An Introduction to Nuclear Power Generation

Christopher E. Brennen
California Institute of Technology
Pasadena, California

Dankat Publishing Company

Library of Congress Card Number 05-???????

A catalogue record for this book is available from the British Library

ISBN-10
ISBN-13

Preface

This book is intended as a introduction to the technology of power generation by nuclear fission. It began many years ago as a series of notes prepared for a graduate student course at the California Institute of Technology. When, following the Three Mile Island accident in 1979, nuclear power became politically unpopular, demand and desire for such a course waned and I set the book aside in favor of other projects. However, as the various oil crises began to accentuate the need to explore alternative energy sources, the course and the preparation of this book was briefly revived. Then came the terrible Chernobyl accident in 1986 and the course and the book got shelved once more. But the pendulum swung back again as the problems of carbon emissions and global warming rose in our consciousness and I began again to add to the manuscript. Even when the prospects for nuclear energy took another downturn in the aftermath of the Fukushima accident (in 2011), I decided that enough was enough and that I should finish the book whatever the future might be for the nuclear power industry. I happen to believe despite the accidents - or perhaps because of them - that nuclear power will be an essential component of electricity generation in the years ahead.

The book is an introduction to a graduate level (or advanced undergraduate level) course in nuclear power generation. It assumes a basic knowledge of physics, fluid mechanics and heat transfer. Of course, the design of a nuclear power plant involves a broad range of engineering expertise. This monograph focuses on the thermohydraulics and neutronics of nuclear power generation and, in particular, on the interplay between these that determines the design of the reactor core. However, no book on nuclear power generation would be complete without some brief description of other critical issues such as nuclear reactor safety. This necessarily includes brief descriptions of the three major accidents (Three Mile Island, Chernobyl and Fukushima) that have influenced the development of nuclear power. However, I have tried to reduce the subject to its essentials for an excess of detail seems to plague many of the texts on nuclear power.

Significant sections of this book (most notably in chapter 7) were adapted from two of my other books, *Cavitation and Bubble Dynamics* and *Fundamentals of Multiphase Flow* and I am most grateful to the publisher of those books, Cambridge University Press, for permission to reproduce those sections and their figures in the present text. Other figures and photographs reproduced

in this book are acknowledged in their respective captions. I would also like to express my gratitude to the senior colleagues at the California Institute of Technology who introduced me to the topic of nuclear power generation, in particular Noel Corngold and Milton Plesset. Milton did much to advance the cause of nuclear power generation in the United States and I am much indebted to him for his guidance. I also appreciate the interactions I had with colleagues in other institutions including Ivan Catton, the late Ain Sonin, George Maise and staff at the Nuclear Regulatory Commission.

This book is dedicated to James MacAteer from whom I first heard the word *neutron* and to the Rainey Endowed School in Magherafelt where the physics *Johnny Mac* taught me stayed with me throughout my life.

Christopher Earls Brennen
California Institute of Technology, November 2013.

Contents

Nomenclature

Roman Letters

a	Amplitude of wave-like disturbance
A	Cross-sectional area
A	Atomic weight
b	Thickness
B_g^2	Geometric buckling
B_m^2	Material buckling
c	Speed of sound
c_p	Specific heat of the coolant
C, C_1, C_2, C_R	Constants
C^*, C^{**}	Constants
C_f	Friction coefficient
d	Diameter
D	Neutron diffusion coefficient
D_h	Hydraulic diameter of coolant channel
E	Neutron kinetic energy
E'	Neutron energy prior to scattering
f	Frequency
g	Acceleration due to gravity
h, h^*	Heat transfer coefficients
H	Height
H_E	Extrapolated height
Hm	Haberman-Morton number, normally $g\mu^4/\rho S^3$
j	Total volumetric flux
j_N	Volumetric flux of component N
J_j	Angle-integrated angular neutron current density vector
J_j^*	Angular neutron current density vector
k	Multiplication factor, number of neutrons/number in preceding generation
k_∞	Multiplication factor in the absence of leakage
k	Thermal conductivity
$\mathcal{K}$	Frictional constants
l	Typical dimension of a reactor

ℓ	Typical dimension
ℓ	Mean free path
ℓ_a	Mean free path for absorption
ℓ_f	Mean free path for fission
ℓ_s	Mean free path for scattering
L	Neutron diffusion length, $(D/\Sigma_a)^{\frac{1}{2}}$
$\mathcal{L}$	Latent heat of vaporization
$\dot{m}$	Mass flow rate
m	Index denoting a core material
M	Number of different core materials denoted by $m = 1$ to M
Ma	Square root of the Martinelli parameter
n	Integer
$n(E)dE$	Number of neutrons with energies between E and $E + dE$ from one collision
N	Number of neutrons or nuclei per unit volume
N_f	Number of fuel rods
$\mathcal{N}$	Number of atoms per unit volume
N^*	Site density, number per unit area
Nu	Nusselt number, hD_h/k_L
p	Pressure
p^T	Total pressure
P	Power
$\mathcal{P}$	Perimeter
$(1 - P_F)$	Fraction of fast neutrons that are absorbed in U^{238}
$(1 - P_T)$	Fraction of thermal neutrons that are absorbed in U^{238}
Pr	Prandtl number
$\dot{q}$	Heat flux per unit surface area
$\mathcal{Q}$	Rate of heat production per unit length of fuel rod
r	Radial coordinate
r, θ, z	Cylindrical coordinates
R	Radius of reactor or bubble
R_E	Extrapolated radius
R_R	Reflector outer radius
R_{RE}	Extrapolated reflector radius
R_P	Fuel pellet radius
R_O	Outer radius
Re	Reynolds number
s	Coordinate measured in the direction of flow
$S(x_i, t, E)$	Rate of production of neutrons of energy, E, due to fission per unit volume.
$\mathcal{S}$	Surface tension
t	Time
T	Temperature
u, U	Velocity
$\bar{u}$	Neutron velocity
u_i	Fluid velocity vector
u_N	Fluid velocity of component N

V	Volume
$\dot{V}$	Volume flow rate
x, y, z	Cartesian coordinates
x_i	Position vector
x_N	Mass fraction of component N
$\mathcal{X}$	Mass quality
z	Elevation

Greek Letters

α	Volume fraction
α_L	Thermal diffusivity of liquid
α_{mf}	Ratio of moderator volume to fuel volume
β	Fractional insertion
β	Volume quality
ϵ	Fast fission factor, number of fast neutrons produced by one fast neutron fission of U^{238}
δ	Boundary layer thickness
η	Efficiency
η	Thermal fission factor, number of fast neutrons produced by one thermal neutron fission of U^{235}
θ	Angular coordinate
κ	Bulk modulus of the liquid
κ	Wavenumber
κ_L, κ_G	Shape constants
λ	Wavelength
$(1 - \Lambda_F)$	Fraction of fast neutrons that leak out of the reactor
$(1 - \Lambda_T)$	Fraction of thermal neutrons that leak out of the reactor
ξ	Time constant
ξ_1, ξ_2	Constants
μ	Dynamic viscosity
ν	Kinematic viscosity
ρ	Density
ρ	Reactivity, $(k-1)/k$
σ	Cross-section
σ_a	Cross-section for absorption
σ_f	Cross-section for fission
σ_s	Cross-section for scattering
Σ	Macroscopic cross-section, $\mathcal{N}\sigma$
Σ_{tr}	Macroscopic transport cross-section, $1/3D$
τ	Half-life
τ_w	Wall shear stress
ϕ	Angle-integrated neutron flux

$\phi_L^2, \phi_G^2, \phi_{L0}^2$	Martinelli pressure gradient ratios
φ	Angular neutron flux
ω	Radian frequency
ω_a	Acoustic mode radian frequency
ω_m	Manometer radian frequency
Ω_j	Unit direction vector

Subscripts

On any variable, Q:

Q_o	Initial value, upstream value or reservoir value
Q_1, Q_2	Values at inlet and discharge
Q_a	Pertaining to absorption
Q_b	Bulk value
Q_c	Critical values and values at the critical point
Q_d	Detachment value
Q_e	Effective value or exit value
Q_e	Equilibrium value or value on the saturated liquid/vapor line
Q_i	Components of vector Q
Q_f	Pertaining to fission or a fuel pellet
Q_s	Pertaining to scattering
Q_w	Value at the wall
Q_A, Q_B	Pertaining to general phases or components, A and B
Q_B	Pertaining to the bubble
Q_C	Pertaining to the continuous phase or component, C
Q_C	Critical value
Q_C	Pertaining to the coolant or cladding
Q_{CI}	Pertaining to the inlet coolant
Q_{CS}	Pertaining to the inner cladding surface
Q_D	Pertaining to the disperse phase or component, D
Q_E	Equilibrium value
Q_F	Pertaining to fast neutrons
Q_{FS}	Pertaining to the fuel pellet surface
Q_G	Pertaining to the gas phase or component
Q_L	Pertaining to the liquid phase or component
Q_M	Mean or maximum value
Q_N	Nominal conditions or pertaining to nuclei
Q_N	Pertaining to a general phase or component, N
Q_R	Pertaining to the reflector
Q_S	Pertaining to the surface
Q_T	Pertaining to thermal neutrons
Q_V	Pertaining to the vapor
Q_∞	Pertaining to conditions far away

Superscripts and other qualifiers

On any variable, Q:

$\bar{Q}$	Mean value of Q
$\dot{Q}$	Time derivative of Q
δQ	Small change in Q
ΔQ	Difference in Q values
Q^m	Pertaining to the material component, m

Chapter 1

INTRODUCTION

1.1 Introduction

Beginning in the early 1950s, the nuclear power industry in the United States grew to become second only to coal in its electrical generation capacity. By 1990, there were 111 commercial nuclear power plants with a combined capacity of $99,000MW$, representing about 19% of the nation's electric power. Nuclear power production in the US was then 530×10^9 kWh, much more than in France and Japan combined though these two countries were among the nations most reliant on nuclear power. France produced 77% of its electricity by nuclear power; in West Germany and Japan the percentages were 33% and 26%. However, in the US no new nuclear plants were ordered after 1978 and the expansion of the US commercial nuclear power industry ceased shortly thereafter. Other countries saw a similar drastic decline in the growth of the nuclear power capacity.

The reasons for this abrupt transition are several. First, the rate of growth of demand for electric power was less than expected. Second, the capital costs associated with new nuclear power plants rose dramatically in the 1970s and 80s, in part because of more stringent regulatory activity. And third, public opposition to nuclear power also rose substantially in the aftermath of the Three Mile Island accident (see section 8.4.1) in 1979, a reaction that was further amplified by the Chernobyl accident in 1986 (see section 8.4.2). These accidents greatly heightened the public fear of nuclear power plants based on three major concerns, two reasonable and one unreasonable. The unreasonable concern was that a nuclear generating plant might explode like a nuclear weapon, an event that can be dismissed on fundamental physical grounds (see, for example, Nero 1979). However, the other two concerns that continue to have validity are the fear of the release of harmful radioactive material and the concern over the storage of nuclear waste. While Chernobyl rightly increased the concern over radioactive release, the improvements introduced as a result of the lessons learned from the nuclear accidents over the past half-century (see sections 8.4

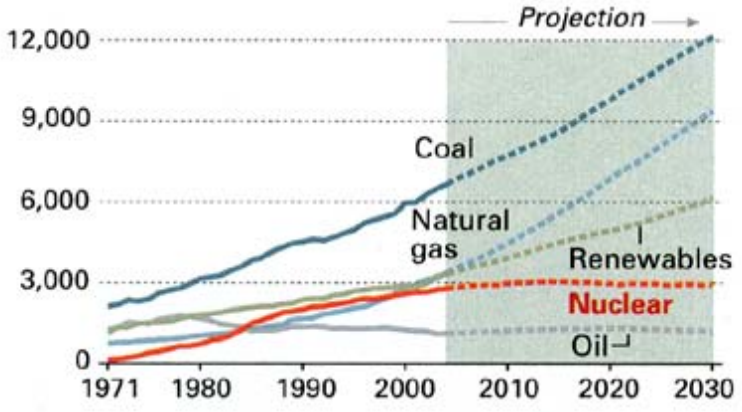

Figure 1.1: Projected worldwide electricity generation by fuel in billion kilowatt-hours. Reproduced by permission of National Geographic, April 2006.

and 8.5) have greatly reduced the risk of such events. Specifically, it is now recognized that, in the past, a lack of standardization in the design and operation of nuclear power plants significantly impaired their safety margins and that world-wide cooperation, oversight and standardization will radically improve safety margins in the future. Great strides have been made in this regard since the end of the Cold War. Similarly, plans for waste storage and/or recycling continue to be developed both nationally and globally. As von Hippel (2006) has pointed out there is no hurry to recycle nuclear waste for many temporary storage options are possible given how small a volume of waste is produced and temporary storage is advisable when a number of reprocessing options may be found to be advantageous in the years ahead.

Of course, no power generating process is devoid of risks and consequences and, though complex, it is necessary to balance both the long and short-term effects while seeking an appropriate mix of energy resources. In 2011, 63% of the world's electricity generation was produced by coal and gas combustion; 12% was from nuclear power (from the Shift Project Data Portal, 2011). This 12% is significantly smaller than in the year 2006, when, as seen in figure 1.1, nuclear power amounted to about 20% of the global generation. That diagram projects that nuclear power generation will remain relatively constant in the decades ahead while the overall demand and generation will continue to grow. This growth is in part caused by population increase and in part by economic development particularly in the developing countries. Efforts to conserve energy in the developed countries have been more than offset by population increases in the less-developed world. Consequently worldwide energy consumption per capita continued to rise and increased by about 20% between 1980 and 2010 (from the Shift Project Data Portal 2011).

However, it is now becoming clear that the increase in the use of combustible fuels, primarily coal and gas, has serious consequences for the earth's

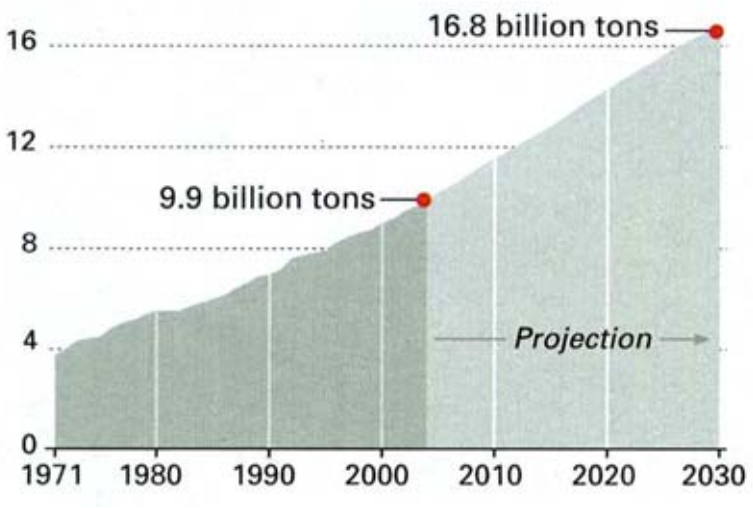

Figure 1.2: Worldwide annual CO_2 emissions from electricity production in billion metric tons. As well as power production the numbers include the mining, preparation and transport of the fuel as well as plant construction. Reproduced by permission of National Geographic, April 2006.

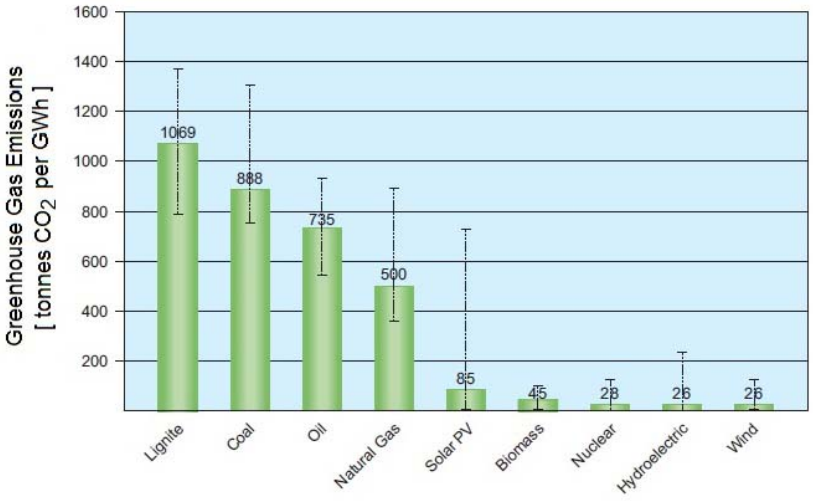

Figure 1.3: The greenhouse gas emissions of the major electricity generating processes in terms of tonnes of CO_2 equivalent per GWh. Large bars are the average values and the vertical error bars represent the scatter in the sources. Taken from the WNA report (2011).

atmosphere and climate. Figure 1.2 shows how the worldwide emissions of CO_2 from electricity production may continue to rise in the decade ahead. Moreover, greenhouse gas emissions are primarily caused by the burning of the combustible fuels coal, natural gas and oil. Indeed, as demonstrated, by the data in figure 1.3 (which includes the emissions generated during mining, preparation, transport and plant construction) the emission of greenhouse gases from coal, oil and natural gas generating processes far exceeds that from the other power sources, in particular nuclear power systems. This advantage of nuclear power generation has led a number of environmental groups to begin to advocate for nuclear power (see, for example, Duffey 2005) as a preferred *green solution* to the energy challenge. Whatever the preferred means of electricity production might be in the future, it seems clear that nuclear power must remain an option and we must therefore be prepared to exercise that option. One of the disturbing consequences of the anti-nuclear public sentiment in the past 30 years is that nuclear engineering became quite unpopular in universities (at least in the USA) and hence the nuclear engineering programs and students dwindled to a small number. If nuclear power generation were to become an important national or global objective, there would have to be a radical increase in that component of our engineering educational effort.

1.2 Book structure

After a brief review of the fundamental physics of nuclear fission and of radioactivity in chapters 2 and 3, the book covers some of the basic features of the neutronics of nuclear reactors in chapter 4. This is followed in chapter 5 by a description of the structure of the fission reactors presently used or envisaged for nuclear power generation. With that structure in mind the reader is then equipped to absorb, in chapter 6, how the heat generated by nuclear fission is transferred to the reactor core coolant and thus transferred out of the core to be used to drive the turbines and generators that complete the structure of the power station. Chapter 7 then reviews some of the basic multiphase flow phenomena that may be associated with those heat transfer processes during both normal operation of a nuclear power plant and during postulated accidents within that reactor. This leads naturally to a discussion in chapter 8 of nuclear reactor safety including descriptions of the three major accidents which dominate the public's impression of the dangers of nuclear power, namely the accidents at Three Mile Island, at Chernobyl and at Fukushima. That discussion naturally includes the important lessons learned from those accidents and other experiences.

1.3 Other texts

There are, of course, some very fine text books on nuclear power generation that the serious student should certainly peruse. My own favorite for the overall en-

gineering of nuclear power systems is the elegant and comprehensive engineering book entitled *Nuclear Power Systems* by C.D. Gregg King (1964). For the more advanced analytical methods it is hard to beat the classic texts by Glasstone and Sesonke (1981) and by Duderstadt and Hamilton (1976). For the thermohydraulics I learnt much from the compact monograph by Winterton (1981). In the present text I have chosen to focus on the neutronics and thermohydraulics that contribute to the design of the nuclear reactor core. There are, of course important ancillary subjects that should form any comprehensive study of nuclear power generation, in particular the energy economics (see, for example, Murray 1993), the safety issues and waste disposal. While I have included discussion of the second, I have chosen not to address the issue of waste disposal since that involves many separate and unconnected facets. The reader may wish to consult texts such as Knief (1980) or Collier and Hewitt (1987) for a discussion of the waste disposal options.

Other valuable texts are referenced at the conclusion of each chapter. Moreover, today a great deal can be learnt from the pages of the internet, for example those constructed by the American Nuclear Society or the World Nuclear Association.

References

Duffey, R.B. (2005). *Green atoms.* Power & Energy, **2**, No.2.

National Geographic Magazine, April 2006.

Nero, A.V. (1979). *A guidebook to nuclear reactors.* Univ. Calif. Press.

The Shift Project Data Portal. (2011). http://www.tsp-data-portal.org/

von Hippel, F.N. (2006). *No hurry to recycle.* ASME Mechanical Engineering, **128**, No.5, 32-35.

WNA report. (2011). *Comparison of lifecycle greenhouse gas emissions of various electricity generation sources.* World Nuclear Association Report.

World Nuclear Association Information Library. (2011). http://www.world-nuclear.org/Information-Library/

Chapter 2

BASIC NUCLEAR POWER GENERATION

2.1 Nuclear power

Nuclear energy is released when atoms are either split into smaller atoms (a phenomenon known as fission) or combined to form a larger atom (a phenomenon known as fusion). This monograph will focus on the production of power by harnessing atomic fission since that is the principle process currently utilized in man-made reactors.

Most of the energy produced by nuclear fission appears as heat in the nuclear reactor core and this heat is transported away from the core by conventional methods, namely by means of a cooling liquid or gas. The rest of the power generation system is almost identical in type to the way in which heat is utilized in any other generating station whether powered by coal, oil, gas or sunlight. Often the heat is used to produce steam which is then fed to a steam turbine that drives electric generators. In some plants hot gas rather than steam is used to drive the turbines. In the case of steam generating nuclear power plants the part of the plant that consists of the reactor and the primary or first-stage cooling systems (pumps, heat exchangers, etc.) is known as the *nuclear steam supply system* and the rest, the conventional use of the steam, is called the *balance of plant* . This monograph will not deal with this conventional power generation technology but will focus on the nuclear reactor, its production of heat and the primary coolant loop that cools the reactor core.

2.2 Nuclear fuel cycle

Though it is possible that power might be derived from nuclear fusion at some point in the distant future, all presently feasible methods of nuclear power generation utilize the energy released during nuclear fission, that is to say the process

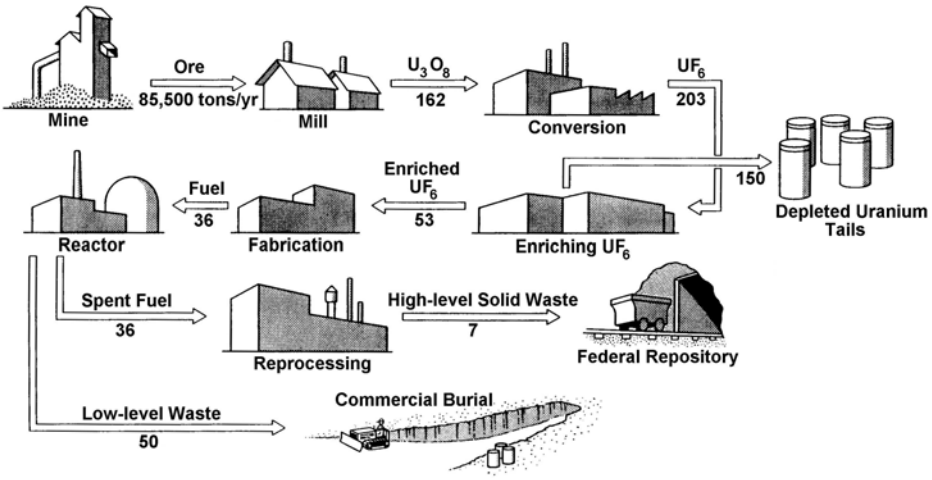

Figure 2.1: Uranium requirements for a pressurized water reactor. The numbers refer to the number of tons of each material required per year for a 1000 MWe power plant. From USAEC (1973).

by which a neutron colliding with an atom causes that atom to split and, as a by product, produces heat. With atoms known as fissile atoms, additional neutrons are released at the same time thus allowing a continuing, naturally regenerating process of fission and a source of heat. The only naturally occurring fissile material is the uranium isotope, ^{235}U but it only occurs along with a much greater quantity of the common isotope ^{238}U. Specifically, naturally occurring uranium contains 99.29% of ^{238}U and only 0.71% of ^{235}U (138 atoms of ^{238}U for every atom of ^{235}U). These proportions are the same everywhere on earth because they date from the original creation of uranium by fusion and the similar decay of these isotopes since that time.

The nuclear fuel cycle refers to the sequence of steps in a nuclear power generation system, from the mining or acquisition of the raw ore, to the refining and enrichment of that material, to its modification during power production and thence to the management of the nuclear waste. Each of the steps in a nuclear fuel cycle involves complex engineering and economics that is beyond the scope of this book (the reader could consult Knief (1992) for a comprehensive summary). Here we provide a brief summary of commonly-envisaged fuel cycles. A basic feature of those cycles is an assay of the mass of the essential material during each step (as well as the waste). Another is the power consumption or generation during each step. One example of a nuclear fuel cycle is shown in figure 2.1 which presents the uranium requirements for a 1000 MWe pressurized water reactor.

Since ^{235}U is the only naturally-occurring fissile material, the nuclear fuel cycle must necessarily begin with the mining and milling of uranium ore. Uranium ore is relatively common and additional recoverable resources are being

discovered at a significant pace; indeed the known resources have increased by a factor of about three since 1975. Some 40% of the known recoverable resources are found in Canada and Australia while Russia and Kazakhstan hold another 21% (the highest grade uranium ore is found in northern Saskatchewan). Thorium, an alternate nuclear reactor fuel, is reputed to be about three times as abundant as uranium (from the World Nuclear Association Information Library (2011)).

Uranium is usually removed from the ore by chemical milling methods that result in the production of U_3O_8, known as yellowcake. The waste or *tailings* present some, primarily chemical disposal problems. With the exception of the CANDU reactor described in section 5.7, all other current reactors require the uranium to be *enriched* , a process in which the fraction of ^{235}U is increased. In preparation for enrichment, the uranium is converted to a gaseous form, namely from U_3O_8 to UF_6 in a process known as *conversion* . Several possible methods have then been used to enrich the UF_6 and this requires the separation of $^{235}UF_6$ from the $^{238}UF_6$, a process that cannot be accomplished chemically since these isotopes are chemically identical. The separation must therefore be accomplished physically by recourse to the small physical differences in the molecules, for example their densities or diffusivities. The most common conversion process uses a gas centrifuge in which the heavier $^{238}UF_6$ is preferentially driven to the sides in a rapidly rotating cylinder. Another is the gaseous diffusion method in which the gas is forced through a porous filter which the $^{235}UF_6$ penetrates more readily. In either case a by-product is a waste known as the *enrichment tailings* .

Whether enriched or not the fuel must next be formed into fuel ready for loading into the reactor. In most reactors this fuel fabrication stage involves conversion to solid pellets of UO_2 or, less commonly, UC. These cylindrical pellets are then packed into long fuel rods (as described in section 5.2.4) and loaded into the reactor.

The fuel cycle clearly continues when the fuel rods are spent and removed from the reactor. However, before resuming our review by a description of those later stages of the nuclear fuel cycle we should briefly review the changes in the fuel that occur during its life in the reactor core.

2.2.1 Fuel changes in the reactor

In a typical 1000 MWe reactor for power generation, the core contains 75 tonnes of low-enriched uranium usually in the form of UO_2 pellets. (One tonne of fuel typically generates about $45kWh$ of electricity). During operation in a critical state, the ^{235}U fissions or splits producing heat in a chain reaction that also produces plutonium, other transuranic elements and fission products. The fission fragments and heavy elements increase in concentration so that after 18-36 months it becomes advantageous to replace the fuel rods. At this point the fuel still contains about 96% of the original uranium but the fissionable ^{235}U is now less than 1% compared with the initial, enriched $3.5 - 5\%$. About 3% of the used fuel is waste product and 1% is plutonium.

2.2.2 The post-reactor stages

Upon removal from a reactor, the fuel in the fuel rods is highly radioactive and is still producing decay heat as described in section 3.2.2. At the time of shutdown of the reactor the decay heat is about 6.5% of the full power level. This declines rapidly falling to about 1.5% after an hour, 0.4% after a day and 0.2% after a week. Spent fuel rods are therefore normally stored in isolated water pools near the generation site for several months not only to keep them cool but also to allow for the radioactive elements with short half-lives to decay substantially before further processing. The water absorbs the decay heat and prevents overheating of the fuel rods. They can be transferred to dry storage after about 5 years.

At the present time there are two subsequent strategies. The fuel may be reprocessed in order to recycle the useful remnants or it may remain in long term storage to await re-evaluation of its potential use or disposal in the future.

Reprocessing involves separating the uranium and plutonium from the waste products by chopping up the fuel rods (cladding and all) and dissolving them in acid to separate their components (see, for example, Nero 1979). This enables the uranium and plutonium to be reused in fuel while the remaining 3% of radioactive waste is disposed of as described below. The recovered uranium is usually a little richer in ^{235}U than in nature and is reused after enrichment. The plutonium can be combined with uranium to make so-called *mixed oxide* (MOX) fuel that can be used as a substitute for enriched uranium in mixed oxide reactors.

All the waste from the nuclear cycle and fuel processing is classified according to the radiation it emits as either low-level, intermediate level or high-level waste. The high-level waste from reprocessing is reduced to powder and entombed in glass to immobilize it. The molten glass is poured into steel containers ready for long term storage. One year of high-level waste from a 1000 MWe reactor produces about 5 tonnes of such high-level waste.

Currently there are no disposal facilities for used fuel or reprocessing waste. These are deposited in storage to await future use or treatment or for the creation of more permanent disposal facilities. The small mass of the material involved makes this wait not only feasible but wise.

As a footnote, we remark that the end of the Cold War created a new source of nuclear fuel from the Russian stockpiles of highly-enriched weapons-grade uranium. Under a US-Russian agreement, this has been diluted for use in nuclear power plants and, since then, has provided fully half of the nuclear fuel used in the USA for the generation of electricity.

2.3 Nuclear physics

2.3.1 Basic nuclear fission

To proceed it is necessary to outline the basic physics of nuclear fission. The speed of individual neutrons is quoted in terms of their kinetic energy in eV

or *electron-volts* where $1eV$ is equivalent to $4.44 \times 10^{-26} kWh$ (kilowatt hours) of power. In 1938/9 Hahn, Meitner, Strassman and Frisch (Hahn and Strassman 1939, Meitner and Frisch 1939, Frisch 1939, Hahn 1958) first showed that any heavy atomic nucleus would undergo fission if struck by a *fast* neutron of sufficiently high kinetic energy, of the order of $1 \rightarrow 2MeV$. Shortly thereafter Bohr and Wheeler (1939) predicted that only very heavy nuclei containing an odd number of neutrons could be fissioned by all neutrons with kinetic energies down to the level of *thermal* neutrons (order $0.1MeV$). The only naturally occuring nucleus that meets this condition is the isotope U^{235} which has 92 protons and 143 neutrons. However, the isotope ^{235}U is rare; in nature it only occurs as one atom for every 138 atoms of the common isotope ^{238}U or, in other words, as 0.71% of natural uranium. We will discuss the consequences of this shortly.

When a neutron strikes a heavy nucleus there are several possible consequences:

- *radiative capture* or absorption , in which the neutron is captured by the nucleus and essentially lost.
- *inelastic scattering* , during which the neutron is momentarily captured and then released without fission but with considerable loss of kinetic energy.
- *fission* , in which the heavy nucleus is split into several *fission fragments*, energy is generated and several *secondary* neutrons are released.

When a heavy nucleus such as ^{235}U is fissioned by a colliding neutron, several important effects occur. First and most fundamentally for our purposes is the release of energy, mostly in the form of heat (as a result of the special theory of relativity, there is an associated loss of mass). On average the fission of one ^{235}U nucleus produces approximately $200MeV$ $(2 \times 10^8 eV)$ of energy. Thus a single fission produces roughly $8.9 \times 10^{-18} kWh$. Since a single ^{235}U atom weighs about $3.9 \times 10^{-22} g$ it follows that the fission of one gram of ^{235}U produces about $23MWh$ of power. In contrast one gram of coal when burnt produces only about $10^{-5} MWh$ and there is a similar disparity in the waste product mass.

The second effect of a single ^{235}U fission is that it releases about 2.5 neutrons. In a finite volume consisting of ^{235}U, ^{238}U and other materials, these so-called *prompt* neutrons can have several possible fates. They can:

- collide with other ^{235}U atoms causing further fission.
- collide with other ^{235}U atoms and not cause fission but rather undergo radiative capture.
- collide with other atoms such as ^{238}U and be similarly absorbed by radiative capture.
- escape to the surroundings of the finite volume of the reactor.

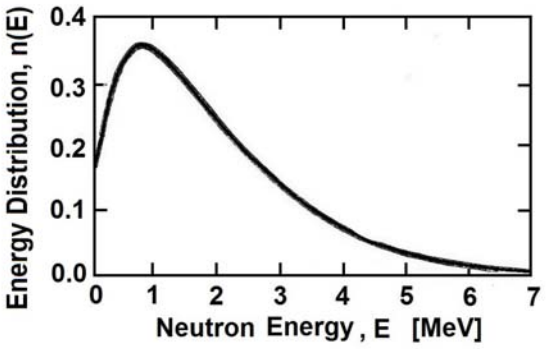

Figure 2.2: Spectrum, $n(E)$, of neutron energies due to fission.

As a consequence we can, at least conceptually, think of counting the number of neutrons in a large mass in one generation and compare it with the number of neutrons in the following generation. The ratio of these two populations is known as the *reproduction factor* or *multiplication factor*, k, where

$$k = \frac{\text{Number of neutrons in a generation}}{\text{Number of neutrons in the preceding generation}} \tag{2.1}$$

In addition to k, it is useful to define a multiplication factor which ignores the loss of neutrons to the surroundings, in other words the multiplication factor for a reactor of the same constituents but infinite size, k_∞. We shall see in the section which follows how k and k_∞ are used in the evaluation of the state of a reactor.

An alternative to k is the frequently used *reactivity*, ρ, defined as

$$\rho = \frac{k-1}{k} \tag{2.2}$$

and this quantity is also widely used to describe the state of a reactor. We postpone further discussion on k (or ρ) and k_∞ and the role these parameters play in the evaluation of the criticality of a reactor until further details of the neutronics of a reactor core have been established.

2.3.2 Neutron energy spectrum

The neutrons that are released during fission have a spectrum of energies as shown in figure 2.2 where $n(E)dE$ is the fraction of neutrons with energies in the range E to $E + dE$. The distribution in figure 2.2 is often described by empirical formulae of the type

$$n(E) = 0.453e^{-1.036E}\sinh\left(\sqrt{2.29E}\right) \tag{2.3}$$

which integrates to unity as it must. It follows that, as quoted earlier, the average energy of a fission neutron is $2MeV$.

2.3.3 Cross-sections and mean free paths

In the context of nuclear interactions or events, a cross-section is a measure of the probability of occurrence of that interaction or event. Consider, for example, a highly simplified situation in which n neutrons per cm^3, all of the same velocity, $\bar{u}$, (or energy, E) are zooming around in a reactor volume of density ρ consisting of only one type of atom of atomic weight, A. The number of atoms per gram is therefore $6.025 \times 10^{23}/A$ where 6.025×10^{23} is Avagadro's number. Hence, the number of atoms per cm^3, $\mathcal{N}$, is given by

$$\mathcal{N} = 6.025 \times 10^{23} \rho / A \tag{2.4}$$

In such a reactor, the rate at which the moving neutrons are colliding with atoms (assumed stationary) within each cm^3 of volume is clearly going to be proportional to $\mathcal{N}$, to n and to the velocity, $\bar{u}$, of the neutrons. The factor of proportionality, σ, or

$$\sigma = \frac{\text{Number of collisions per unit time per unit volume}}{\mathcal{N} n \bar{u}} \tag{2.5}$$

has units of area and is known as a cross-section . It can be visualized as the effective frontal area of the atom which would lead to the given collision rate per unit volume (zero area would, of course, not lead to any collisions). Cross-sections are measured in units called *barns* where $1barn = 10^{-24} cm^2$. They are a measure of the probability of a particular event occurring in unit volume per unit time. Thus, for example, the probability of a collision causing fission is proportional to the *fission cross-section*, σ_f, the probability of a collision resulting in neutron capture or absorption is proportional to the *absorption cross-section*, σ_a, and the probability of a collision resulting in scattering is proportional to the *scattering cross-section*, σ_s.

The typical distance traveled by a neutron between such interaction events is called the mean free path, ℓ, and this is related to the cross-section as follows. Consider a given interval of time. Then the mean free path, ℓ, will be given by the total distance traveled by all neutrons in a unit volume during that time divided by the number of neutrons undergoing a particular interaction during that time. Or

$$\ell = \frac{n\bar{u}}{\mathcal{N} n \bar{u} \sigma} = \frac{1}{\mathcal{N}\sigma} \tag{2.6}$$

More specifically, the *fission mean free path*, $\ell_f = 1/\mathcal{N}\sigma_f$, will be the typical distance traveled by a neutron between fission events, the *absorption mean free path*, $\ell_a = 1/\mathcal{N}\sigma_a$ will be the typical distance traveled by a neutron between absorption events and so on. For this and other reasons, it is convenient to define *macroscopic cross-sections* , Σ, where $\Sigma = \mathcal{N}\sigma$; these macroscopic cross-sections therefore have units of inverse length.

Note that most of the cross-sections, σ, which we shall need for reactor analysis are strong and often complicated functions of the neutron energy, E. This complicates the quantitative analyses of most reactors even when the conceptual

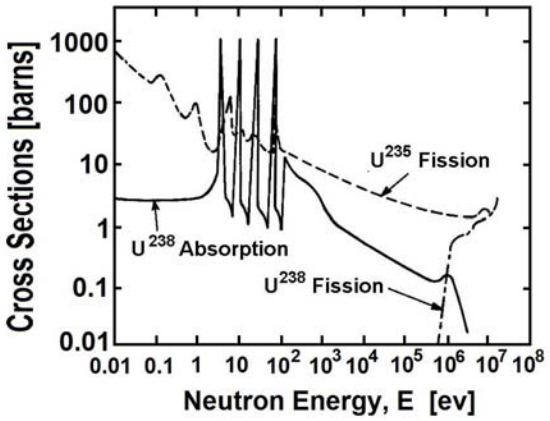

Figure 2.3: Qualitative representations of how the fission cross-sections for ^{235}U and ^{238}U as well as the absorption cross-section for ^{238}U vary with the neutron energy.

processes are quite straightforward. Qualitative examples of how some cross-sections vary with E are included in figure 2.3. Rough models of how σ_a, σ_f, and σ_s depend on E (or $\bar{u}$) are as follows.

In many materials, thermal neutrons have σ_a and σ_f cross-sections that are inversely proportional the velocity, $\bar{u}$, and therefore vary like $E^{-\frac{1}{2}}$. In such materials it is conventional to use a factor of proportionality, $\sigma E^{\frac{1}{2}}$, at a reference state corresponding to a velocity of $2200m/s$ (or an energy of $E = 0.0253eV$). The average cross-section so defined at $E = 0.0253eV$ is called the *thermal cross-section reduced to* $0.0253eV$ and will be denoted here by $\hat{\sigma}$.

Of course, some materials like ^{238}U have strong absorption peaks or resonances near particular energies and, in these, the model described above requires modification. This is often effected by supplementing the $E^{-\frac{1}{2}}$ dependence with one or more resonance peaks.

Another useful observation is that scattering cross-sections, σ_s, are often independent of E except at high velocities and can therefore be modeled using a single uniform value.

2.3.4 Delayed neutrons and emissions

Another important feature of nuclear fission is that although almost all of the neutrons are produced essentially instantaneously a small fraction (about 0.7%) are delayed and emerge up to about $80sec$ after the fission event. Most of these delayed neutrons occur because some fission products produced by the event undergo radioactive decay and, in one or more stages of that decay, emit a neutron. One of the most common of these post-fission decays occurs when the fission product ^{87}Br decays, though there are many fission products each having several stages of decay so that delay times may range from 0.6 to $80sec$.

These delayed neutrons play a crucial role in the control of a nuclear reactor. As we will describe later in sections 4.9 and 5.2.5without these delayed neutrons, a nuclear reactor would be very difficult to control since a slight excess in the neutron population would grow exponentially in a matter of microseconds. The delayed neutrons increase this response time by several orders of magnitude and make reactor control quite manageable.

2.4 Natural reactors

A useful and appropriate starting point is to consider the state of naturally-occurring uranium. As stated earlier the most common isotope is ^{238}U and the fission cross-section for ^{238}U has the form shown in figure 2.3. Thus only high energy or *fast neutrons* with energies greater than about $2MeV$ can cause fission of ^{238}U. However, the absorption and scattering cross-sections are much larger and therefore any population of neutrons in ^{238}U rapidly declines; such a *reactor*is very subcritical.

Now consider a naturally occurring mixture of ^{238}U and ^{235}U. As previously stated and illustrated in figure 2.3, ^{235}U can be fissioned even with low energy neutrons and therefore the presence of the ^{235}U causes an increase in the reactivity of the mixture. However, the high absorption cross-section of the ^{238}U still means that the reactivity of the mixture is negative. Thus no chain reaction is possible in natural uranium. One can visualize that if it were possible then this would have happened at some earlier time in the earth's evolution and that no such unstable states or mixtures could be left today. Such has also been the fate of higher atomic weight elements that may have been produced during nuclear activity in the past.

There are several different ways in which the naturally occurring uranium mixture might be modified in order to produce a critical or supercritical chain reaction in which the neutron population is maintained. One obvious way is to create a mixture with a higher content of ^{235}U than occurs naturally. This is called enriched uranium and requires a process of separating ^{238}U and ^{235}U in order to generate the enriched mixture. Since ^{238}U and ^{235}U are almost identical chemically and physically, separation is a difficult and laborious process, the main hurdle during the Manhattan project. In an atomic bomb two or more subcritical masses of enriched uranium (typically enriched so that the percentage of ^{235}U is of the order of 10%) are brought together to form a supercritical reactor size in which the high energy neutron population explodes uncontrollably.

2.5 Thermal reactors

2.5.1 Moderator

An alternative which avoids the costly and difficult enrichment process and eliminates the need to handle weapons grade uranium is hinged on a characteristic

of the absorption cross-section of ^{238}U which has the form shown in figure 2.3. This has strong peaks at intermediate neutron energies, the so-called *capture resonances*, so that many neutrons, slowed down by scattering, are absorbed by the ^{238}U before they can reach low or *thermal* energies. This is important because, as shown in figure 2.3, ^{235}U has a very high fission cross-section at thermal energies and this potential source of fast neutrons is attenuated because so few neutrons can pass through the resonance barrier. (We note that neutrons that are in the process of being slowed down are termed *epithermal neutrons* .)

However, if it were possible to remove the fast neutrons from the reactor, slow them down to thermal energies and then reintroduce them to the core, then the reactivity of the reactor could be increased to critical or supercritical levels. In practice, this can be done by including in the reactor a substance that slows down the neutrons without absorbing them. These slowed down neutrons then diffuse back into the uranium and thus perpetuate the chain reaction. This special substance is known as the *moderator* and it transpires that both water and carbon make good moderators. Such a reactor is called a *thermal* reactor since its criticality is heavily dependent on the flux of low energy, thermal neutrons. Virtually all the nuclear reactors used today for power generation are thermal reactors and this monograph will therefore be focussed on this type of reactor.

To summarize, a conventional thermal reactor core comprises the following components:

- Natural or slightly enriched uranium fuel, usually in the form of an oxide and encased in fuel rods to prevent the escape of dangerous fission products.
- Moderator, usually water (sometimes heavy water) or carbon.
- Control rods made of material that is highly absorbent of neutrons so that the insertion or withdrawal of the rods can be used to control the reactivity of the core.
- A cooling system to remove the heat, the energy produced. In many reactors water serves as both the coolant and the moderator.

A variety of thermal reactors have been developed and used to produce power in the world. These comprise three basic types:

1. Light water reactors (LWRs) are by far the most common type used for power generation and include the common pressurized water reactors (PWRs) and boiling water reactors (BWRs) (see sections 5.2.1 and 5.2.3). They use regular water (so called *light* water) as both the coolant and the moderator but need somewhat enriched uranium fuel (about 2% ^{235}U).
2. Heavy water reactors (HWRs) use natural, unenriched uranium fuel and achieve the needed increase in reactivity by using deuterium oxide (*heavy* water) as the moderator and coolant rather than light water. The Canadian CANDU reactor is the best known example of this type.

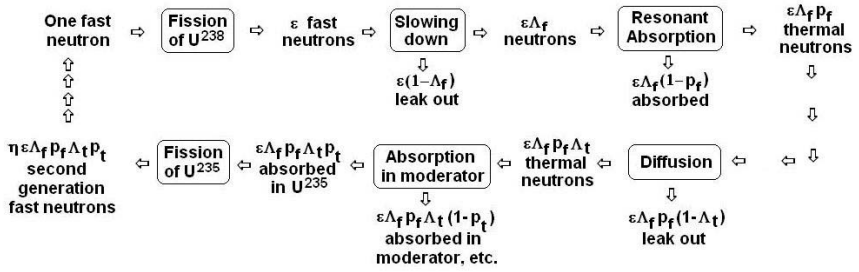

Figure 2.4: Simplified history of neutrons in a thermal reactor.

3. Gas-cooled reactors (GCRs) in which the primary coolant loop utilizes a gas (for example carbon dioxide or helium) rather than water. Typically these use graphite as the moderator. Examples are the high temperature gas-cooled reactor (HTGR) and the advanced gas-cooled reactor (AGR) manufactured respectively in the USA and UK.

This list focuses on the large thermal reactors for power generation. There is a much greater variety of design in the smaller reactors used for research and for power-sources in vehicles such as submarines, space probes, etc. We will be examining the various types of thermal reactors in much greater detail in the chapter 5.

2.5.2 Neutron history in a thermal reactor

Figure 2.4 delineates the typical neutron history in a thermal reactor. Using a single fast neutron as an arbitrary starting point (upper left), this fast neutron fissions a ^{238}U atom and produces ϵ fast neutrons. Some fraction, $(1 - \Lambda_F)$, of these fast neutrons leak out through the boundaries of the reactor and another fraction, $(1 - P_F)$ are absorbed in ^{238}U leaving $\epsilon\Lambda_F P_F$ that have been slowed down to thermal speed either in the moderator or otherwise. Some fraction, $(1 - \Lambda_T)$, of these thermal neutrons also leak out through the boundaries and another fraction, $(1 - P_T)$, are absorbed in the ^{238}U or the moderator or other material. This finally leaves $\epsilon\Lambda_F P_F \Lambda_T P_T$ thermal neutrons to cause fission of ^{235}U and thus produce $\eta\epsilon\Lambda_F P_F \Lambda_T P_T$ second generation fast neutrons. In this history, η is the *thermal fission factor of* ^{235}U, ϵ is the *fast fission factor*, Λ_F is the *fast neutron non-leakage probability*, Λ_T is the *thermal neutron non-leakage probability*, P_F is the *resonance escape probability*, and P_T is the *thermal utilization factor for* ^{235}U.

It follows that the multiplication factors, k and k_∞, are given by

$$k = \eta\epsilon\Lambda_F P_F \Lambda_T P_T \qquad ; \qquad k_\infty = \eta\epsilon P_F P_T \tag{2.7}$$

known respectively as the *six-factor formula* and the *four-factor formula*. It also follows that a reactor operating at steady state will have $k = \eta\epsilon\Lambda_F P_F \Lambda_T P_T = 1$

and the control system needed to maintain such steady state operation must be capable of adjusting one or more of the factors P_F and P_T.

The thermal energy resulting from this process comes mostly from the fission process and therefore both the neutron population and the neutron flux (see section 4.2) are roughly proportional to the rate of generation of heat within a reactor core. Thus an evaluation of the neutron flux by the methods of chapter 4 can be used to estimate the generation of heat within the components of the core as described in chapter 6.

2.6 Fast reactors

An alternative to the thermal reactor strategy is to strive to attain criticality using, primarily, fast neutrons. Various fuels and combinations of fuels can provide the required self-sustaining reaction. Highly enriched uranium (over 20% ^{235}U) is possible and in this process ^{238}U produces several isotopes of plutonium including ^{239}Pu and ^{241}Pu by neutron capture. Then the ^{239}Pu and ^{241}Pu undergo fission and produce heat in the same way as ^{235}U or ^{233}U. The ^{238}U is referred to as the *fertile* material while, like ^{235}U or ^{233}U, the ^{239}Pu and ^{241}Pu are referred to as *fissile* materials. An alternative is the fertile thorium, ^{232}Th, that yields fissile thorium.

While fast reactors could use enriched uranium, they are more efficiently fueled with fissile plutonium or a mixture of uranium and plutonium. In the latter case the ^{238}U will produce more plutonium. Reactors in which the net change of plutonium content is negative is called a *burner* fast reactor while those in which the plutonium content is increasing is termed a *fast breeder reactor*. (FBR) Commonly fast breeder reactors are cooled using liquid metal (sodium, lead or mercury) rather than water and so are referred to as *liquid metal fast breeder reactors* (LMFBR). Almost all the commercial fast reactors constructed to date are LMFBRs and so we focus on this type in the pages that follow.

The advantage of a fast reactor is that it makes much better use of the basic uranium fuel, indeed by an estimated factor of 60. Moreover, since an FBR breeds new fuel there are subsequent savings in fuel costs since the spent fuel can be reprocessed to recover the usable plutonium. Examples of LMFBRs are the French-built Phenix (and Superphenix)(see section 5.7) and the gas-cooled fast breeder reactor (GCFR). However, the safety issues associated with these reactors are much more complex than with thermal reactors.

2.7 Criticality

We now resume discussion of the criticality of a nuclear reactor. It is self-evident that a finite reactor will manifest an accelerating chain reaction (a bomb) when $k > 1$ (or $\rho > 0$); such a reactor is termed *supercritical*. Moreover a reactor for which $k = 1$ ($\rho = 0$) is termed *critical* and one for which $k < 1$ ($\rho < 0$) is *subcritical*. Note that since the neutron escape from a finite reactor of typical

linear dimension, l, is proportional to the surface area, l^2, while the neutron population and production rate will be proportional to the volume or l^3 it follows that k will increase with the size, l, of the reactor and hence there is some *critical size* at which the reactor will become critical. It is clear that a power plant needs to maintain $k = 1$ to produce a relatively stable output of energy while gradually consuming its nuclear fuel.

Consequently there are two sets of data which determine the criticality of a reactor. First there is the basic neutronic data (the fission, scattering and absorption cross-sections, and other details that are described previously in this chapter); these data are functions of the state of the fuel and other constituents of the reactor core but are independent of the core size. These so-called *material properties* of a reactor allow evaluation of k_∞. The second set of data is the geometry of the reactor that determines the fractional leakage of neutrons out of the reactor. This is referred to as the *geometric property* of a reactor and this helps define the difference between k and k_∞. These two sets of data are embodied in two parameters called the *material buckling*, B_m^2, and the *geometric buckling*, B_g^2, that are used in evaluating the criticality of a reactor. These will be explicitly introduced and discussed in chapter 4.

2.8 Fuel cycle variations

To conclude the discussion of nuclear fuel cycles, it is appropriate to reprise the variations in the fuel cycle represented by the present family of nuclear power generating reactors. The basic fuel cycle for a light water reactor (LWR) (see section 5.2.1) is depicted in figure 2.5 but without the dashed line indicating plutonium recycling. As described above, the basic cycle begins with enriched uranium ($3.5 - 5\%$ ^{235}U as compared to the 0.71% in natural uranium). The depleted uranium from the fuel preparation process contains about 0.2% ^{235}U. Spent fuel removed from the reactor contains about 0.8% ^{235}U and the fission products described previously, as well as plutonium. As indicated by the dashed line in figure 2.5, the plutonium can be recycled and used again in a fuel in which it is mixed with uranium that might typically only need to be enriched to about 2.0% ^{235}U. Such a *mixed oxide fuel* (MOX) consisting of UO_2 and PuO_2 needs to be carefully adjusted to have the desired neutronic activity.

As a second example, note the very different fuel cycle for the high temperature gas reactor, HTGR, (see section 5.5) depicted in figure 2.6 that utilizes thoriumas the primary fertile material. This is mixed with highly enriched uranium (93% ^{235}U) to provide the necessary neutron activity. In the reactor the thorium produces ^{233}U which can then be recycled in mixed fuel.

As a third example, the fuel cycle for a typical liquid metal fast breeder reactor, LMFBR, (see section 5.7) is shown in figure 2.7. This may be fueled with a mix of natural, depleted (recycled) or enriched uranium as well as recycled plutonium. As described in sections 5.6 and 5.7 the driver core of an LMFBR is surrounded by a blanket in which natural uranium produces plutonium that can later be recycled in new fuel. This recycling of plutonium (as well as uranium)

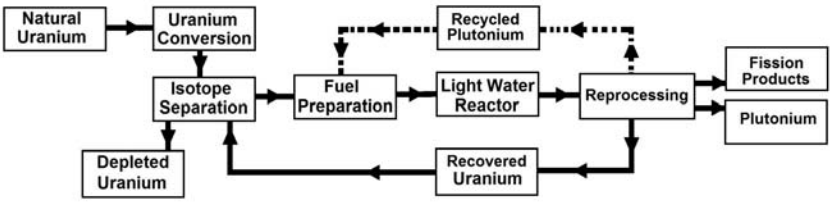

Figure 2.5: The conventional light water reactor (LWR) fuel cycle (solid line) with plutonium recycling (dashed line) and without (no dashed line).

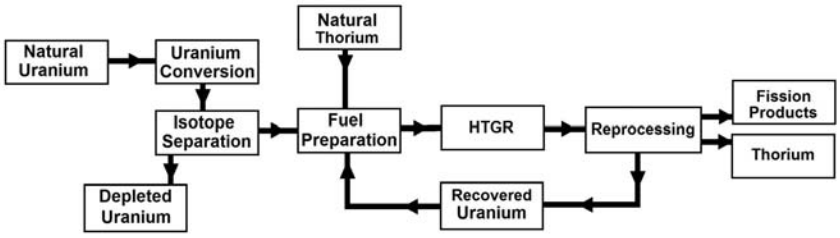

Figure 2.6: The Thorium fuel cycle for the high temperature gas reactor (HGTR).

makes much more thorough and efficient use of the basic uranium fuel and therefore not only extends the potential use of our natural uranium resource but also reduces the cost of the power produced.

Finally we should note that there is significant potential for interactions between the various fuel cycles. These interactions also allow for increased efficiency in the utilization of limited natural resources but also improved cost effectiveness. Moreover, the potential for the development of improved fuel cycles in the future means that temporary or retrievable storage of nuclear waste may be the optimum strategy.

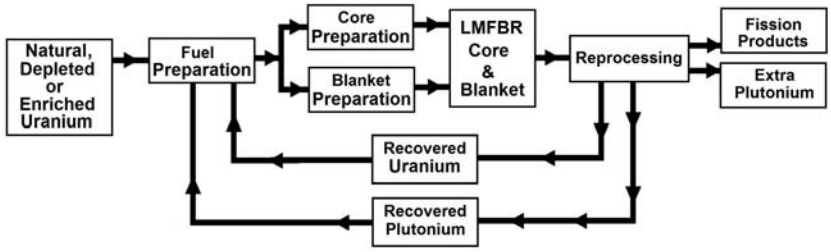

Figure 2.7: The liquid metal fast breeder reactor (LMFBR) fuel cycle.

References

Bohr, N. and Wheeler, J.A. (1939). The mechanism of nuclear fission. *Phys. Rev.*, **56**, 426-450.

Hahn, O. and Strassmann, F. (1939). On the detection and characteristics of the alkaline earth metals formed by irradiation of uranium with neutrons. *Die Naturwissenschaften*, **27**, 11.

Meitner, L. and Frisch, O.R. (1939). Disintegration of uranium by neutrons: a new type of nuclear reaction. *Nature*, **143**, 3615.

Frisch, O.R. (1939). Physical evidence for the division of heavy nuclei under neutron bombardment. *Nature*, **143**, 3616.

Hahn, O. (1958). The discovery of fission. *Scientific American*, **198**, No.2, 76.

Knief, R.A. (1992). *Nuclear engineering: Theory and practice of commercial nuclear power.* Hemisphere Pub. Corp.

Nero, A.V. (1979). *A guidebook to nuclear reactors.* Univ. Calif. Press.

USAEC. (1973). *The nuclear industry.* US Atomic Energy Commission Rep. WASH-1174-73.

World Nuclear Association Information Library. (2011). http://www.world-nuclear.org/Information-Library/

Chapter 3

RADIOACTIVITY

3.1 Introduction

In this chapter we will consider additional nuclear issues that effect power generation and its auxiliary activities. Most of these are related to the by-products of nuclear fission, namely the fission products and fission radiation. Apart from the release of neutrons which was the focus of the preceding chapter, nuclear fission also results in fission products and these elements and isotopes have a number of important consequences. It also results in the emission of various types of radiation whose consequences need to be discussed. We begin with a brief description of radioactive decay.

3.2 Radioactive decay

3.2.1 Half-Life

A fundamental process that effects the behavior of a nuclear reactor and the treatment of its waste is the radioactive decay of the atomic constituents of the fuel, the fuel by-products and the containment structures. All the heavier, naturally occurring elements of the earth and other planets were formed by fusion in the enormous thermonuclear furnace that eventually resulted in the formation of our planet and, indeed, are part of any cataclysmic astronomical event like a supernova. Only such an event could have produced the incredible temperatures (of order 10^9 $^\circ C$ that are required for such fusion. Many of the heavier elements and isotopes formed in that event are unstable in the sense that they decay over time, fissioning into lighter elements and, at the same time, releasing radiation and/or neutrons. This release leads directly to the generation of heat through collisions (or interactions with the surrounding material) in which the kinetic energy associated with the radiation/neutrons is converted to thermal motions of the molecules of the surrounding material.

However the rates at which these heavier elements decay differ greatly from

element to element and from isotope to isotope. The rate of decay is quoted in terms of a half-life, τ, namely the length of time required for one half of the material to be transformed and one half to remain in its original state. Note that $\tau = 0.693/\xi$ where ξ is known as the radioactive decay constant. It describes the rate of decay of the number of original nuclei of a particular isotope, $N(t)$, according to

$$-\frac{dN(t)}{dt} = \xi N(t) \tag{3.1}$$

Isotopes with extremely long half lives, like ^{238}U (whose half life is 4.47×10^9 years), are therefore almost stable and, in a given period of time, exhibit very few (if any) fission events and consequently generate very little thermal energy. Rare elements with short half lives like ^{107}Pd may have existed at one time but have now disappeared from the earth. In between are isotopes like ^{235}U (half life like 7.04×10^8 years) which are now much rarer than their longer lived cousins, in this case ^{238}U.

3.2.2 Decay of a nuclear reactor

In the unnatural environment of a nuclear reactor, the high neutron flux causes the formation of a number of unstable isotopes. These decay to other unstable isotopes and the chain thus followed can be long and complex before finally coming to an end with the formation of stable elements and isotopes. A full catalog of these decay chains is beyond the scope of this book but several important examples should be given.

First we note the decay of ^{235}U (half life 4.47×10^9 years) which results in ^{231}Th which, after 25.5 hours, emits radiation and becomes ^{231}Pa. This decays with a half life of 3.28×10^4 years to ^{227}Ac and the chain continues with many intermediate stages eventually resulting in the stable lead isotope, ^{207}Pb.

One of the most important isotopes produced in a nuclear reactor is the unstable element plutonium, ^{239}Pu, formed when a ^{238}U atom absorbs a neutron. Plutonium does not occur in nature because it has a relatively short half life (2.44×10^4 years). Because of this short half life it is highly radioactive, decaying back to ^{235}U which then decays as described above.

This process of decay has a number of important consequences. First, the thermal energy generated by the decay adds to the heat generated within the nuclear reactor. Thus, although the primary source of heat is the energy transmitted to the molecules of the core as a result of nuclear fission and neutron flux, the additional heat generated by decay is an important secondary contribution. This heat source is referred to as *decay heat* .

But there is an important additional consequence for although the primary fission contribution vanishes when the reactor is shut down (when the control rods are inserted) and the neutron flux subsides, the radioactive decay continues to generate heat for some substantial time following reactor shutdown. The decrease in heat generation occurs quite rapidly after shutdown; thus the reactor heat production decreases to 6.5% after one second, 3.3% after one minute, 1.4% after one hour, 0.55% after one day, and 0.023% after one year. Though these

numbers may seem small they represent a substantial degree of heating and coolant must be circulated through the core to prevent excessive heating that might even result in core meltdown. The production of decay heat also means that fuel rods removed from the core must be placed in a cooled environment (usually a water tank) for some time in order to avoid overheating.

3.3 Radiation

Nuclear fission and radioactive decay also result in the emission of various forms of radiation aside from the emission of neutrons which may be referred to as *neutron radiation* . Those additional forms of radiation are:

- Alpha radiation is the emission of two protons and two neutrons, an *alpha particle* being identical in composition to a nucleus of helium. It is emitted, for example, in the decay of ^{235}U to ^{231}Th.

- Beta radiation is small charged particles, namely electrons and other similarly small particles. It is emitted, for example, in the decay of ^{239}Np to ^{239}Pu.

- Gamma radiation is short wavelength electromagnetic radiation and is emitted in the form of photons. It is emitted, for example, during fission or radiative capture in ^{235}U.

Since all of the above radiation emissions are associated with the decay of an isotope, a measure of radioactivity is the number of disintegrations per second, given by $\lambda N(t)$ in the notation of equation 3.1. One disintegration per second is known as *one becquerel* ($1Bq$) and is related to the more traditional unit of a *curie* (Ci) by $1Ci = 3.7 \times 10^{10}Bq$.

Some comments on typical magnitudes of radioactivity are appropriate here. Room air has a typical radioactivity of $10^{-12}Ci/l$ or about $10^{-8}Ci/kg$. Typical radiation treatments for cancer range up to about $10^{4}Ci$ and the activity in the core of a typical thermal reactor just after it has been shut down is about $1.5 \times 10^{9}Ci$.

Though they are beyond the scope of this text, the effects of radiation on materials (see, for example, Foster and Wright 1977, Cameron 1982) or on biological tissue (see, for example, Lewis 1977, Murray 1993) are clearly important and therefore it is useful to have some measures of the changes in a material or tissue brought about by exposure to radiation. These measures will clearly be a function not only of the strength and type of radiation but also of the nature of the material (or tissue) exposed to that radiation. A number of such measures are used:

- One *roentgen* (R), a traditional unit for x-rays and gamma radiation, is defined in terms of the ionization produced in air and is equivalent to the deposition in air of $87ergs/g$.

- To address the fact that the absorption of radiation in biological tissue differs from the ionization in air, the *rad* (rad) was introduced as a measure of the radiation energy absorbed per unit mass ($1rad = 100ergs/g$). One *gray* (Gr) is $100rads$.

- To address the fact that the damage done depends on the type of radiation, the *roentgen-equivalent-man* (or *rem* for short) was introduced and defined to be the dose (energy) of $250keV$ x-rays that would produce the same damage or effect as the dose (energy) of the radiation being measured. Thus $1rem$ is the equivalent dose of $250keV$ x-rays that would produce the same effect as $1rad$ of the radiation being measured. Similarly one *sievert* (Sv) is equivalent to $1Gr$.

- The ratio of the number of *rems* to the number of *rads* is called the *quality factor* . Clearly then x-rays (and gamma radiation) have a quality factor of unity. In comparison, the quality factor for alpha radiation and fission fragments is 20 while that for neutrons varies from 5 to 20 depending on the neutron energy.

The biological effects of radiation are beyond the scope of this text (see, for example, Lewis 1977 or Murray 1993). It is sufficient for present purposes to observe that the potential damage that might be caused by the nuclear fuel before, during and after use in a nuclear reactor requires that the fuel (and other components of a reactor that may have been irradiated within the core and its immediate surroundings) be confined within a secure containment system for as long as the destructive levels of that radiation continue. Such assurance is only achieved by a system that is necessarily comprised of multiple systems and multiple levels of containment.

3.4 Containment systems

3.4.1 Radioactive release

The main safety concern with nuclear reactors has always been the possibility of an uncontrolled release of radioactive material leading to contamination and radiation exposure outside the plant. To prevent this modern nuclear reactors incorporate three levels of containment. First the fuel and radioactive fission products contained in the fuel pellets are packed and sealed in zirconium alloy fuel rods (see section 5.2.4). These, in turn, are contained inside the large, steel primary containment vessel with walls that are about $30cm$ thick. The associated primary cooling piping is similarly strong. All this is then enclosed in a massive reinforced concrete structure with walls that are at least $1m$ thick. Moreover, these three barriers are monitored continuously. The fuel rod walls are monitored by checking for any radioactivity in the primary cooling water and that cooling system is monitored for any water leakage. Finally the concrete structure is monitored for any air leakage.

One of these systems is the containment surrounding the operational reactor core, a strategy that is known as reactor shielding. We begin our discussion of containment with a review of that topic.

3.4.2 Reactor shielding

Clearly the nuclear reactor surroundings must be shielded from the intense radiation emerging from the reactor core. Man and his natural surroundings must obviously be protected from damage, but, in addition, the material of the plant must be shielded in order to minimize both heat damage and undesirable changes in the properties of the material such as embrittlement (see, for example, Foster and Wright 1977). Moreover, shielding is not only necessary for the core and the equipment enclosed in the primary reactor vessel but also for other components of the primary coolant loop such as the pumps and heat exchangers.

In a water-cooled reactor the first level of protection is the primary cooling water surrounding the core; this water slows down the fast neutrons and provides attenuation of the gamma radiation. To supplement this many reactor cores (including PWR cores) are surrounded by a *thermal shield*, a $3 - 7cm$ thick steel (usually stainless steel) barrel that reduces the neutron and gamma-radiation impacting the inside surface of the primary pressure vessel. Incoming cooling water usually flows up the outside of the thermal shield and then down the inside before turning to flow up through the core. The steel walls of the primary pressure vessel, more than $20cm$ thick, provide yet another layer of protection against the neutron and gamma-ray radiation so that inside the concrete secondary containment structure the levels are very low. That thick, reinforced concrete building ensures that the levels of radiation outside are normally very low indeed. To quantify the attenuation provided by each of these barriers, one needs to know the attenuation distances for each of the materials used and each of the proton energies. Typical data of this kind is shown in figure 3.1.

We should also note that the primary coolant water flowing through the core of a reactor carries some radioactivity out of the primary containment vessel mainly because of the radioactive nuclides, ^{16}N and ^{19}O, formed when water is irradiated. These isotopes, ^{16}N and ^{19}O, have a half-lives of only $7sec$ and $29sec$ respectively though they produces gamma radiation during decay (Gregg King 1964). Thus, for example, access to secondary containment structures is restricted during reactor operation.

References

Cameron, I.R. (1982). *Nuclear fission reactors.* Plenum Press, New York & London.

Foster, A.R. and Wright Jr., R.L. (1977). *Basic nuclear engineering.* Allyn & Bacon, Inc.

Gregg King, C.D. (1964). *Nuclear power systems.* The Macmillan Company, New York.

Harrison, J.R. (1958). *Nuclear reactor shielding.* Temple Press Ltd., London.

Lewis, E.E. (1977). *Nuclear power reactor safety.* John Wiley & Sons.

Murray, R.L. (1993). *Nuclear energy.* Pergamon Press.

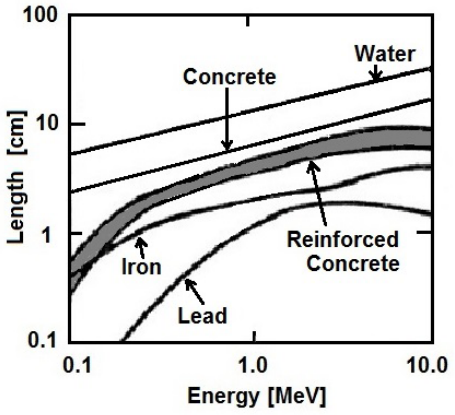

Figure 3.1: Typical distances required for a tenfold decrease in gamma radiation in various shielding materials as a function of the energy. Adapted from Harrison (1958).

Chapter 4

CORE NEUTRONICS

4.1 Introduction

In order to analyze the power generated in the reactor core and thus the temperature distribution one must first calculate the neutron population distribution and neutron flux and examine how they vary with the control devices. In this chapter we discuss how this can be done.

4.2 Neutron density and neutron flux

We begin defining several characteristic features of neutron transport, by introducing the concept of neutron density, N, a measure of the number of free neutrons per unit volume . Of course, this may be a function of time, t, and of position, x_i, within the core. Furthermore, these neutrons may have a range of different energies, E, and the number traveling in a particular angular direction, Ω_j (a unit vector), may have a different density than those traveling in another direction. Consequently, if we wish to fully describe the neutron density then N must be considered to be a function of x_i, t, E and Ω_j and the number of neutrons in a differential volume dV that have energies between E and $E+dE$ and are traveling within the small solid angle, $d\Omega$, around the direction Ω_j would be

$$N(x_i, t, E, \Omega_j)\ dV\ dE\ d\Omega \tag{4.1}$$

and therefore N has units of number per unit volume per unit eV per unit solid angle. Even for a simple core geometry N, when discretized, is a huge matrix, especially since the energy spectrum may require very fine discretization in order to accurately portray the variation with E (see, for example, figure 2.3).

Denoting the magnitude of the neutron velocity by $\bar{u}(x_i, t, E)$ (which will be a function of position, time and energy but is assumed independent of direction, Ω_j) it is conventional to define the *angular neutron flux* , φ, by

$$\varphi(x_i, t, E, \Omega_j) = N(x_i, t, E, \Omega_j)\ \bar{u}(x_i, t, E) \tag{4.2}$$

The conventional semantics here are somewhat misleading since φ is not a flux in the sense that term is commonly used in physics (indeed φ as defined above is a scalar whereas a conventional flux is a vector); it is perhaps best to regard φ as a convenient mathematical variable whose usefulness will become apparent as we proceed.

A more physically recognizable characteristic is the conventional vector quantity known as the *angular current density* , J_j^*, given by

$$J_j^*(x_i, t, E, \Omega_j) = \bar{u}\ \Omega_j\ N(x_i, t, E, \Omega_j) = \Omega_j\ \varphi(x_i, t, E, \Omega_j) \tag{4.3}$$

since $\bar{u}\Omega_j$ is the vector velocity of a neutron traveling in the direction Ω_j. This angular current density, J_j^*, might be more properly called the neutron flux but we will avoid the confusion that would be introduced by altering the standard semantics. Here the physical interpretation is that $J_j^* dE d\Omega$ is the number of neutrons (with energies between E and $E + dE$) traveling within the solid angle $d\Omega$ about the direction Ω_j per unit area normal to that direction per unit time. Note that since Ω_j is a unit vector, the magnitude of J_j^* is φ.

The above definitions allow for the fundamental quantities φ and J_j^* to vary with the angular orientation Ω_j. However we will often assume that these variations with orientation are small or negligible. Then we will wish to integrate over all orientations and define an angle-integrated neutron flux, $\phi(x_i, t, E)$ (later abbreviated to *neutron flux*), and an angle-integrated current density, $J_j(x_i, t, E)$, by:

$$\phi(x_i, t, E) = \int_{4\pi} \varphi(x_i, t, E, \Omega_j) d\Omega \tag{4.4}$$

$$J_j(x_i, t, E) = \int_{4\pi} J_k^*(x_i, t, E, \Omega_j) d\Omega \tag{4.5}$$

Note that if $\varphi(x_i, t, E, \Omega_j)$ and/or $J_j^*(x_i, t, E, \Omega_j)$ are isotropic and therefore independent of Ω_j then

$$\phi = 4\pi\varphi \qquad ; \qquad J_j = 4\pi J_j^* \tag{4.6}$$

In the simpler neutronics calculations later in this book, the *neutron flux* , ϕ, is normally the dependent variable used in the calculations.

4.3 Discretizing the energy or speed range

In order to calculate the neutron distribution in every detail one would need to consider the population of neutrons with a particular energy and direction of motion at every location and at every moment in time and be able to analyze their collisions, production, and capture. This is an enormous computational challenge particularly since the cross-sections for those interactions are all complicated functions of the neutron energy. The problem is further complicated by the fact that the mean free paths are comparable with the dimensions of the detailed interior structure of the reactor core (for example the fuel rod diameter or coolant channel width). The general approach to this problem is known

as *neutron transport theory*. The details of the general theory, for which the reader is referred to other classic texts such as Glasstone and Sesonske (1981) or Duderstadt and Hamilton (1976), are beyond the scope of this monograph. In part, this is because most practical calculations are performed only after radical simplifications that are necessary to arrive at a practical computation of the neutron dynamics in a practical reactor.

Before further deliberation of neutron transport theory we will anticipate some of the approximations that will be made later in the analysis. As implied in the preceding section the neutron energies represented in a reactor cover a wide range of speeds and, since each speed may have different cross-sections to various reactions, it becomes extremely complicated to incorporate all of these intricate details. Fortunately, it is sufficient for many purposes to discretize the energy range in very crude ways. The crudest approach is to assume that all the neutrons have the same energy, a thermal energy in thermal reactors since most of the heat produced is generated by fission which is proportional to the thermal neutron flux. We will pursue this approach further in section 4.6.3.

One of the first hurdles experienced in implementing a method with a very crude discretization of the energy spectrum is the need to find average cross-sections that are applicable to the assumed, uniform energy within each sub-range. This can be effected by using the *reduced thermal models* described in section 2.3.3. Thus a one-speed thermal neutron model could have a single neutron energy of $E = 0.0253eV$ and an absorption cross-section of $\hat{\sigma}$. If the corresponding thermal neutron flux (called the *flux reduced to* $0.0253eV$) is also denoted by a hat, or $\hat{\phi}$, then the rate of absorption would be given by $\mathcal{N}\hat{\phi}\hat{\sigma}$. Henceforth, we shall adopt this averaging and, for the sake of simplicity, we shall omit the $\hat{}$ and use just σ and ϕ to denote the averaged cross-section and the averaged neutron flux.

4.4 Averaging over material components

The above averaging referred, of course, to the process of averaging within one (or sometimes two) range(s) of neutron energy within a given material. However, we must now recognize that a reactor core consists of many different physical components each of which may have different absorption and scattering properties. Thus in addition to the energy averaging described above, the simplest models homogenize this core by also averaging over these components as follows. The total reaction or absorption rate (per unit total core volume) in the homogenized core is clearly the sum of the reaction rates in each of the M materials present (denoted by the superscript $m = 1$ to $m = M$). The reaction rate in the material m per unit total core volume will be given by $\mathcal{N}^m\alpha^m\sigma^m\phi^m = \alpha^m\Sigma^m\phi^m$ where $\mathcal{N}^m$ is the number atoms of material m per unit volume of m, α^m is the volume of m per unit total core volume, σ^m is the reaction cross-section for the material m, Σ^m is the corresponding macroscopic cross-section (see section 2.3.3) and ϕ^m is the neutron flux in the material m. It follows that the average neutron flux, ϕ, and the average macroscopic absorption cross-section, Σ, will

be related by

$$\Sigma\phi = \sum_{m=1}^{M} \mathcal{N}^m \alpha^m \sigma^m \phi^m \tag{4.7}$$

Note that in the special case in which the typical physical dimensions of the components are much smaller than the neutron mean free path then the neutron flux should be considered identical in all the materials ($\phi^m = \phi$) so that

$$\Sigma = \sum_{m=1}^{M} \mathcal{N}^m \alpha^m \sigma^m = \sum_{m=1}^{M} \alpha^m \Sigma^m \tag{4.8}$$

This allows evaluation of the effective cross-sections for a core with physically different components. Of course, each interaction or event will have its own effective cross-section so that there will be cross-sections for fission, Σ_f, for absorption, Σ_a, for scattering, Σ_s, etc.

4.5 Neutron transport theory

The first simplification of *neutron transport theory* is to assume that the range of neutron energies can be discretized into a small number of energies ranges (sometimes, as we have described in the preceding section, we may make the even more radical assumption that all neutrons have the same energy). Then the heart of neutron transport theory is a neutron continuity equation known as the *neutron transport equation* that simply represents the neutron gains and losses for an arbitrary control volume, V, within the reactor for each of the ranges of neutron energies being considered. In evaluating this neutron balance for each of the energy ranges it is necessary to account for:

[A] The rate of increase of those neutrons within the volume V.

[B] The rate of appearance of those neutrons in V as a result of flux through the surface of the volume V.

[C] The loss of those neutrons as a result of absorption (and as a result of scattering to an energy level outside of the entire range of discretized energies).

[D] The rate of appearance of those neutrons that, as a result of a scattering interaction, now have energies of the magnitude being evaluated.

[E] The rate of production of those neutrons in V, most importantly by fission.

We will retain these alphabetical labels when we evaluate these terms in the analysis that follows.

The second simplification, mentioned earlier, recognizes that the angular variations in the neutron flux are rarely of first order importance. Hence non-isotropic details can be laid aside and the neutron flux can be integrated over

the angular orientation, Ω_j, as described in equations 4.4 and 4.5. When this integration is performed on the neutron transport equation in order to extract an equation for the integrated neutron flux, $\phi(x_i, t, E)$, the result takes the following form (Glasstone and Sesonske 1981, Duderstadt and Hamilton 1976):

$$\frac{1}{\bar{u}}\frac{\partial \phi}{\partial t} + \frac{\partial J_j}{\partial x_j} + \Sigma_a \phi = \int_0^\infty \Sigma_s(E' \rightarrow E)\phi(x_i, t, E')dE' + S(x_i, t, E) \qquad (4.9)$$

which is known as the *neutron continuity equation* . The five terms each represent a contribution to the population (per unit volume) of neutrons of energy E at the location x_i and the time t; specifically:

[A] The first term is the rate of increase of neutrons in that unit volume.

[B] The second term is the flux of neutrons out of that unit volume.

[C] The third term is the rate of loss of neutrons due to absorption.

[D] The fourth term is the rate of increase of neutrons of energy E due to scattering where the energy before the scattering interaction was E'. Thus we must integrate over all possible previous energies, E'.

[E] The fifth term is the rate of production of neutrons of energy E within the unit volume due to fission, $S(x_i, t, E)$.

Consequently the following nomenclature pertains in equation 4.9: $\phi(x_i, t, E)$ and $J_j(x_i, t, E)$ are the angle-integrated flux and current density as defined by equations 4.4 and 4.5, $\bar{u}$ represents the magnitude of the neutron velocity (assumed isotropic), $\Sigma_a(x_i, E)$ is the macroscopic cross-section at location x_i for collisions in which neutrons of energy, E, are absorbed, $\Sigma_s(E' \rightarrow E)$ is the macroscopic cross-section for scattering of neutrons of energy E' to energy E, and $S(x_i, t, E)$ is the rate of production in a unit volume at x_i and t of neutrons of energy E.

Assuming that the macroscopic cross-sections and the source term are given, equation 4.9 is the equation that determines the population of neutrons for each energy level E as a function of position x_i and time t. Ideally we would wish to solve this equation for the neutron flux, $\phi(x_i, t, E)$. However, there remains a problem in that the equation involves two unknown functions, $\phi(x_i, t, E)$ and $J_j(x_i, t, E)$, a problem that was further complicated by the integration over the angle. Specifically, whereas $\varphi(x_i, t, E, \Omega_j)$ and $J_j^*(x_i, t, E, \Omega_j)$ are simply related by equation 4.3, the functions, $\phi(x_i, t, E)$ and $J_j(x_i, t, E)$, defined respectively by equations 4.4 and 4.5, are not so easily related.

To proceed with a solution, another relation between $\phi(x_i, t, E)$ and $J_j(x_i, t, E)$ must be found. One simple way forward is to heuristically argue that in many transport processes (for example the conduction of heat), the concentration (in this case ϕ) and the flux (in this case J_j) are simply connected by a relation known as Fick's law in which the flux is proportional to the gradient of the concentration, the factor of proportionality being a diffusion coefficient. We shall

make this assumption or approximation here by heuristically declaring that

$$J_j(x_i, t, E) = -D(x_i)\frac{\partial \phi(x_i, t, E)}{\partial x_j} \tag{4.10}$$

where D is a diffusion coefficient that may be a function of position. This diffusive process could be viewed as the effective consequence of neutrons undergoing multiple scattering interactions.

This is the model we will focus on here. However, it is valuable to point out that this Fick's law for neutrons can also be derived from the basic conservation laws in the following way. Returning to the neutron continuity principle, one can propose an expansion for the neutron flux, φ, that includes the angle-integrated average used above plus a perturbation term that is linear in the angle Ω_j. Assuming that this second term is small (that the flux is only weakly dependent on the angle), one can then establish the equation for this linear perturbation term that emerges from the neutron continuity principle. Making some further assumptions (neglect of the time dependent term, assumption of isotropic source term), the result that emerges from this perturbation analysis is:

$$\frac{1}{3}\frac{\partial \phi}{\partial x_j} + \Sigma_{tr} J_j = 0 \tag{4.11}$$

where Σ_{tr} is called the *macroscopic transport cross-section* and is given by $\Sigma_{tr} = \Sigma_a + \Sigma_s - \mu\Sigma_s$ where μ is the cosine of the average scattering angle. (For further detail and a rigorous derivation of these relations the reader should consult texts such as Glasstone and Sesonske 1981 or Duderstadt and Hamilton 1976). Comparing equation 4.11 with equation 4.10 we see that J_j and ϕ do, indeed, connect via Fick's law and that the *neutron diffusion coefficient* , $D(x_i)$, is given by

$$D(x_i) = \frac{1}{3\Sigma_{tr}} \tag{4.12}$$

Equation 4.11 can then be used to substitute for J_j in equation 4.9 and thus generate an equation for the single unknown function, $\phi(x_i, t, E)$.

Computational methods based on the assumption of equation 4.10 are known as diffusion theories and these will be the focus of the sections which follow.

4.6 Diffusion theory

4.6.1 Introduction

It is appropriate to recall at this point that diffusion theory for the neutronics of a reactor core avoids much complexity posed by the interior structure of the reactor core by assuming:

1. that the reactor core can be considered to be homogeneous. As described in section 4.3 this requires the assumption that the neutron mean free paths are long compared with the typical interior dimensions of the reactor

core. This then allows us to characterize the dynamics by a single neutron flux, ϕ, though one which varies with time and from place to place. Fuel rods are typically only a few cm in diameter and with neutron diffusion lengths, L (see equation 4.19), of about $60cm$ this criterion is crudely satisfied in most thermal reactors.

2. that the characteristic neutron flux does not vary substantially over one mean free path. This is known as a *weakly absorbing* medium.

3. that the reactor core is large compared with the neutron mean free paths so that a neutron will generally experience many interactions within the core before encountering one of the core boundaries. Most thermal reactor cores are only a few neutron diffusion lengths, L, in typical dimension so this criterion is only very crudely satisfied.

These last two assumptions effectively mean that neutrons diffuse within the core and the overall population variations can be characterized by a diffusion equation.

In addition to the governing equation, it is necessary to establish both initial conditions and boundary conditions on the neutron flux, ϕ. Initial conditions will be simply given by some known neutron flux, $\phi(x_i, 0)$ at the initial time, $t = 0$. The evaluation of boundary conditions requires that we develop relations for the one-way flux of neutrons through a surface or discontinuity. To establish such relations we will denote the one-way flux of neutrons through any surface or boundary (we define the coordinate x_n normal to this boundary in the positive direction) by J_n^+ in the positive direction and by J_n^- in the negative direction. Clearly the net flux of neutrons will be equal to J_n so that

$$J_n^+ - J_n^- = J_n = -D\frac{\partial \phi}{\partial x_n} \tag{4.13}$$

using equations 4.11 and 4.12. On the other hand the sum of these same two fluxes must be related to the neutron flux; specifically

$$J_n^+ + J_n^- = J_n = \frac{1}{2}\phi \tag{4.14}$$

(see, for example, Glasstone and Sesonske 1981). The factor of one half is geometric: since the flux ϕ is in all directions, the resultant in the direction x_n requires the average value of the cosine of the angle relative to x_n.

It follows from equations 4.13 and 4.14 that

$$J_n^+ = \frac{1}{4}\phi - \frac{D}{2}\frac{\partial \phi}{\partial x_n} \qquad ; \qquad J_n^- = \frac{1}{4}\phi + \frac{D}{2}\frac{\partial \phi}{\partial x_n} \tag{4.15}$$

These relations allow the establishment of boundary conditions when the condition involves some constraint on the neutron flux. Two examples will suffice.

At an interface between two different media denoted by subscripts 1 and 2 (and with diffusion coefficients D_1 and D_2), the neutron flux into medium 1 must

be equal to the neutron flux out of medium 2 and, conversely, the neutron flux out of medium 1 must be equal to the neutron flux into medium 2. Therefore from equations 4.15 it follows that, at the interface, we must have:

$$\phi_1 = \phi_2 \qquad \text{and} \qquad D_1 \frac{\partial \phi_1}{\partial x_n} = D_2 \frac{\partial \phi_2}{\partial x_n} \tag{4.16}$$

A second, practical example is the boundary between one medium (subscript 1) and a vacuum from which there will be no neutron flux back into the first medium. This is an approximation to the condition at the boundary of a reactor. Then on that boundary it is clear that $J_n^- = 0$ where x_n is in the direction of the vacuum. Then it follows that at the boundary

$$\phi_1 = -2D \frac{\partial \phi_1}{\partial x_n} \tag{4.17}$$

One way to implement this numerically is to use a linear extrapolation and set ϕ_1 to be zero at a displaced, virtual boundary that is a distance $1/2D$ into the vacuum from the actual boundary. This displacement, $1/2D$, is known as the *linear extrapolation length* .

4.6.2 One-speed and two-speed approximations

As described earlier, the crudest approach to the energy discretization is to assume that all the neutrons have the same energy, a thermal energy in thermal reactors since the heat produced is mostly dependent on the thermal neutron flux. This basic approach is termed the *one-speed approximation* and the diffusion theory based on this approximation is *one-speed diffusion theory*. The next level of approximation is to assume two classes of neutrons each with a single neutron energy. This *two-speed model* applied to thermal reactors assumes one class of thermal neutrons and a second class of fast neutrons combined with a model for the slowing down of the fast neutrons to the thermal neutrons.

We will focus first on the simplest approach, namely the one-speed approximation. With this approximation, scattering between energy levels is no longer an issue and the fourth (or [D]) term in the neutron continuity equation 4.9 drops out. The result is the following governing equation for the neutron flux, $\phi(x_i, t)$ (where the independent variable, E, is now dropped since all neutrons are assumed to have the same speed):

$$\frac{1}{\bar{u}} \frac{\partial \phi}{\partial t} - \frac{\partial}{\partial x_j} \left(D(x_i) \frac{\partial \phi}{\partial x_j} \right) + \Sigma_a \phi = S(x_i, t) \tag{4.18}$$

This is called the *one-speed neutron diffusion equation* and its solution is known as *one-speed diffusion theory* .

Before moving to examine this theory in some detail, we note that the ratio, D/Σ_a, is a key parameter that appears in the diffusion equation 4.18. The square root of this ratio has the dimension of length and allows the definition

of a quantity, L, known as the *neutron diffusion length*:

$$L = \left[\frac{D}{\Sigma_a}\right]^{\frac{1}{2}} \tag{4.19}$$

A neutron moving within an absorbing and scattering medium will exhibit classical random walk and, by Rayleigh's scattering theory, a single neutron will therefore typically travel a distance of $6^{\frac{1}{2}}L$ before it is absorbed. Typical values for L at normal temperatures are of the order of $60cm$. Note that this is not small compared with the dimensions of a reactor core and therefore diffusion theory can only provide a crude (but nevertheless useful) approximation for reactor neutronics.

4.6.3 Steady state one-speed diffusion theory

The most elementary application of diffusion theory is to the steady state operation of a reactor in which the neutron flux is neither increasing or decreasing in time. Then, with the time-derivative term set equal to zero, the one-speed diffusion equation 4.18 becomes:

$$-D \bigtriangledown^2 \ \phi = S - \Sigma_a \phi \tag{4.20}$$

assuming that the diffusion coefficient, D, is uniform throughout the reactor. Here the left-hand side is the flux of neutrons out of the control volume per unit volume. Thus, in steady state, this must be equal to the right-hand side, the excess of the rate of neutron production over the rate of neutron absorption per unit volume. This excess is a basic property of the fuel and other material properties of the reactor, in other words a *material property* as defined in section 2.7. Furthermore, by definition this excess must be proportional to $(k_\infty - 1)$ (not $(k-1)$ since the loss to the surroundings is represented by the left hand side of equation 4.20). Consequently it follows that the appropriate relation for the source term is

$$S = k_\infty \Sigma_a \phi \tag{4.21}$$

so that, using the relation 4.19, the one-speed diffusion equation, equation 4.20, can be written as

$$\bigtriangledown^2 \ \phi + \frac{(k_\infty - 1)}{L^2}\phi = 0 \tag{4.22}$$

The material parameter $(k_\infty - 1)/L^2$ is represented by B_m^2 and, as indicated in section 2.7, is called the *material buckling* :

$$B_m^2 = \frac{(k_\infty - 1)\Sigma_a}{D} = \frac{(k_\infty - 1)}{L^2} \tag{4.23}$$

where, we note that $(B_m)^{-1}$ has the dimensions of length. Thus the diffusion equation 4.22 that must apply to the steady state operation of the reactor is written as

$$\bigtriangledown^2 \ \phi + B_m^2 \phi = 0 \tag{4.24}$$

Equation 4.24 (or 4.22) is Helmholtz' equation. It has convenient solutions by separation of variables in all the simple coordinate systems. Later we examine detailed eigensolutions to equation 4.24 for various reactor geometries. These solutions demonstrate that, in any particular reactor geometry, solutions only exist for specific values (eigenvalues) for the parameter B_m^2. These specific values are called the *geometric buckling* and are represented by B_g^2; as described in section 2.7 the values of B_g^2 are only functions of the geometry of the reactor and not of its neutronic parameters. It follows that steady state critical solutions only exist when

$$B_m^2 = B_g^2 \tag{4.25}$$

and this defines the conditions for steady state criticality in the reactor. Moreover it follows that supercritical and subcritical conditions will be defined by the inequalities

$$\text{Subcritical condition:} \quad B_m^2 < B_g^2 \tag{4.26}$$

$$\text{Supercritical condition:} \quad B_m^2 > B_g^2 \tag{4.27}$$

since, in the former case, the production of neutrons is inadequate to maintain criticality and, in the latter, it is in excess of that required.

As a footnote, the multiplication factor, k, in the finite reactor can be related to the geometric buckling as follows. From equation 2.1, k may be evaluated as

$$k = \frac{\text{Rate of neutron production}}{\text{Sum of rates of neutron absorption and escape}} \tag{4.28}$$

and, in the diffusion equation solution, the rate of escape to the surroundings is represented by $-D \bigtriangledown^2 \ \phi$ and therefore by $DB_g^2\phi$. The corresponding rate of production is given by $Dk_\infty\phi/L^2$ and the rate of neutron absorption by $D\phi/L^2$. Substituting these expressions into the equation 4.28 we find that in steady state operation

$$k = \frac{Dk_\infty\phi/L^2}{(D\phi/L^2) + DB_g^2\phi} = \frac{k_\infty}{(1 + B_g^2L^2)} \tag{4.29}$$

4.6.4 Two-speed diffusion theory

The next level of approximation is to assume that there are two speeds of neutrons, namely one group of fast neutrons that are all traveling at the same speed and a second group of thermal neutrons also all traveling with the same speed. We denote these two neutron fluxes by ϕ_F and ϕ_T respectively. We also need to model the slowing down from the fast to the thermal neutron group by defining a macroscopic cross-section for slowing denoted by Σ_{FT}. Focusing first on the diffusion equation for the thermal neutron flux, ϕ_T, the source term in equation 4.20 represents the rate of supply of thermal neutrons due to the slowing down of fast neutrons and will therefore be given by $P_F\Sigma_{FT}\phi_F$ and the first of the two coupled differential equations that constitute the two-speed diffusion model becomes

$$\bigtriangledown^2 \ \phi_T - \frac{\phi_T}{L_T^2} = - \ \frac{P_F\Sigma_{FT}}{D_T} \ \phi_F \tag{4.30}$$

where L_T is the neutron diffusion length for the thermal neutrons.

Turning to the fast neutrons, we neglect the absorption of fast neutrons in comparison with the slowing down and therefore Σ_{FT} is analogous to Σ_a for the thermal neutrons. Therefore we can define a neutron diffusion length for the fast neutrons as $L_F^2 = D_F/\Sigma_{FT}$. It remains to establish the source term for the fast neutrons, the rate at which fast neutrons are produced by fission. Beginning with the expression 4.21 for S from the one-speed model, we argue that the appropriate ϕ in this two-speed model is ϕ_T/P_F or the flux of thermal neutrons causing fission in the absence of resonant absorption. Thus the source term in the fast neutron continuity equation will be $k_\infty \Sigma_a \phi_T/P_F$ and the second of the two coupled differential equations, namely that for the fast neutrons, becomes

$$\bigtriangledown^2 \ \phi_F - \frac{\phi_F}{L_F^2} = -\frac{k_\infty \Sigma_a}{D_F P_F}\phi_T \tag{4.31}$$

Since $\Sigma_a = D_T/L_T^2$ and $\Sigma_{FT} = D_F/L_F^2$ the two equations 4.31 and 4.30 may be written as

$$\bigtriangledown^2 \ \phi_F - \frac{\phi_F}{L_F^2} = -\frac{D_T}{D_F}\frac{k_\infty}{P_F L_T^2}\phi_T \tag{4.32}$$

$$\bigtriangledown^2 \ \phi_T - \frac{\phi_T}{L_T^2} = -\frac{D_F}{D_T}\frac{P_F}{L_F^2}\phi_F \tag{4.33}$$

The solution of these coupled differential equations is simpler than might first appear for it transpires that the solutions for ϕ_F and ϕ_T take the same functional form as those of the one-speed equation 4.24 provided the constant B_g is appropriately chosen. With this tip-off we try for a solution of the form

$$\bigtriangledown^2 \ \phi_F = -B_g^2 \phi_F \qquad ; \qquad \bigtriangledown^2 \ \phi_T = -B_g^2 \phi_T \tag{4.34}$$

Substituting into equations 4.32 and 4.33, it transpires that B_g^2 must satisfy

$$(1 + B_g^2 L_T^2)(1 + B_g^2 L_F^2) = k_\infty \tag{4.35}$$

Consequently solutions to the two speed diffusion equations are of the form given in equations 4.34 where B_g^2 must satisfy the quadratic relation 4.35. It follows from equation 4.35 that there are two possible values for B_g^2. In the cases of interest $k_\infty > 1$ and therefore one of the values of B_g^2 is positive and the other is negative. In most circumstances (though not all) the component of the solution arising from the negative root can be neglected or eliminated leaving only the component resulting from the positive root. Moreover in the common circumstance in which k_∞ is just slightly greater than unity, the positive root is given approximately by

$$B_g^2 \approx k_\infty/(L_T^2 + L_F^2) \tag{4.36}$$

Thus both the fission and thermal neutrons are governed by the same diffusion equation as in the one speed diffusion theory and with a geometric buckling that is a minor modification of that used in the earlier theory. It follows that the one-speed solutions that we will detail in sections 4.7.1 to 4.7.4 can be readily developed into two-speed solutions.

4.6.5 Multigroup diffusion theories and calculations

Before proceeding with derivations from the one and two speed diffusion theories, it is appropriate to pause and comment on the many approximations that were made in developing these models and to outline the more accurate efforts that are required for detailed reactor analysis and design. In reviewing the extensive assumptions that were made in the preceding sections it is surprising that the simple diffusion theories work at all; indeed to the extent that they do, that success is largely a result of judicious choice of the averaging used to arrive at the effective cross-sections.

One set of assumptions was that the angular neutron flux was isotropic (or nearly so). This assumption is reasonably valid in most large reactors except perhaps in the neighborhood of non-isotropic material that is, for example, highly absorbing, or a boundary that results in a highly non-isotropic neutron flux. Such regions or boundaries may require special treatment but the issue is not as important as those detailed below so we do not dwell on it here.

A second and more important set of assumptions was the very limited discretization of the energy spectrum. In practice it is necessary to discretize the energy spectrum much more finely than in either the one or two speed models and to use 20 or 30 energy levels. These are called *multigroup diffusion models* and in them each level is governed by a diffusion equation with source terms appropriately chosen to model the slowing down of neutrons from the higher energy levels. Sophisticated numerical schemes have been developed for the solution of all these coupled differential equations (see, for example, Glasstone and Sesonske 1981, Duderstadt and Hamilton 1976) and modern reactor designs rely on these detailed calculations that are beyond the scope of this monograph. We observe that these calculations are only as good as the accuracy of the source terms and cross-sections assumed. Therefore careful analysis and modeling of the scattering process is critical as is accurate representation and averaging of the cross-sections within each energy level.

4.6.6 Lattice cell calculations

A third set of assumptions concern the averaging over the various materials that make up a reactor core. The fuel rods, control rods, moderator, coolant channels, etc. in a reactor are usually arranged in *lattice cells* that are repeated across the cross-section of the core (see section 5.2.4 and figure 5.10). Thus there are several structural or material scales (dimensions), a small common scale being the diameter of the fuel rods. Another, larger scale would be the dimension of the lattice. In the preceding sections it was assumed that the core was effectively homogeneous; this is the case when the material inhomogeneity dimension is small compared with the typical mean free path of the neutrons. In a light water reactor (LWR) the typical mean free path is of the order of a centimeter and therefore comparable with the diameter of a fuel rod. In contrast, a fast breeder reactor has typical mean free paths of the order of tens of centimeters but similar fuel rod dimensions and so the inhomogeneity is less

important in fast reactor calculations.

When, as in a LWR, the inhomogeneity is important there will be significant differences between the neutron flux within the fuel rods and that in the moderator or coolant. Practical reactor analysis and design requires detailed calculation of these differences and this is effected using numerical codes called *heterogeneous lattice cell calculations*. Though these are beyond the scope of the present monograph, they are important to include in considering the application of diffusion theories to real reactors.

4.7 Simple solutions to the diffusion equation

4.7.1 Spherical and cylindrical reactors

Notwithstanding the limitations of the one-speed diffusion theory, we will continue some reactor analysis because it yields qualitatively useful results and concepts. As previously mentioned, the Helmholtz diffusion equation 4.24 permits solution by separation of variables in many simple coordinate systems. Perhaps the most useful are the solutions in cylindrical coordinates since this closely approximates the geometry of most reactor cores.

However, the solutions in spherical coordinates are also instructive and we begin with these. It is readily seen that, in a spherically symmetric core (radial coordinate, r) the solution to equation 4.24 takes the form

$$\phi = C_1 \frac{\sin B_g r}{r} + C_2 \frac{\cos B_g r}{r} \tag{4.37}$$

where C_1 and C_2 are constants to be determined. For ϕ to be finite in the center, C_2 must be zero. Next we apply the boundary condition at the surface, $r = R$, of this spherical reactor which is assumed to be surrounded by a vacuum so the appropriate boundary condition is given by equation 4.17, or more conveniently $\phi = 0$ at the extrapolated boundary at $r = R_E = R + 1/2D$. Thus

$$\sin B_g R_E = 0 \qquad \text{or} \qquad B_g R_E = n\pi \tag{4.38}$$

where n is an integer. Since B_g and n are positive and ϕ cannot be negative anywhere within the core, the only acceptable, non-trivial value for n is unity and therefore

$$R_E = \pi / B_g \qquad \text{and thus} \qquad R = \pi / B_g - 1/2D \tag{4.39}$$

Therefore, $R = R_C = \pi / B_m - 1/2D$ is the critical size of a spherical reactor, that is to say the only size for which a steady neutron flux state is possible for the given value of the material buckling, B_m. It is readily seen from equation 4.9 that $\partial\phi/\partial t$ will be positive if $R > R_C$ and that the neutron flux will then grow exponentially with time. Conversely when $R < R_C$, the neutron flux will decay exponentially with time.

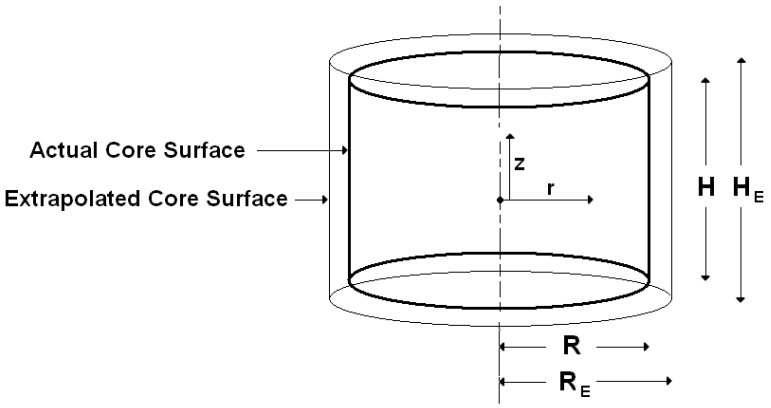

Figure 4.1: Sketch of a simple cylindrical reactor.

In summary, the neutron flux solution for the steady state operation of a spherically symmetric reactor is

$$\phi = C_1 \frac{\sin B_g r}{r} \qquad \text{for} \qquad 0 < r < R_C \tag{4.40}$$

Note that the neutron flux is largest in the center and declines near the boundary due to the increased leakage. Also note that though the functional form of the neutron flux variation has been determined, the magnitude of the neutron flux as defined by C_1 remains undetermined since the governing equation and boundary conditions are all homogeneous in ϕ.

Most common reactors are cylindrical and so, as a second example, we construct the solution for a cylinder of radius, R, and axial length, H, using cylindrical coordinates, (r, θ, z), with the origin at the mid-length of the core. It is assumed that the reactor is homogeneous so that there are no gradients in the θ direction and that both the sides and ends see vacuum conditions. Again it is convenient to apply the condition $\phi = 0$ on extrapolated boundary surfaces at $r = R_E = R + 1/2D$ and at $z = \pm H_E/2 = \pm(H/2 + 1/2D)$ as depicted in figure 4.1. Obtaining solutions to equation 4.24 by separation of variables and eliminating possible solutions that are singular on the axis, it is readily seen that the neutron flux has the form:

$$\phi = C_1 \cos\left(\frac{\pi z}{H_E}\right) J_0\left(\frac{2.405 r}{R_E}\right) \tag{4.41}$$

where, as before, C_1 is an undetermined constant and $J_0()$ is the zero-order Bessel function of the first kind (2.405 is the argument that gives the first zero of this function). As in the spherical case we reject the higher order functions since they would imply negative neutron fluxes within the cylindrical reactor. Substituting this solution into the governing equation 4.24 yields the expression

that determines the critical size of this cylindrical reactor namely

$$\left(\frac{\pi}{H_E}\right)^2 + \left(\frac{2.405}{R_E}\right)^2 = B_g^2 \tag{4.42}$$

If H_E and R_E are such that the left-hand side is greater than the material buckling, B_m^2, then the reactor is supercritical and the neutron flux will grow exponentially with time; if the left hand side is less than B_m^2 the flux will decay exponentially. In the critical reactor, the neutron flux is greatest in the center and decays toward the outer radii or the ends as the leakage is greatest near the boundaries.

These two examples assumed homogeneous reactors surrounded by vacuum conditions. There are a number of ways in which these simple solutions can be modified in order to incorporate common, practical variations. Often the reactor core is surrounded, not by a vacuum, but by a *blanket* of moderator that causes some of the leaking neutrons to be scattered back into the core. Such a blanket is called a reflector; examples of diffusion theory solutions that incorporate the effect of a reflector are explored in the next section. Another practical modification is to consider two core regions rather than one in order to model that region into which control rods have been inserted. Section 4.7.4 includes an example of such a two-region solution.

4.7.2 Effect of a reflector on a spherical reactor

In the examples of the last section it was assumed that all neutrons leaking out were lost. In practice, reactor cores are usually surrounded by a reflector that scatters some of the leaking neutrons back into the core. In this section we shall detail two examples of diffusion theory solutions with reflectors.

Perhaps the simplest example is the spherically symmetric reactor of the preceding section now surrounded by a reflector of inner radius R and outer radius R_R. Since there is no source of neutrons in the reflector the diffusion equation which governs the neutron flux in the reflector (denoted by ϕ_R) is then

$$\bigtriangledown^2 \phi_R - \frac{1}{L_R^2}\phi_R = 0 \tag{4.43}$$

where L_R is the diffusion length in the reflector. The boundary conditions that must be satisfied are as follows. At the interface between the core and the reflector both the neutron flux and the net radial neutron current (see section 4.2) must match so that

$$(\phi)_{r=R} = (\phi_R)_{r=R} \qquad \text{and} \qquad D\left(\frac{\partial\phi}{\partial r}\right)_{r=R} = D_R\left(\frac{\partial\phi_R}{\partial r}\right)_{r=R} \tag{4.44}$$

where D and D_R are the diffusion coefficients in the core and in the reflector. At the outer boundary of the reflector we use the vacuum condition and set $\phi_R = 0$ at $r = R_R + 1/2D_R = R_{RE}$.

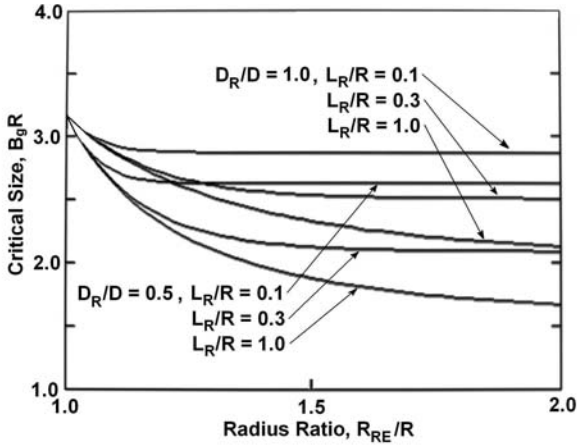

Figure 4.2: The non-dimensional critical size or geometric buckling, $B_g R$, for a spherical reactor with a reflector as a function of the radius ratio, R_{RE}/R, for various values of L_R/R and D_R/D.

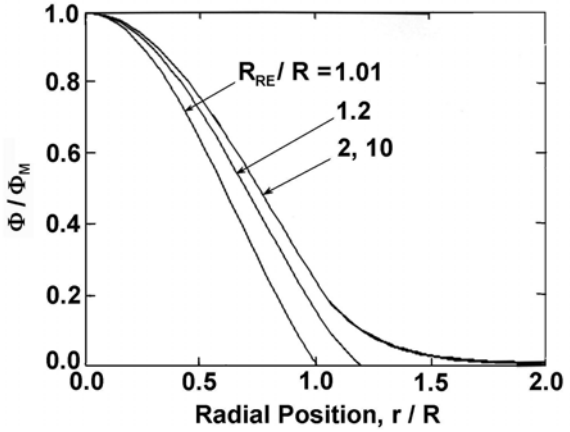

Figure 4.3: The shape of the neutron flux distribution , ϕ (normalized by the maximum neutron flux, ϕ_M) for various radius ratios, R_{RE}/R, as shown and for $D_R/D = 1$.

As in the preceding section the appropriate solution for the neutron flux in the core is

$$\phi = \frac{C}{r} \sin B_g r \tag{4.45}$$

where C is an undetermined constant. Moreover, the appropriate solution to equation 4.43 in the reflector is

$$\phi_R = \frac{C_R}{r} \sinh\left(\frac{r^* - r}{L_R}\right) \tag{4.46}$$

where C_R and r^* are constants as yet undetermined. Applying the above boundary conditions it follows that

$$r^* = R_{RE} \qquad \text{and} \qquad C \sin B_g R = C_R \sinh\left(\frac{R_{RE} - R}{L_R}\right) \tag{4.47}$$

and

$$\begin{aligned} &DC\left(\sin B_g R - B_g R \cos B_g R\right) \\ &= D_R C_R \left(\frac{R}{L_R} \cosh\left(\frac{R_{RE} - R}{L_R}\right) + \sinh\left(\frac{R_{RE} - R}{L_R}\right)\right) \end{aligned} \tag{4.48}$$

Eliminating the ratio C/C_R from the last two relations yields

$$D\left(1 - B_g R \cot B_g R\right) = D_R \left(1 + \frac{R}{L_R} \coth\left(\frac{R_{RE} - R}{L_R}\right)\right) \tag{4.49}$$

Given all the material constants involved this relation can be solved numerically to determine the critical size (or critical geometric buckling) of such a spherical reactor.

Sample results are shown in figure 4.2 which presents the non-dimensional critical size or geometric buckling, $B_g R$, as a function of the radius ratio, R_{RE}/R, for various values of L_R/R and D_R/D. The change in the shape of the neutron flux as the size of the reflector is increased is shown in figure 4.3; note that the uniformity of the neutron flux within the core can be somewhat improved by the presence of the reflector.

4.7.3 Effect of a reflector on a cylindrical reactor

As a second example of the effect of a reflector, consider the cylindrical reactor of section 4.7.1 surrounded at larger radii by a reflector as shown in figure 4.4 (for simplicity we continue to assume vacuum conditions at both ends of the core and the reflector). Then, as in section 4.7.1, the appropriate, non-singular solution to equation 4.24 for the neutron flux in the core is

$$\phi = C \cos\left(\frac{\pi z}{H_E}\right) J_0(\xi_1 r) \tag{4.50}$$

where $H_E = H + 1/D$ as before and C and ξ_1 are constants as yet undetermined. Turning now to the solution for equation 4.43 in the cylindrical annulus occupied

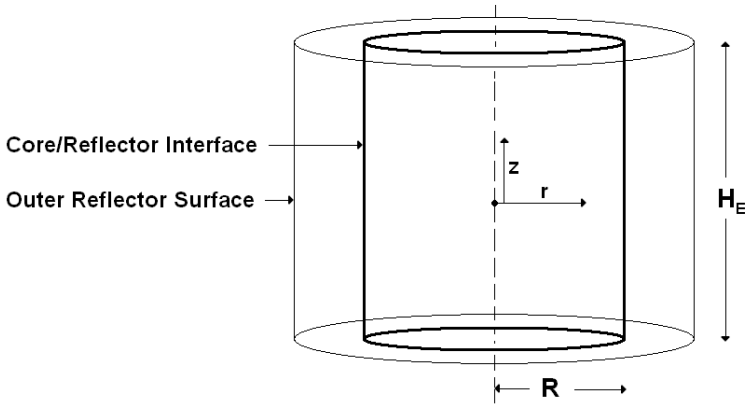

Figure 4.4: Cylindrical reactor with reflector.

by the reflector we will, for simplicity, assume this extends all the way from $r = R$ to $r \to \infty$ and that the reflector has the same height H_E as the core. Then, omitting terms which are singular as $r \to \infty$, the appropriate solution to equation 4.43 in the reflector is

$$\phi_R = C_R \cos\left(\frac{\pi z}{H_E}\right) K_0(\xi_2 r) \tag{4.51}$$

where ξ_2 is to be determined and K_0 is the modified Bessel function. Applying the boundary conditions at the core-reflector interface, $r = R$, (equations 4.44) yields the relations

$$CJ_0(\xi_1 R) = C_R K_0(\xi_2 R) \quad \text{and} \quad \xi_1 DCJ_1(\xi_1 R) = \xi_2 D_R C_R K_1(\xi_2 R) \tag{4.52}$$

and, upon elimination of C_R/C, these yield

$$D\xi_1 J_1(\xi_1 R)K_0(\xi_2 R) = D_R \xi_2 K_1(\xi_2 R)J_0(\xi_1 R) \tag{4.53}$$

and, in a manner analogous to equation 4.49, this equation must be solved numerically to determine R, the critical size of such a cylindrical reactor. The corresponding solutions for a reflector with a finite outer radius or with a reflector at the ends, though algebraically more complicated, are conceptually similar.

4.7.4 Effect of control rod insertion

A second example of a practical modification of the diffusion theory solutions is to consider a core into which control rods have been partially inserted so that, as sketched in figure 4.5, the reactor core consists of two regions with different levels of neutron absorption. We denote the fractional insertion by β. Assuming

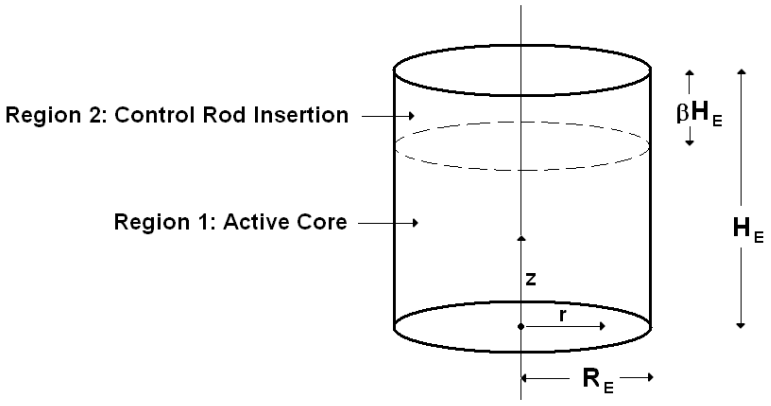

Figure 4.5: Cylindrical reactor with partial control rod insertion.

that the control rod absorption is sufficiently large so that the conditions in the controlled region are subcritical the equations governing the neutron flux in the two regions are

$$\bigtriangledown^2 \phi_1 + B_g^2 \phi_1 = 0 \qquad \text{in} \qquad 0 \leq z \leq (1-\beta) H_E \tag{4.54}$$

$$\bigtriangledown^2 \phi_2 - \frac{\phi_2}{L_2^2} = 0 \qquad \text{in} \qquad (1-\beta) H_E \leq z \leq H_E \tag{4.55}$$

where subscripts 1 and 2 refer to the two regions indicated in figure 4.5, L_2 is the neutron diffusion length in region 2 and, for convenience, the origin of z has been shifted to the bottom of the core. The boundary conditions on the cylindrical surface $r = R_E$ are $\phi_1 = \phi_2 = 0$ (as in section 4.7.1) and on the radial planes they are

$$\phi_1 = 0 \quad \text{on} \quad z = 0 \quad ; \quad \phi_2 = 0 \quad \text{on} \quad z = H_E \quad ; \tag{4.56}$$

$$\phi_1 = \phi_2 \quad \text{and} \quad \frac{\partial \phi_1}{\partial z} = \frac{\partial \phi_2}{\partial z} \quad \text{on} \quad z = (1-\beta) H_E \tag{4.57}$$

where, for simplicity, we have assumed that the neutron diffusivities are the same in both regions. By separation of variables, the appropriate solutions to equations 4.54 and 4.55 are

$$\phi_1 = \left[C_1 \sin \xi_1 z + C_2 \cos \xi_1 z \right] J_0(2.405 r / R_E) \tag{4.58}$$

$$\phi_2 = \left[C_3 e^{\xi_2 z} + C_4 e^{-\xi_2 z} \right] J_0(2.405 r / R_E) \tag{4.59}$$

where C_1, C_2, C_3, C_4, $\xi_1$and ξ_2 are constants as yet undetermined and we have already applied the boundary conditions at $r = R_E$. The governing equations 4.54 and 4.55 require that

$$\xi_1^2 = B_g^2 - (2.405/R_E)^2 \quad ; \quad \xi_2^2 = (1/L_2)^2 + (2.405/R_E)^2 \tag{4.60}$$

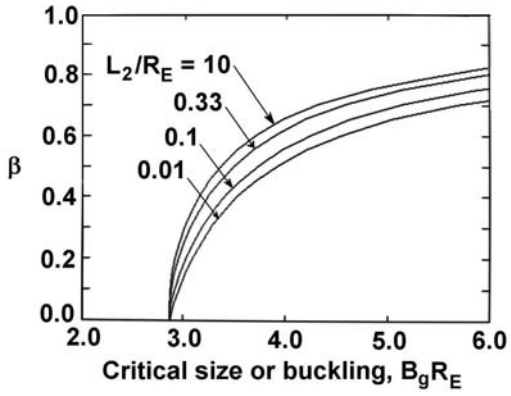

Figure 4.6: The critical non-dimensional size or geometric buckling, $B_g R_E$, as a function of the fractional control rod insertion, β, for a cylindrical reactor with $H_E/R_E = 2.0$ and several values of L_2/R_E as indicated.

The boundary conditions 4.56 require that

$$C_2 = 0 \quad ; \quad C_4 = -C_3 e^{2\xi_2 H_E} \tag{4.61}$$

and using these with the boundary conditions 4.57 yields

$$C_1 \sin\{\xi_1(1-\beta)H_E\} = -C_3 e^{\xi_2 H_E}\left[e^{\xi_2 \beta H_E} - e^{-\xi_2 \beta H_E}\right] \tag{4.62}$$

$$\xi_1 C_1 \cos\{\xi_1(1-\beta)H_E\} = \xi_2 C_3 e^{\xi_2 H_E}\left[e^{\xi_2 \beta H_E} + e^{-\xi_2 \beta H_E}\right] \tag{4.63}$$

Eliminating the ratio C_1/C_3 from these last two expressions we obtain

$$\xi_2 \tan\{\xi_1(1-\beta)H_E\} + \xi_1 \tanh\{\xi_2 \beta H_E\} = 0 \tag{4.64}$$

Since ξ_1 and ξ_2 are given by equations 4.60 this constitutes an expression for the critical size of the reactor, R_E (or R) given the aspect ratio H_E/R_E as well as B_g, L_2 and α. Equivalently it can be seen as the value of β needed to generate a critical reactor given R_E, H_E, B_g and L_2.

As a non-dimensional example, we present in figure 4.6 critical values for the fractional insertion, β, as a function of the quantity $B_g R_E$ (which can be thought of as a non-dimensional size or non-dimensional geometric buckling) for a typical aspect ratio, H_E/R_E, of 2.0 and several values of L_2/R_E. Naturally the critical size increases with the insertion, β; equivalently the insertion, β, for a critical reactor will increase with the *size* given by $B_g R_E$. Note that the results are not very sensitive to the value of L_2/R_E.

The way in which the neutron flux distribution changes as the control rods are inserted will become important when the temperature distribution is analyzed in later chapters. Evaluating the neutron flux in the above solution and

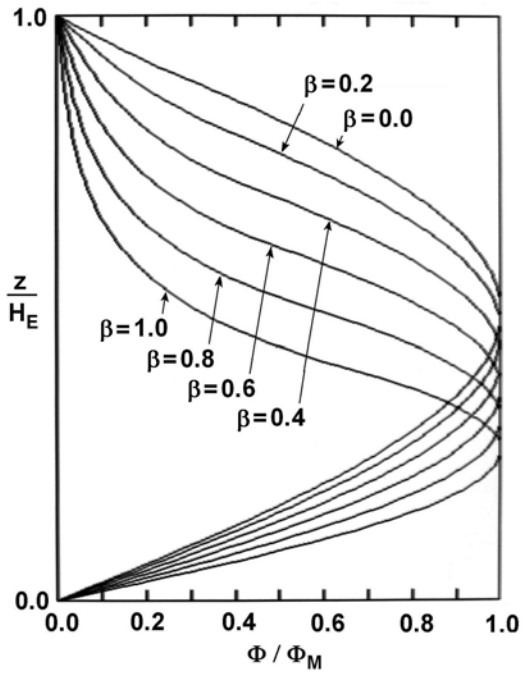

Figure 4.7: The change in the shape of the axial distribution of the neutron flux, ϕ (normalized by the maximum neutron flux, ϕ_M), with fractional control rod insertion, β, for the case of $H_E/R_E = 2.0$ and $L_2/R_E = 0.36$.

normalizing each distribution in the z direction by the maximum value of ϕ occuring within it (denoted by ϕ_M) the distribution becomes:

$$\begin{aligned} \phi/\phi_M &= \sin\{\xi_1 z\} \quad \text{for} \quad 0 \le z \le (1-\beta)H_E \\ &= \frac{\sin\{\xi_1(1-\beta)H_E\}}{\left\{e^{\xi_2\beta H_E} - e^{-\xi_2\beta H_E}\right\}} \left\{e^{\xi_2(H_E - z)} - e^{-\xi_2(H_E - z)}\right\} \\ &\quad \text{for} \quad (1-\beta)H_E \le z \le H_E \end{aligned} \tag{4.65}$$

Typical examples of these neutron flux distributions are shown in figure 4.7; as the fractional insertion, β, increases note how the neutron flux in the region of insertion decreases and the distribution becomes skewed toward the lower part of the core.

4.8 Steady state lattice calculation

4.8.1 Introduction

The preceding sections addressed solutions for the distribution of the neutron flux in reactors that were assumed to be homogeneous. As previously described in section 4.6.1, the assumption of homogeneity was based on the fact that the typical mean free path of the neutrons is normally large compared with the small scale structure within the reactor (for example, the fuel rod diameter). On the other hand the neutron mean free path is somewhat smaller than the overall reactor geometry and this provides some qualitative validity for variations in the neutron flux within the reactor that are derived from analytical methods such as those based on the diffusion equation (or any other more detailed methodology).

As described in section 4.6.6 the typical mean free path in a LWR is of the order of a centimeter and therefore comparable with the diameter of a fuel rod. Consequently the variation of the neutron flux within and around the fuel rod of a LWR may be substantial and therefore important to take into account in the design of those components. In contrast, a fast breeder reactor has typical mean free paths of the order of tens of centimeters. With fuel rod dimensions similar to a LWR, it follows that the inhomogeneity is less important in a fast reactor. In either case, practical reactor analysis and design requires detailed calculation of the variations in the neutron flux at these smaller scales and this is effected using numerical codes called *heterogeneous lattice cell calculations*.

Thus we now turn to consider analytical methods that might be used to determine the variations in the neutron flux associated with the finer structure within a reactor core, for example the variations around a fuel rod or a control rod. In this endeavor, it is convenient to take advantage of the fact that much of this finer structure occurs in lattices or *units* that are repeated over the cross-section of the reactor (or at least parts of that cross-section). For example, each of the fuel rods are surrounded by coolant channels and other fuel rods in patterns that are exemplified in figure 5.10. Thus a fuel rod plus an appropriately allocated fraction of the surrounding coolant constitute a *unit* and those units are repeated across the reactor cross-section. Moreover since the neutron mean free path is comparable to or larger than the dimensions of this unit, it may be adequate to adjust the geometry of the unit to facilitate the mathematical solution of the neutron flux. Thus, as shown in figure 4.8, we might model the geometry of a fuel rod unit as consisting of a central cylinder of fuel pellets of radius, R_1, surrounded by a cylinder of neutronically passive and moderating components, $R_1 < r < R_2$, where the ratio of the areas of the two regions is the same as the ratio of the cross-sectional area of fuel pellet to the cross-sectional area of allocated non-pellet material within the reactor.

Before outlining some typical examples of the calculation of neutron flux variations within a lattice cell, we need to consider the nature of the boundary conditions that might be applied at the interfaces and boundaries of a cell such as that of figure 4.8. As described in section 4.6.1, at an interface such as $r = R_1$ not only should the neutron fluxes in the two regions be the same but the one-

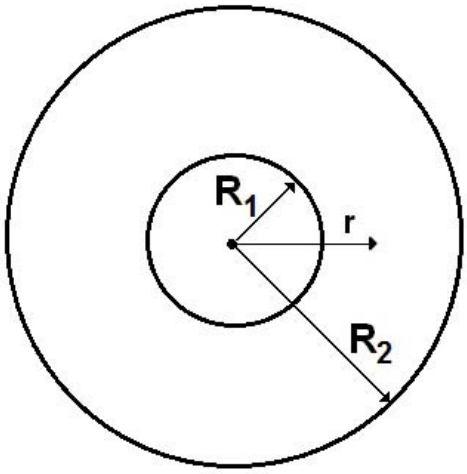

Figure 4.8: Generic circular lattice cell.

way fluxes must also be the same. In the context of diffusion theory these imply that at the interface the conditions should be as given in equation 4.16. With the geometry of figure 4.8 these become:

$$\phi_1 = \phi_2 \qquad \text{and} \qquad D_1 \frac{\partial \phi_1}{\partial r} = D_2 \frac{\partial \phi_2}{\partial r} \tag{4.66}$$

Now consider the conditions on the outer boundary of the lattice cell ($r = R_2$ in figure 4.8). If the reactor is in a steady critical state each of the unit cells should be operating similarly with little or no net neutron exchange between them and therefore the condition on the outer boundary should be

$$\frac{\partial \phi_2}{\partial r} = 0 \quad \text{on} \quad r = R_2 \tag{4.67}$$

or the equivalent in more complex neutron flux models.

In the sections which follow we will use diffusion theory solutions to explore some of the features of lattice cell models.

4.8.2 Fuel rod lattice cell

The diffusion theory solution for the single fuel rod lattice cell requires the solution of the following forms of the diffusion equation 4.22 for the neutron fluxes ϕ_1 and ϕ_2 in the two regions of cell sketched in figure 4.8:

$$\bigtriangledown^2 \, \phi_1 + B_g^2 \phi_1 = 0 \qquad \text{in} \qquad r \leq R_1 \tag{4.68}$$

$$\bigtriangledown^2 \, \phi_2 - \frac{\phi_2}{L_2^2} = 0 \qquad \text{in} \qquad R_1 \leq r \leq R_2 \tag{4.69}$$

subject to the boundary conditions 4.66 and 4.67 and neglecting any gradients in the direction normal to the figure 4.8 sketch (the z direction). The appropriate general solutions are

$$\phi_1 = C_1 J_0(B_g r) + C_2 Y_0(B_g r) \tag{4.70}$$

$$\phi_2 = C_3 I_0(r/L_2) + C_4 K_0(r/L_2) \tag{4.71}$$

where $J_0()$ and $Y_0()$ are Bessel functions of the first and second kind, $I_0()$ and $K_0()$ are modified Bessel functions of the first and second kind and C_1, C_2, C_3, and C_4 are constants yet to be determined. Since ϕ_1 must be finite at $r = 0$, C_2 must be zero. If, for the convenience of this example, we assume the diffusivities are the same in both regions ($D_1 = D_2 = D$) then the boundary conditions 4.61 require that

$$C_1 J_0(B_g R_1) = C_3 I_0(R_1/L_2) + C_4 K_0(R_1/L_2) \tag{4.72}$$

$$-C_1 B_g J_1(B_g R_1) = C_3 I_1(R_1/L_2)/L_2 - C_4 K_1(R_1/L_2)/L_2 \tag{4.73}$$

where $J_1()$, $I_1()$ and $K_1()$ denote Bessel functions of the first order. In addition the outer boundary condition 4.62 requires that

$$-C_3 I_1(R_2/L_2) + C_4 K_1(R_2/L_2) = 0 \tag{4.74}$$

and equations 4.72, 4.73 and 4.74 lead to the eigenvalue equation

$$J_0(B_g R_1)\left[I_1(R_2/L_2)K_1(R_1/L_2) - I_1(R_1/L_2)K_1(R_2/L_2)\right] =$$

$$L_2 B_g J_1(B_g R_1)\left[I_0(R_1/L_2)K_1(R_2/L_2) + I_1(R_2/L_2)K_0(R_1/L_2)\right] \tag{4.75}$$

Given the non-dimensional parameters R_2/R_1 and L_2/R_1 the solution to this equation yields the non-dimensional geometric buckling, $B_g R_1$, for this configuration. When the neutron mean free path, L_2, is large relative to R_1 and R_2 the approximate solution to equation 4.75 is

$$B_g^2 L_2^2 \approx (R_2^2 - R_1^2)/R_1^2 \tag{4.76}$$

More precise solutions for the non-dimensional geometric buckling, $B_g^2 R_1^2$, are shown in figure 4.9 for various values of L_2/R_1 and R_2/R_1. These lead to different neutron flux profiles as exemplified by those presented in figure 4.10. As expected the flux inside the fuel rod is larger than in the surroundings but the profile flattens out as the neutron mean free path increases.

4.8.3 Control rod lattice cell

The obverse of the fuel rod lattice cell is the control rod lattice cell in which an individual control rod ($0 < r < R_1$) is surrounded by an annulus ($R_1 < r < R_2$) containing a homogeneous mix of fuel rod and coolant as can also be depicted by figure 4.8. Then the governing equations for the neutron flux are:

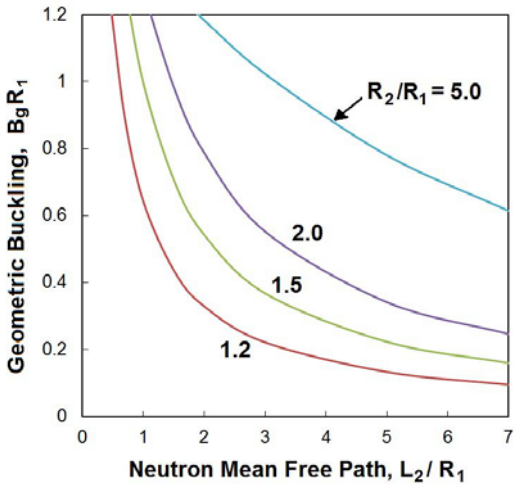

Figure 4.9: Values of the non-dimensional geometric buckling for the fuel rod lattice cell as a function of L_2/R_1 for four values of R_2/R_1 as shown.

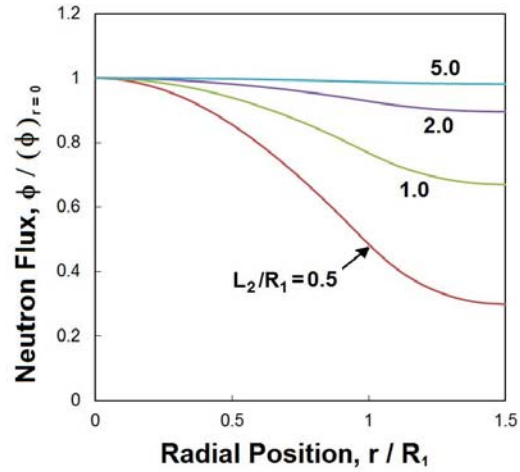

Figure 4.10: Typical neutron flux profiles for the fuel rod lattice cell with $R_2/R_1 = 1.5$ for four values of L_2/R_1 as shown.

$$\bigtriangledown^2 \phi_1 - \frac{\phi_1}{L_1^2} = 0 \qquad \text{in} \qquad r \leq R_1 \tag{4.77}$$

$$\bigtriangledown^2 \phi_2 + B_g^2 \phi_2 = 0 \qquad \text{in} \qquad R_1 \leq r \leq R_2 \tag{4.78}$$

where gradients in the direction normal to the sketch (the z direction) are neglected and L_1 is the neutron mean free path in the control rod. The boundary conditions are the same as in the fuel rod lattice cell and it follows that the appropriate general solutions are

$$\phi_1 = C_1 I_0(r/L_1) + C_2 K_0(r/L_1) \tag{4.79}$$

$$\phi_2 = C_3 J_0(B_g r) + C_4 Y_0(B_g r) \tag{4.80}$$

Since ϕ_1 must be finite at $r = 0$, C_2 must be zero. If, again for convenience, we assume the diffusivities are the same in both regions ($D_1 = D_2 = D$) then the boundary conditions 4.61 require that

$$C_1 I_0(R_1/L_1) = C_3 J_0(B_g R_1) + C_4 Y_0(B_g R_1) \tag{4.81}$$

$$C_1 I_1(R_1/L_1)/L_1 = -C_3 B_g J_1(B_g R_1) - C_4 B_g Y_1(B_g R_1) \tag{4.82}$$

In addition the outer boundary condition 4.62 requires that

$$C_3 J_1(B_g R_2) + C_4 Y_1(B_g R_2) = 0 \tag{4.83}$$

and equations 4.81, 4.82 and 4.83 lead to the eigenvalue equation

$$I_1(R_1/L_1)\left[J_0(B_g R_1)Y_1(B_g R_2) - J_1(B_g R_2)Y_0(B_g R_1)\right] =$$

$$B_g L_1 I_0(R_1/L_1)\left[J_1(B_g R_2)Y_1(B_g R_1) - J_1(B_g R_1)Y_1(B_g R_2)\right] \tag{4.84}$$

and, given the non-dimensional parameters R_2/R_1 and L_1/R_1, the solution to this equation yields the non-dimensional geometric buckling, $B_g R_1$, for this configuration. When the neutron mean free path, L_1, is large relative to R_1 and R_2 the approximate solution to equation 4.84 is

$$B_g^2 L_1^2 \approx R_1^2/(R_2^2 - R_1^2) \tag{4.85}$$

More precise solutions for the non-dimensional geometric buckling, $B_g^2 R_1^2$, are shown in figure 4.11 for various values of L_1/R_1 and R_2/R_1. These lead to different neutron flux profiles as exemplified by those presented in figure 4.12. As expected the flux inside the control rod ($r < R_1$) is smaller than in the surroundings but the profile flattens out as the geometric buckling decreases.

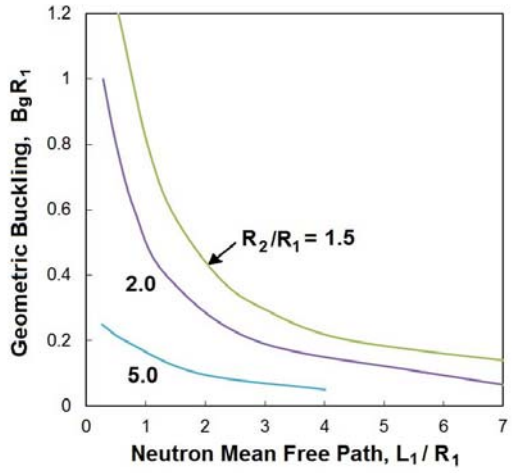

Figure 4.11: Values of the non-dimensional geometric buckling for the control rod lattice cell as a function of L_1/R_1 for three values of R_2/R_1 as shown.

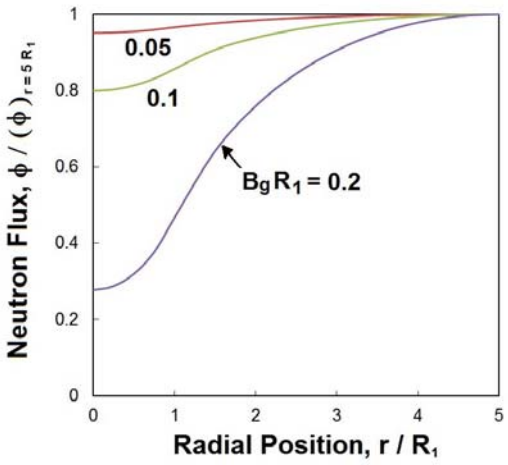

Figure 4.12: Typical neutron flux profiles for the control rod lattice cell with $R_2/R_1 = 5$ for three values of non-dimensional geometric buckling, B_gR_1, as shown.

4.8.4 Other lattice scales

The preceding two sections illustrated the use of the lattice cell approach, first on the small scale associated with an individual fuel rod and then on the somewhat larger scale associated with an individual control rod. Finally we briefly note that many other lattice cell approaches are possible. For example the square cross-section fuel assembly sketched in figure 4.8 is repeated across a PWR core and this can be utilized to investigate inhomogeneous effects on that scale. For such square crossection lattice cells the diffusion equation 4.24 has solutions of the form

$$\phi = C \cos B_m x/2^{1/2} \cos B_m y/2^{1/2} \tag{4.86}$$

where the origin of the (x, y) coordinate system is taken to be the center of the square cross-section. Solutions like equation 4.86 combined with the fact that the diffusion equations permit superposition of solutions allow the construction of a variety of other lattice cell solutions to that equation.

However, it is important to note in closing that these diffusion equation approaches involve many approximations and can only be considered to provide qualitative estimates and guidance. Precise, quantitative assessment of the neutronics of a reactor core are much more complex (see, for example, Duderstadt and Hamilton 1976) and require large computational effort.

4.9 Unsteady or quasi-steady neutronics

The preceding sections in this chapter referred to steady state calculations, and therefore we should end this brief introduction to reactor core neutronics with some mention of the corresponding time dependent processes. Clearly, it is important to consider the growth or decay rates for the neutron flux when the reactor becomes supercritical or subcritical. This is needed not only in order to design control systems for the reactor but also to evaluate scenarios that would follow reactor transients or accidents. There are two sets of unsteady perturbations that are commonly considered: (1) perturbations caused by changes in the reactor core neutronics, for example the insertion or withdrawal of control rods or (2) perturbations caused by changes in the thermohydraulic conditions such as as change in the power level. The former perturbations are governed by what are called the *nuclear reactor kinetics*, whereas the latter are termed the *nuclear reactor dynamics*. The latter therefore involve the response of the entire plant including the steam generators and are not further discussed in this text. Instead we confine our attention to the nuclear reactor kinetics.

To exemplify the nature of the nuclear reactor kinetics we return to the basic diffusion equation 4.18, and now retain the unsteady term $\partial\phi/\partial t$:

$$\frac{1}{\bar{u}} \frac{\partial \phi}{\partial t} - D \bigtriangledown^2 \ \phi = S - \Sigma_a \phi \tag{4.87}$$

where we will assume that the diffusivity is uniform throughout the reactor and does not change with time. Recall that equation 4.87 is a statement of neutron

conservation in some small piece of the core in which the excess of the neutrons produced over the neutrons absorbed (the right hand side) is balanced by the rate of increase of the neutrons in that piece plus the net flux of neutrons out of that piece of core (the left hand side). As before we set the left hand side equal to $(k_\infty - 1)\Sigma_a\phi$ so the diffusion equation 4.87 becomes

$$\frac{1}{\bar{u}D}\frac{\partial\phi}{\partial t} - \bigtriangledown^2\ \phi = \frac{(k_\infty - 1)\Sigma_a}{D}\ \phi \tag{4.88}$$

Fortunately, equation 4.88 is linear in the neutron flux, ϕ, and therefore solutions are superposable. Consequently, for simplicity, we can focus on a single basic solution knowing that more complex solutions may be constructed by superposition. This basic solution for the neutron flux, $\phi(x_i, t)$, takes the form:

$$\phi(x_i, t) = C\exp(-\xi t)\phi^*(x_i) \tag{4.89}$$

where C is a constant, ξ is the time constant associated with the transient and ϕ^* is a time-independent neutron flux function. Substituting from equation 4.89 into the governing equation 4.88 yields the following relation for ϕ^*:

$$\bigtriangledown^2\ \phi^* + \left\{\frac{(k_\infty - 1)\Sigma_a}{D} + \frac{\xi}{D\bar{u}}\right\}\phi^* = 0 \tag{4.90}$$

Note that, as in the steady state case, Σ_a could be replaced using $\Sigma_a = D/L^2$ where L is the neutron diffusion length, L (see the definition 4.19). In parallel with the steady state equation 4.24, we can write equation 4.90 as the eigenequation

$$\bigtriangledown^2\ \phi^* + B_g^2\phi^* = 0 \tag{4.91}$$

where the geometric buckling, B_g, is the specific eigenvalue for the particular geometry of the reactor under consideration. Since equation 4.91 is identical to that governing ϕ in the steady case, and since the boundary conditions are usually the same, the geometric buckling, B_g, will be the same as in the steady case. In addition, from equations 4.90 and 4.91 it follows that

$$B_g^2 = \frac{(k_\infty - 1)}{L^2} + \frac{\xi}{D\bar{u}} \tag{4.92}$$

so that, using equation 4.19, we find that

$$\xi = D\bar{u}B_g^2 + \bar{u}\Sigma_a - k_\infty\bar{u}\Sigma_a \tag{4.93}$$

in which the left hand side consists of contributions to ξ from the neutron leakage, absorption and production respectively. Alternatively we could write

$$\xi = \frac{(k-1)}{t^*} \tag{4.94}$$

where k is the multiplication factor and t^* is the mean lifetime of a neutron in the reactor where using equations 4.29 and 4.19

$$k = \frac{k_\infty}{1 + L^2B_g^2} \qquad \text{and} \qquad t^* = \frac{1}{\bar{u}\Sigma_a(1 + L^2B_g^2)} \tag{4.95}$$

Note that $(\bar{u}\Sigma_a)^{-1}$ is the typical time before absorption and $(\bar{u}\Sigma_a L^2 B_g^2)^{-1}$ is the typical time before escape; combining these it follows that t^* is the typical neutron lifetime in the reactor.

Hence the solution to the characteristic unsteady problem may be written as

$$\phi = C \exp(-\frac{(k-1)}{t^*}t)\phi^* \tag{4.96}$$

where ϕ^* is the solution to the steady diffusion problem with the same geometry and boundary conditions. The characteristic response time of the reactor, t_R, is known as the *reactor period* . In the absence of other factors, this analysis and equation 4.96 suggest that t_R might be given by

$$t_R = \frac{t^*}{(k-1)} \tag{4.97}$$

Since the typical lifetime of a neutron, t^*, in a LWR is of the order of $10^{-4} sec$, equation 4.97 suggests that a very small perturbation in the multiplication factor k of 0.1% to 1.001 might result in a reactor period, t_R, of $0.1 sec$ and therefore more than a 2×10^4 fold increase in the neutron population in one second. This would make any reactor very difficult to control. Fortunately, as described in section 2.3.4, delayed neutron emission causes a more than 100 fold increase in the mean neutron lifetime in an LWR and a corresponding increase in the reactor period, making reactor control much more manageable (see section 5.2.5).

4.10 More advanced neutronic theory

As we described in the earlier sections of this chapter, there are many approximations that were made during the development of the diffusion theory described above. Consequently, though the one-speed diffusion theory results presented have qualitative instructional value they are not adequate for practical reactor design. For this much more detailed and complex analyses have been developed but are beyond the scope of this text.

Perhaps the most glaring deficiency of the one-speed diffusion theory is the assumption that all the neutrons have the same speed or energy. Consequently the most obvious next step is to allow a variety of neutron energies and to incorporate a model for the transfer of neutrons from one energy level to another. Such models are termed *multigroup diffusion models* and the simplest among these is the *two-speed diffusion model* in which the neutron population consists of one population of fast neutrons and another of thermal neutrons. This is particularly useful in a LWR in which the moderator helps maintain a balance between the two groups. More sophisticated models with many more energy levels are needed in order to accommodate the complexities of the neutron energy spectra described in section 2.3.2. For further information on these more advanced calculational methods the reader is referred to texts like Glasstone and Sesonske (1981) or Duderstadt and Hamilton (1976).

References

Bell, G.I. and Glasstone, S. (1970). *Nuclear reactor engineering.*Van Nostrand Reinhold Co.

Duderstadt, J.J. and Hamilton, L.J. (1976). *Nuclear reactor analysis.* John Wiley and Sons, New York.

Glasstone, S. (1955). *Principles of nuclear reactor engineering.* Van Nostrand Co., Inc.

Glasstone, S. and Sesonske, A. (1981). *Nuclear reactor engineering.* Van Nostrand Reinhold Co. [See also, Glasstone (1955) and Bell and Glasstone (1970)].

Glasstone, S. (1955). *Principles of nuclear reactor engineering.* Van Nostrand Co., Inc.

Syrett, J.J. (1958.) *Nuclear reactor theory.* Temple Press Ltd., London.

Chapter 5

SOME REACTOR DESIGNS

5.1 Introduction

Before proceeding with further analysis of nuclear power generation reactors, it is useful to provide some engineering context by briefly describing the design and components of a number of power generation reactors. As illustrated in

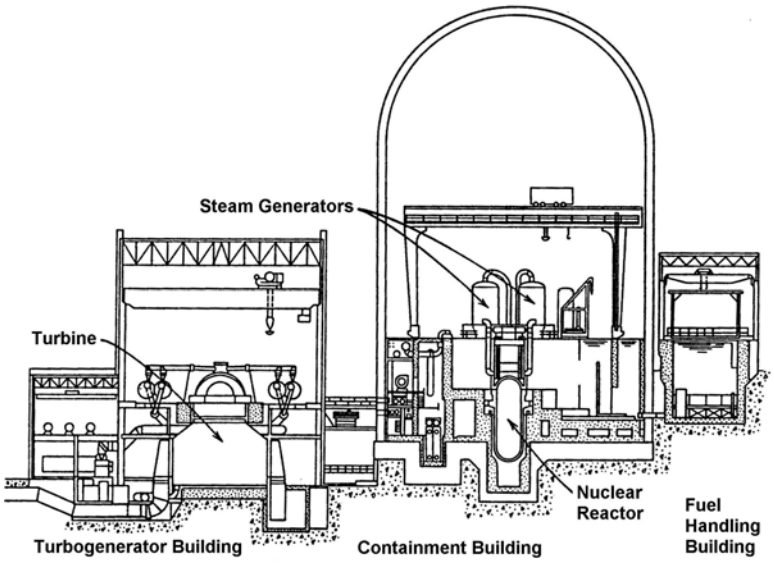

Figure 5.1: Schematic of a nuclear power plant. From Duderstadt and Hamilton (1976).

Table 5.1: Some typical nuclear power plant data. Extracted from Duderstadt and Hamilton (1976).

Type of Reactor	PWR (LWR)	BWR (LWR)	CANDU (HWR)	LMFBR (FNR)
Electrical Output (MW)	$1150 - 1300$	1200	500	1000
Efficiency(%)	$33 - 34$	33	31	39
Fuel	U_2O	U_2O	U_2O	U_2O, PuO_2
Primary Coolant	H_2O	H_2O	D_2O	Na
Moderator	H_2O	H_2O	D_2O	None
Coolant Pressure (atm)	155	72	89	14
Coolant Inlet ($^\circ C$)	$296 - 300$	269	249	380
Coolant Outlet ($^\circ C$)	$328 - 333$	286	293	552
Flow Rate (10^6 kg/hr)	65	47	24	50
Max. Fuel Temp.($^\circ C$)	$1788 - 2021$	1829	1500	2000

figure 5.1, a nuclear power plant is similar to any other coal, gas or oil fired plant except that the source of the heat creating the steam that drives the steam turbines and therefore the electrical generators is the nuclear reactor core rather than the fossil fuel furnace. We focus here on that core, what is known as the *nuclear steam supply system* or *NSSS*, assuming the reader is familiar with the rest of the equipment (known as the *balance of plant*).

Some typical data on some of the principal types of nuclear power generation reactors is listed in table 5.1. These differ primarily in terms of the nuclear fuel being utilized and therefore the nuclear fuel cycle involved (see section 2.2) and this distinguishes the LWRs from the HWRs and the FBRs. The two LWR types are then distinguished by the strategy to handle the possibility of the cooling water boiling and therefore by the pressure of the primary cooling water system and the corresponding safety systems. We will address each of these features in remainder of the book.

5.2 Light water reactors (LWRs)

5.2.1 Types of light water reactors (LWRs)

By far the greatest fraction of nuclear reactors used to produce power around the world belong to the class known as light water reactors (LWRs), in other words reactors that utilize *light* water (as opposed to *heavy water*) as the moderator and primary coolant. To be self-sustaining neutronically, a LWR with natural uranium fuel must use heavy water as the moderator in order to maintain the neutron flux. The Canadian-designed CANDU heavy water reactor operates on this basis and is described in more detail in section 5.7. LWRs, on the other hand require enriched uranium fuel in order to be self-sustaining. However, because light water absorbs neutrons as well as slowing them down it is less

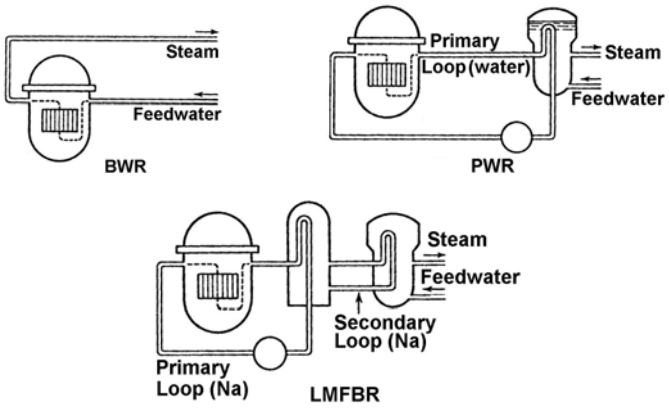

Figure 5.2: Schematics of a boiling water reactor, BWR, a pressurized water reactor, PWR, and a liquid metal fast breeder reactor, LMFBR. From Duderstadt and Hamilton (1976).

efficient as a moderator than heavy water or graphite.

Besides serving as both moderator and primary coolant, water has many advantages in this context. It is inexpensive and the technology of water cooling is very well known and tested; it also has a high heat capacity and a low viscosity so that the heat can be removed with relatively low flow rates and pressure drops. Burnable poisons which absorb neutrons are often added to the primary coolant water to provide some additional control over the reactivity and to even it out over time. Most importantly, in most (though not all) designs of LWRs, boiling of the water within the core leads to a decrease of reactivity and serves as an automatic reactor shutdown mechanism (see section 8.3).

Various types of light water reactors have been developed in the past decades. These can be subdivided into two principal types, namely Pressurized Water Reactors (PWRs) and Boiling Water Reactors (BWRs) that are described in sections 5.2.2 and 5.2.3.

5.2.2 Pressurized water reactors (PWRs)

The majority of light water reactors (LWRs) in operation in the world are known as *pressurized water reactors* (PWRs) because water is used to remove the heat from the core and because that primary coolant loop is pressurized in order to suppress boiling. In 2013 there were about 270 of these in commercial operation worldwide. An acceptably large thermodynamic efficiency is only achieved by having a primary cooling system that operates at a high maximum temperature, and these high temperatures would result in boiling unless that primary coolant loop were pressurized. The alternative would be to allow boiling and to remove most of the heat from the core in the form of latent heat; that alternative strategy is followed in the other major design, namely the boiling

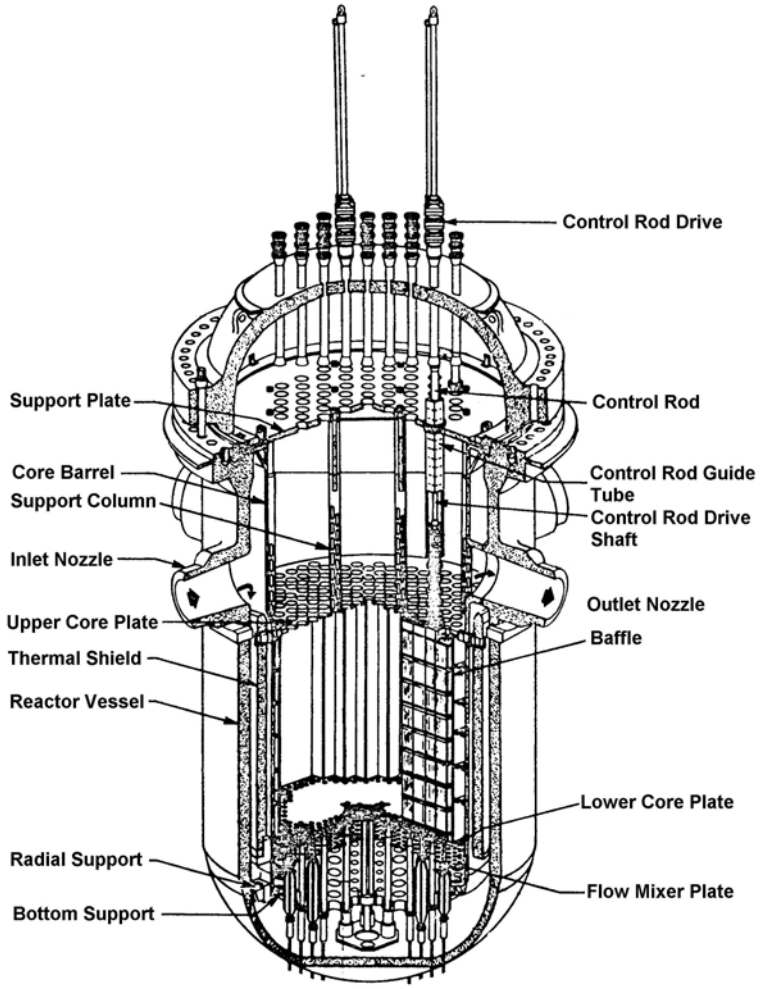

Figure 5.3: Internals of a typical PWR reactor vessel. Adapted from USAEC (1973).

water reactors (or BWRs) that are covered in the section that follows.

The typical PWR in the Unites States consists of a reactor vessel such as that illustrated in figure 5.3, that is serviced by a primary coolant system like that of figure 5.4 installed in a containment building such as that shown in figure 5.5 (see USNRC 1975). The primary coolant inlet and outlet temperatures (from the reactor vessel) are about $300°C$ and $330°C$ respectively but with the high specific heat of water this modest temperature difference is adequate to transport the heat at reasonable water flow rates of the order of $65 \times 10^6 kg/hr$. However to avoid boiling at these temperatures the pressure in the primary

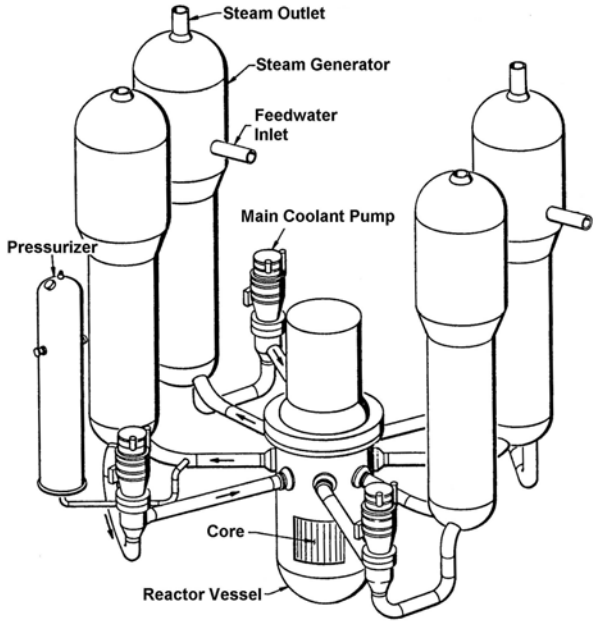

Figure 5.4: PWR coolant system. Adapted from USAEC (1973).

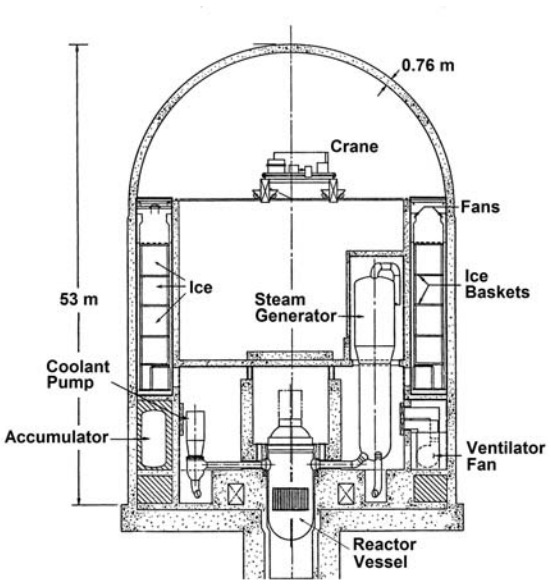

Figure 5.5: Typical PWR primary coolant loop and containment system. Adapted from USNRC (1975).

coolant loop is $155atm$; this is maintained by pressurizers (see figure 5.4) contained within the containment structure (figure 5.5). The high pressure makes for a compact reactor with a high power density. However, the high pressure is also a liability in an accident scenario and therefore this primary coolant loop is secured inside a heavy and strong containment building. A secondary coolant loop which operates at much lower pressure and is less susceptible to radioactive contamination communicates thermally with the primary loop in a heat exchanger and steam generator (figures 5.4, 5.5) within the containment building. The steam thus generated moves the heat outside of that building and is used to drive the steam turbines and electrical generators.

While this double coolant loop system involves some thermal inefficiency and some added equipment it has the advantage of confining the high pressure coolant water (and the radioactivity it contains) within the containment building. The building also houses extensive safety equipment that is described later in section 8.3.

5.2.3 Boiling water reactors (BWRs)

The concept behind the boiling water reactor (in 2013 there were about 84 of these in commercial operation worldwide) is to avoid the high pressures of PWRs (and thus the associated dangers) by allowing the primary coolant water to boil as it progresses through the reactor core. The steam thus generated is fed directly to the turbines, thus eliminating the secondary coolant loop (figure 5.6). Details of the reactor core of a BWR are shown in figure 5.7. By avoiding the high primary coolant loop pressures, this design reduces the need for a large and

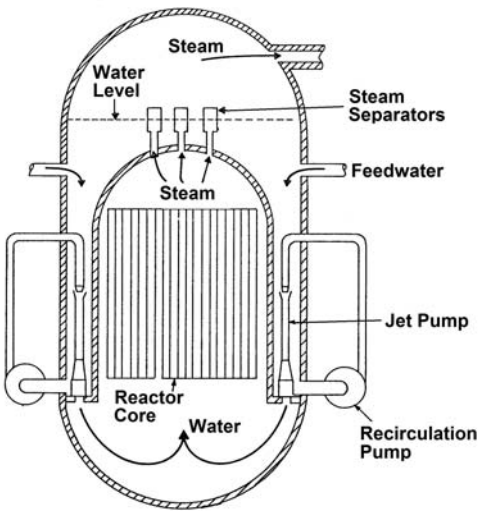

Figure 5.6: Schematic of the BWR coolant and steam supply systems. Adapted from USAEC (1973).

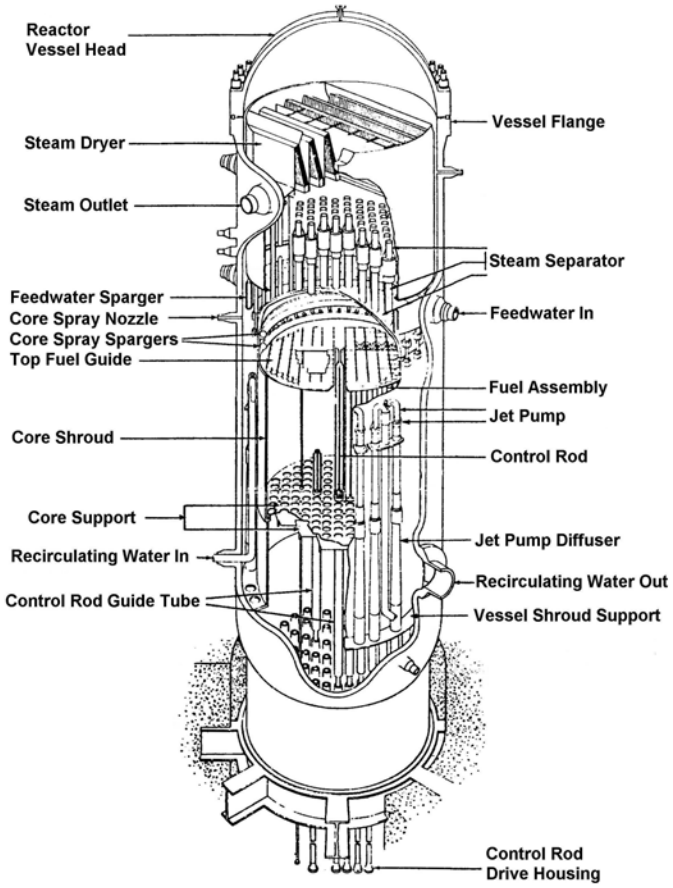

Figure 5.7: Typical BWR reactor vessel. Adapted from USAEC (1973).

costly containment structure since a rupture in the primary coolant loop would not lead to such a high build up of pressure inside that secondary containment.

Furthermore, General Electric who designed and built the BWRs devised a secondary containment structure which, in the event of a primary coolant loop rupture, would direct the steam down through pipes into a large body of water (known as a suppression pool) where it would be condensed. This would minimize the build up of steam pressure within the secondary containment. The first (or Mark I) suppression pool was toroidal in shape as shown in figures 5.8. Later several other pressure suppression configurations were produced. Further comment on the issues associated with primary coolant loop rupture in a BWR are delayed until later (section 8.3).

The elimination of the secondary or intermediate coolant loops is advantageous for the thermal efficiency of the unit but it also means increased build-up of radioactivity in the turbines. Other features of the BWR include the effect

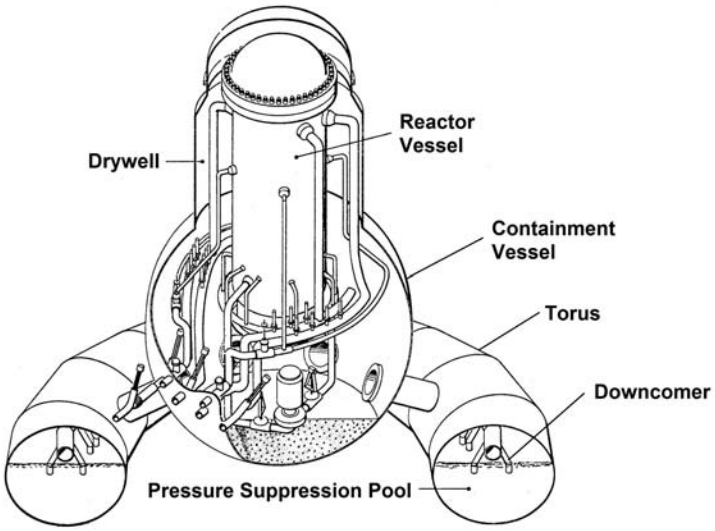

Figure 5.8: Schematic of the BWR (Mark I) primary containment and pressure suppression systems. Adapted from USAEC (1973).

of the steam/water mixture on the moderator role played by the coolant (see section 8.3 on reactor control).

5.2.4 Fuel and Control Rods for LWRs

The uranium dioxide fuel in a PWR or BWR is formed into cylindrical pellets that are packed into zircaloy tubes about $3.5m$ in length known as fuel rods (figure 5.9). In a typical PWR the pellets are $0.97cm$ in diameter and the fuel rods have an outside diameter of $1.07cm$; in a typical BWR the corresponding diameters are $1.24cm$ and $1.43cm$ respectively. Typically the core contains $55,000$ and $47,000$ fuel rods respectively in a PWR and BWR. As we shall see in section 6.3 these dimensions imply cylindrical reactor core dimensions (height and diameter) of about $3.6m$ and $4.4m$ respectively.

The fuel rods are arranged in *fuel assemblies* or *fuel bundles* as shown in figure 5.9. In a PWR the typical arrangement in a fuel assembly consists of a square cross-sectioned cell (figure 5.10, left) containing about 200 equally spaced fuel rods interspersed with about 20 circular control rod channels; the coolant in the cell flows in the spaces between these elements. There are about 200 of these assemblies arranged, lattice-like in a PWR core. A BWR core also consists of cells (figure 5.10, right) each containing about 64 fuel rods arranged in a square channel through which the coolant flows. Four of these cells are grouped together with the rectilinear space between them containing the cruciform-shaped control blade. There are about 180 such groups of four assemblies in a BWR core.

Thus the fuel rods, control rods, moderator, coolant channels, etc. in a

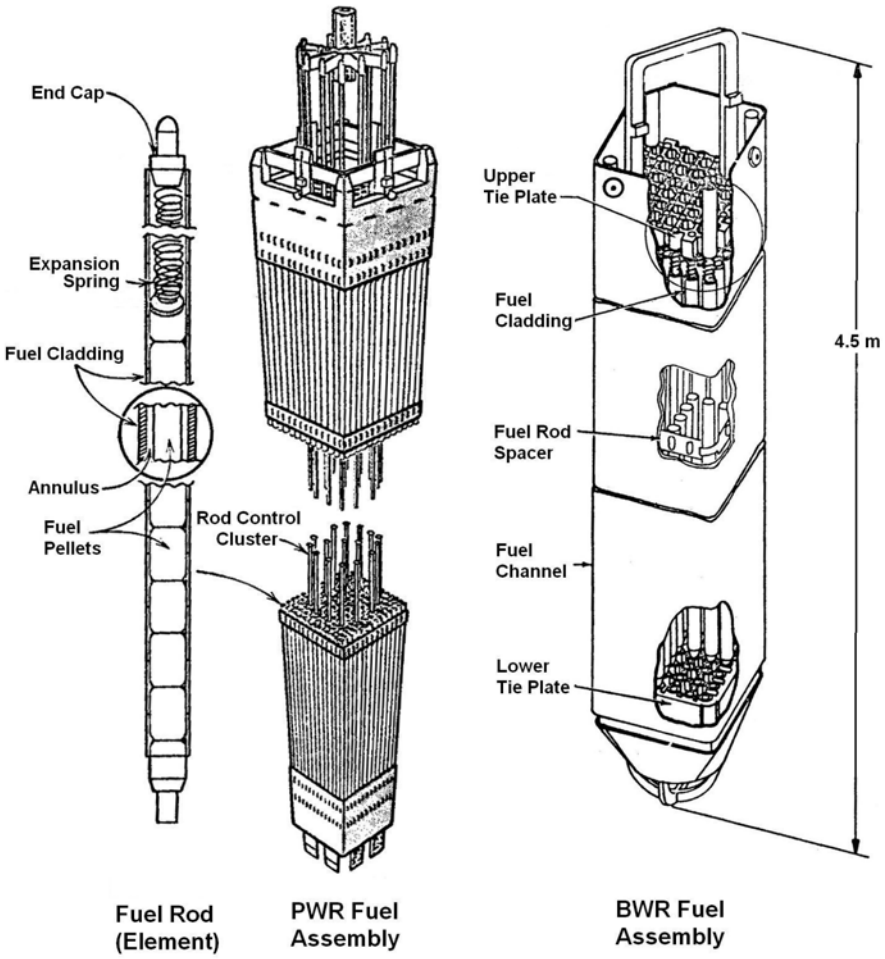

Figure 5.9: Fuel element and PWR fuel assembly (from Duderstadt and Hamilton 1976) and BWR fuel assembly (from USAEC 1973).

reactor are usually arranged in *lattice cells* that are repeated across the cross-section of the core. Consequently there are several structural or material scales within the core and these various scales of inhomogeneity become important in some of the more detailed calculations of the neutron flux within the reactor (see section 4.6.6).

5.2.5 LWR control

The need to maintain tight control on the operation of a nuclear reactor is self-evident and this control is maintained using a variety of tools, managerial,

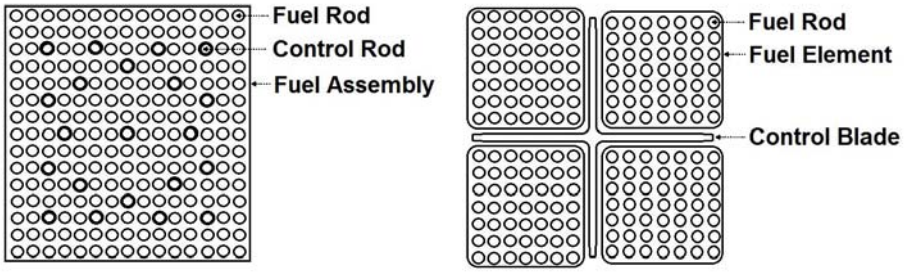

Figure 5.10: Cross-sections of PWR (left) and BWR (right) fuel assemblies.

mechanical and chemical. In section 4.9 we found that control was made much easier, indeed one might say made practical, by the delayed neutrons which extend the neutronic response time of the reactor core by several orders of magnitude. Indeed if the neutron population consisted only of prompt neutrons the calculations of section 4.9 demonstrate that the reactor control system would have to respond in fractions of a second in order to maintain control. The presence of delayed neutrons allows response times of the order of tens or hundreds of seconds to maintain control. The corollary is that the prompt neutron population of a reactor must always be maintained well below the critical level in all sections of the reactor core and throughout the history of the fuel load. It is the delayed neutrons that are used to reach criticality and are manipulated to increase or decrease the power level.

The primary mechanical devices that are used to effect control are the control rods (or structures) that are inserted into channels in the core as described in the preceding section. These are fabricated from material that absorbs neutrons and, when inserted, decrease the reactivity of the core. The materials used include boron, cadmium and gadolinium. As indicated in figure 5.9 the control rods are usually motor-driven from above and sometimes set to drop into the core without power in emergency situations. A full control rod insertion under emergency conditions is referred to as a *scram* and the process as *scram control*. The control rods are also used to adjust the power output from the reactor and to compensate for the aging of the fuel over longer periods of time (known as *shim control*). Typically a LWR is initially loaded with enough fuel to achieve a multiplication factor, k, (see section 2.3.1) of as much as 1.25 and therefore sufficient control rod insertion is needed to balance the reactor. As fuel life is expended the insertion is correspondingly decreased.

In addition to the control rods, several other methods are used to adjust the power level of the reactor, to compensate for the aging of the fuel and to balance the power produced in different regions of the core. Absorbing materials are sometimes fixed in the core in order to age with the fuel and even out the long term power production. Another strategy is to dissolve absorbing or *burnable* poison such as boric acid in the coolant.

5.3 Heavy water reactors (HWRs)

An alternative thermal reactor design that uses natural rather than enriched uranium is the heavy water reactor (HWR). The principal representative of this class of reactors is the Canadian-built CANDU reactor (see, for example, Cameron 1982) of which there are about 48 in commercial operation worldwide (in 2013). A schematic of the CANDU reactor is included in figure 5.11. The use of natural uranium fuel avoids the expense of the enrichment process. In an HWR the reactivity is maintained by using heavy water (D_2O) rather than light water as the moderator.

One of the unique features of the CANDU reactor is the refueling technique employed that is made possible by the natural uranium fuel. As depicted in figure 5.11, the fuel is contained in horizontal tubes and refueling is done continuously rather than in the batch process used in LWRs. Fueling machines inside the secondary containment push the natural uranium *fuel bundles* into the core and remove the spent fuel bundles at the other side of the reactor. The coolant, instead of being contained in a primary pressure vessel as in the LWRs, flows through the core in horizontal pressure tubes surrounding the fuel channels of which there are typically 380-480 in a CANDU reactor.

The cylindrical fuel bundles that are pushed through the core in the fuel

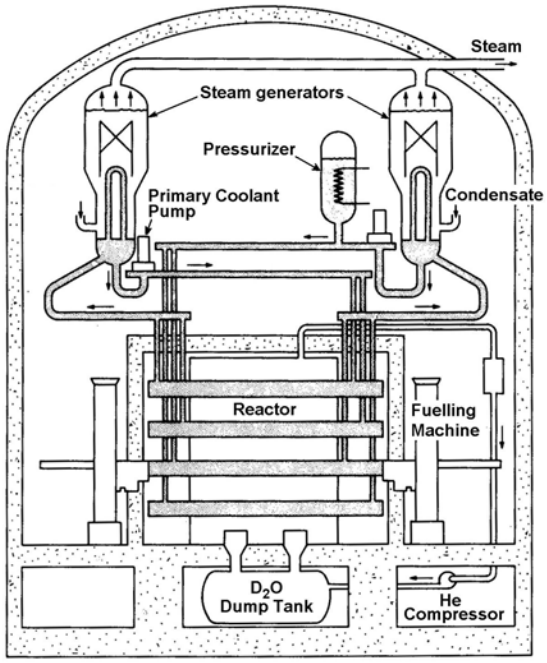

Figure 5.11: Schematic of the CANDU heavy water reactor. From Collier & Hewitt (1987).

channels are about $10cm$ in diameter and $50cm$ long. They consist of a zircaloy package of about $30-40$ zircaloy fuel tubes that contain the fuel in pellet form. In an older model there were twelve of these fuel bundles lying end-to-end within each fuel channel. Light water coolant flows through high-pressure tubes surrounding the fuel channels and these high-pressure coolant tubes are in turn surrounded by a *calandria tube* containing a thermally-insulating flow of carbon dioxide gas. All of this tube assembly is contained in a much larger, low-pressure tank known as the *calandria* that contains most of the heavy water moderator. The carbon dioxide flow placed between the light-water coolant and the heavy water moderator is needed to prevent the hot coolant from boiling the moderator. Note that a cooling system is also needed for the heavy water moderator; this moderator mass represents a heat sink that provides an additional safety feature.

As described in section 2.5.1, the heavy water moderator is needed with natural uranium fuel because the heavy water absorbs a lesser fraction of the neutrons and thus allows a sustainable chain reaction. However, a larger presence of heavy water moderator is needed to slow the neutrons down to thermal energies (because the heavier deuterium molecule needs more collisions to slow down the neutrons) and therefore the CANDU reactor requires a larger thickness of moderator between the fuel bundles. This means a proportionately larger reactor core.

One of the disadvantages of the CANDU reactor is that it has a positive void coefficient (see section 7.7.2). In other words, steam formed by coolant boiling would cause an increase in the reactivity that, in turn, would generate more steam. However, the much larger and much cooler mass of moderator in the calandria would mitigate any potential disassembly. Other features of the design that improve the margin of safety include the basic fact that natural uranium fuel is not critical in the light water coolant and the fact that any distortion of the fuel bundles tends to reduce the reactivity. The CANDU reactor also contains a number of active and passive safety features. As well as the normal control rods, shut-off emergency control rods are held above the core by electromagnets and drop into the core if needed. Another high pressure safety system injects a neutron absorber into the calandria in the event of an emergency.

5.4 Graphite moderated reactors

One of the older Russian designs, notorious because of the Chernobyl disaster, is the enriched uranium, water-cooled BWR known by the initials RBMK. This is shown schematically in figure 5.12. There are still more than 10 of these in commercial operation worldwide though substantial modifications have been made since the disaster. For moderator, these reactors utilize graphite as well as the coolant water and have the severe disadvantage that additional boiling within the core does not necessarily lead to a decrease in reactivity. Rather, the reactivity can increase as a result of a loss of coolant and this was a major

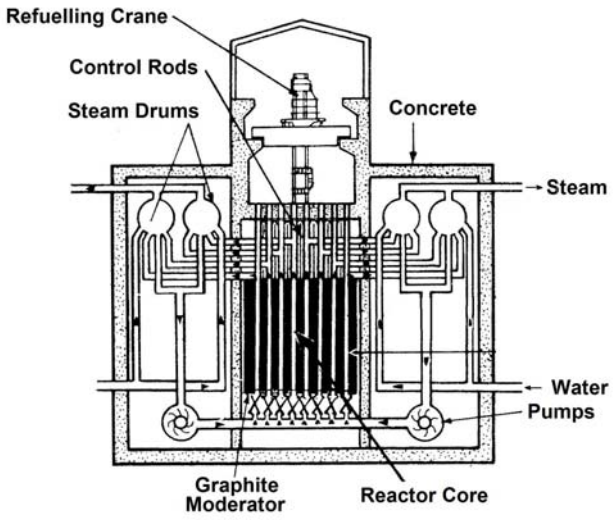

Figure 5.12: Schematic of the Chernobyl RBMK boiling water reactor. Adapted from Mould (2000).

factor in the Chernobyl accident (see section 8.4.2).

5.5 Gas cooled reactors

Yet another alternative is the gas-cooled reactor design (see, for example, Gregg King 1964). Some 17 of these are currently (2013) in commercial operation (mostly in the UK), cooled by CO_2 and moderated by graphite. Early versions (now superseded) utilized natural uranium though this required large cores. The more recent, advanced gas reactors (AGR) use enriched uranium as fuel. Their design is shown conceptually in figure 5.13 (Winterton 1981). The CO_2 flows up through channels in the bricks of the graphite moderator. These channels are interspersed with control rod channels. The entire core is surrounded by a thermal shield and the CO_2 flow loop includes passes up the outside of the shield and down its inside before entering the bottom of the core. Heat exchanger/steam generator tubes to transfer the heat to the secondary water coolant circuit are enclosed with core in the primary containment structure, a pre-stressed concrete vessel.

We should also take note of the more recently proposed design in the USA, the high-temperature gas-cooled reactor (HTGR) that utilizes high pressure helium as the coolant (Duderstadt and Hamilton 1976). This design has a quite different fuel cycle with an initial reactor core loading of highly enriched uranium carbide along with thorium oxide or carbide and graphite moderator. The design has the advantage of more efficient use of the uranium though whether it will

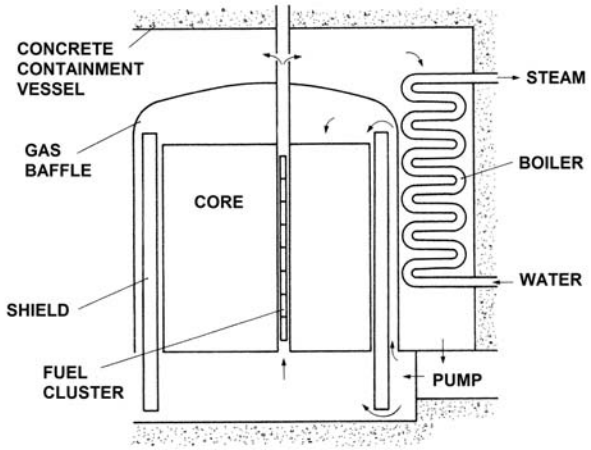

Figure 5.13: Schematic of the typical advanced gas reactor. Adapted from Winterton (1981).

be used for power generation remains to be seen.

5.6 Fast neutron reactors (FNRs)

As described in section 2.6, the label *fast neutron reactor* (FNR) refers to a broad class of reactors that rely on fast neutrons alone to sustain the chain reaction. Consequently there is no moderator. Various fuels and combinations of fuels can provide the required self-sustaining reaction. However, they are most often fueled with plutonium or a mixture of uranium and plutonium. Since there is a large store of highly enriched uranium that has been produced for military purposes, this is sometimes added to the fuel of fast reactors.

Often the core of a fast reactor is surrounded by a *blanket* of fertile ^{238}U in which the neutron flux from the central core produces or breeds additional plutonium; indeed in the presently constructed fast breeder reactors (FBRs) most of the ^{239}Pu is produced in this blanket. Alternatively, an FBR may be fueled by weapons-grade plutonium as in the Russian BN-600 reactor (see below) and, in that case, the blanket is removed to be replaced by a reflector.

5.7 Liquid metal fast breeder reactors (LMFBRs)

Since their power density is significantly higher than LWRs, the FBRs that have been constructed have been cooled by liquid metal since the moderator effect of water is unwanted and liquid metals have low moderating effect. Moreover, liquid metals have the advantage that they have a high thermal conductivity

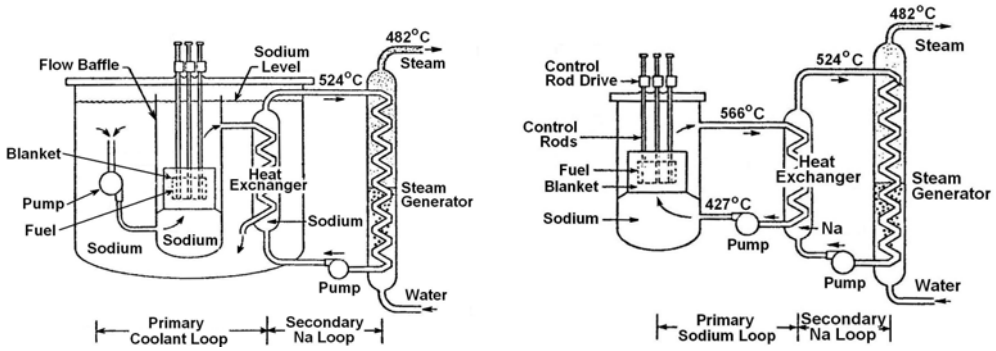

Figure 5.14: Schematics of a pool-type and a loop-type liquid metal fast breeder reactor. Adapted from Wilson (1977).

and can be operated at low pressures. This avoids the dangers that are associated with the high pressures in water-cooled reactors. Despite this there are substantial safety issues associated with FBRs that are addressed in section 8.6 and that have limited their deployment to date. Nevertheless there are some 20 LMFBRs in the world that are currently producing electricity and many more proposals have been put forward.

Sodium has been the universal choice for the primary coolant in LMFBRs for several reasons. First, with a low atomic weight of 23, the scattering cross-section for sodium is small and therefore the neutron loss due to slowing is limited (lithium is another possibility though, as yet, unused). Sodium also has high thermal conductivity making it a good coolant even though its heat capacity is about one third that of water. Though it does have a high melting point that requires a high primary coolant loop temperature ($380 - 550°C$), its boiling point is also very high so the pressure of the loop does not have to be very high to suppress boiling ($14atm$). Of course, the violent reactions with air and water require a very tight coolant loop system and some well-designed safety systems. Sodium also becomes radioactive when bombarded with neutrons and so the primary coolant loop must be confined within a containment system and the heat removed by means of a heat exchanger and a secondary coolant loop. This secondary loop also uses liquid sodium, but does not have the radioactivity of the primary coolant.

Two types of LMFBRs have been designed and constructed, the distinction being the configuration of the primary coolant loop. The so-called loop-type and pool-type LMFBRs are sketched diagrammatically in figure 5.14. In the loop-type the primary coolant is circulated through the core by a primary coolant pump in the conventional way. Because of the high radioactivity all these components require substantial shielding. These shielding requirements are significantly simplified in the other pool-type reactor in which the core is submerged in a pool of sodium that is part of the primary coolant loop and this pool as well as the heat exchanger to the secondary coolant loop are all enclosed

in a large containment vessel. The Russian BN-600 reactor (figure 5.15) and the French Phenix reactors (figure 5.16) are both examples of pool-type LMFBRs.

In most LMFBRs the fuel rods consist of stainless steel tubes about $0.6cm$ in diameter containing the fuel pellets of oxides of uranium and plutonium. The rods are held apart by spacers and packed in fuel assemblies contained in stainless steel cans about $7.6cm$ across and $4.3m$ long. There are typically 217 fuel rods in each assembly and 394 assemblies in a reactor core. Arranged around the periphery of the core are the *blanket* fuel rods, that contain only uranium dioxide. Such a design creates a central *driver* section in the core surrounded on all sides by the blanket whose primary purpose is the breeding of new plutonium fuel (see section 5.6). The core is quite small compared to a LWR core, measuring about $90cm$ high and $220cm$ in diameter for a core volume of $6.3m^3$. It therefore has an *equivalent* cylindrical diameter and height of about $2.0m$. We comment on these reactor dimensions in section 6.4. The flow pattern is similar to that of a PWR core in that the liquid sodium coolant flows upward though the core assembly and exits through the top of the core.

The BN-600 (figure 5.15) is a Russian, pool-type, liquid sodium cooled LMFBR that has been generating $600MW$ of electricity since 1980 and is currently (2013) the largest operating fast breeder reactor in the world. The core (about $1m$ tall with a diameter of about $2m$) has 369, vertically mounted fuel assemblies each containing 127 fuel rods with uranium enriched to $17 - 26\%$. The control and shutdown system utilizes a variety of control rods and the entire primary coolant vessel with its emergency cooling system is contained in a heavily reinforced concrete containment building. The primary sodium cooling loop proceeds through a heat exchanger transferring the heat to a secondary sodium loop that, in turn, transfers the heat to a tertiary water and steam cooling loop that drives the steam turbines. The world of nuclear power generation watches this reactor (and a sister reactor under construction, the BN-800) with much interest as a part of their assessment of safety issues with fast breeder reactors and therefore with their future potential. Though there have been a number of incidents involving sodium/water interactions and a couple of sodium fires, the reactor has been repaired and resumed operation.

The Phenix was a small prototype $233MW$ LMFBR constructed by the French government. Shown diagrammatically in figure 5.16 it was a pool-type, liquid sodium cooled reactor that began supplying electricity to the grid in 1973. This led to the construction of the larger Superphenix that began producing electricity in 1986 though it was notoriously attacked by terrorists in 1982. Despite this and other public protests it was connected to the grid in 1994. As a result of public opposition and some technical problems, power production by the Superphenix was halted in 1996. The Phenix continued to produce power until it, too, was closed in 2009. It was the last FBR operating in Europe.

The Clinch River Breeder Reactor was an experimental reactor constructed by the US government as part of an effort to examine the feasibility of the LMFBR design for commercial power generation. It was a $350MW$ electric, sodium-cooled, fast breeder reactor (see figure 5.17) whose construction was first authorized in 1970. Funding of the project was terminated in 1983, in part

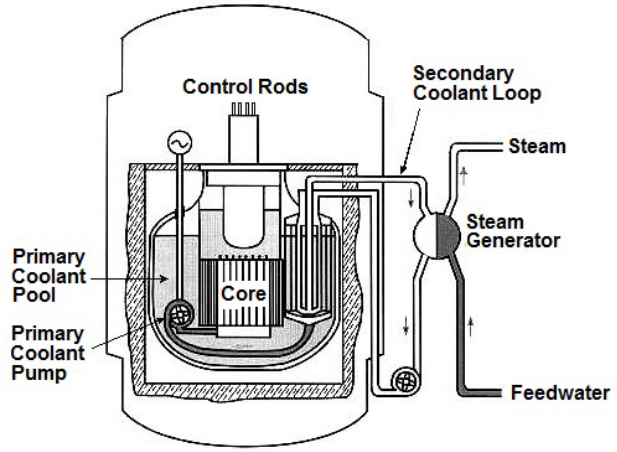

Figure 5.15: Schematic of Russian BN-600 pool-type LMFBR.

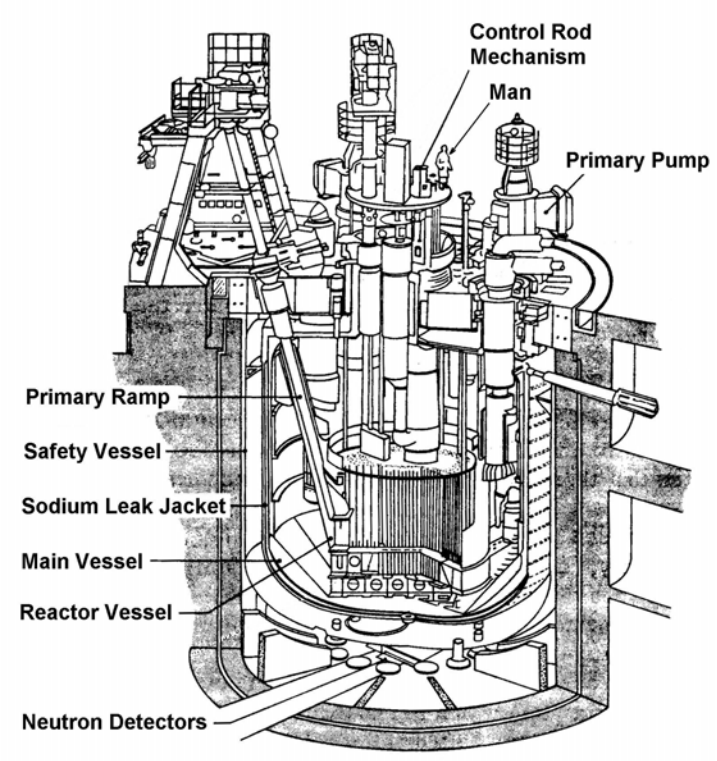

Figure 5.16: Schematic of the Phenix reactor in Marcoule, France. Adapted from Wilson (1977).

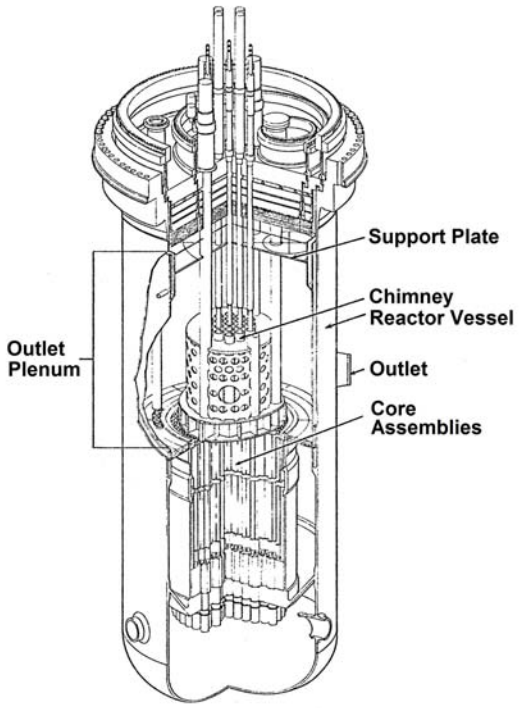

Figure 5.17: Clinch River breeder reactor. Adapted from CRBRP (1976).

because of massive cost overruns. The project demonstrated the potentially high costs of constructing and operating a commercial LMFBR reactor. Moreover, in 1979 as these problems were emerging, the Three Mile Island accident (see section 8.4.1) occurred. This clearly demonstrated that more attention needed to be paid to the safety of existing LWR plants and highlighted the potentially more serious safety issues associated with LMFBRs (see section 8.5.3). Despite these issues, the potential technical advantages of the breeder reactor cycle mean that this design will merit further study in the years ahead.

Although virtually all present day LMFBRs operate with uranium-plutonium oxide fuel, there is considerable interest in the future use of fuel composed of uranium-plutonium carbide, since large breeding ratios are possible with this kind of fuel. This, in turn, is due to the fact that while there are two atoms of oxygen per atom of uranium in the oxide, there is only one atom of carbon per uranium atom in the carbide. Light atoms such as carbon and oxygen tend to moderate fission neutrons, and since there are fewer of the atoms in the carbide than in the oxide, it follows that the energy distribution of neutrons in a carbide-fueled LMFBR is shifted to energies higher than in a comparable oxide-fueled reactor.

References

Cameron, I.R. (1982). *Nuclear fission reactors.* Plenum Press, New York & London.

CRBRP (1976). *Clinch river breeder reactor plant technical review.* CRBRP-PMC 76-06.

Collier, J.G. and Hewitt, G.F. (1987). *Introduction to nuclear power.* Hemisphere Publ. Co.

Duderstadt, J.J. and Hamilton, L.J. (1976). *Nuclear reactor analysis.* John Wiley and Sons, New York.

Gregg King, C.D. (1964). *Nuclear power systems.* The Macmillan Company, New York.

Jones, O.C. and Bankhoff, S.G. (editors) (1977a). *Symposium on the Thermal and Hydraulic Aspects of Nuclear Reactor Safety. Volume 1: Light Water Reactors.* ASME, New York.

Jones, O.C. and Bankhoff, S.G. (editors) (1977b). *Symposium on the Thermal and Hydraulic Aspects of Nuclear Reactor Safety. Volume 2: Liquid Metal Fast Breeder Reactors.* ASME, New York.

Lahey, R.T. Jr. (1977). *The status of boiling water nuclear reactor safety analysis.* In Jones, O.C. and Bankhoff, S.G.(1977a).

Mould, R.F. (2000). *Chernobyl record : the definitive history of the Chernobyl catastrophe.* Publ. Institute of Physics.

USAEC (1973). The safety of nuclear power reactors (light water cooled) and related facilities. *U.S. Atomic Energy Commission*, Rep. WASH-1250.

USNRC (1975). Reactor safety study. An assessment of accident risks in U.S. commercial nuclear power plants. *U.S. Nuclear Regulatory Commission*, Rep. WASH-1400.

Wilson, R. (1977). Physics of liquid metal fast breeder reactor safety. *Rev. Mod. Phys.*, **49**, No.4, 893-924.

Winterton, R.H.S. (1981). *Thermal design of nuclear reactors.* Pergamon Press.

Chapter 6

CORE HEAT TRANSFER

6.1 Heat production in a nuclear reactor

6.1.1 Introduction

In this chapter we analyze the heat transfer process within a normally operating reactor core and thereby establish the conditions in the core during the normal power-production process. It is best to begin with an individual fuel rod and gradually move outward toward an overview of the entire core. For more detailed analyses, the reader is referred to texts such as Gregg King (1964), Tong and Weisman (1970), Todres and Kazimi (1990) and Knief (1992).

6.1.2 Heat source

As discussed earlier, heat is produced within a nuclear reactor as a result of fission. The energy released is initially manifest primarily as the kinetic energy of fission products, of fission neutrons and of gamma radiation. Additional energy is released as the fission products later decay as discussed in section 2.3.4. The kinetic energy is then converted to thermal energy as a result of the collisions of the fission products, fission neutrons and gamma radiation with the rest of molecules in the reactor core. The majority of this energy (about 80%) is derived from the kinetic energy of the fission products. The fission neutrons and gamma radiation contribute about another 6% of the immediate heat production. This immediate energy deposition is called the *prompt heat release* to distinguish it from the subsequent, *delayed heat release* generated by the decay of the fission products. This decay heat is significant and contributes about 14% of the energy in an operating thermal reactor. As discussed earlier in section ES1a, the fission product decay not only produces heat during normal reactor operation but that heat release continues for a time after reactor shutdown. Typically, after shutdown, the heat production decreases to 6.5% after one second, 3.3% after one minute, 1.4% after one hour, 0.55% after one day, and 0.023% after one year.

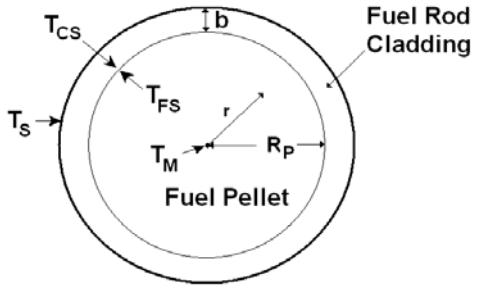

Figure 6.1: Schematic of the cross-section of a fuel pellet and fuel rod.

Most of this chapter focuses on how the heat deposited in the core is transferred out of the fuel and into the core during normal reactor operation. Since almost all of the heat deposited, whether prompt or delayed, is proportional to the neutron flux it will be assumed in the rest of this chapter that the rate of heat production is directly proportional to that neutron flux. At the scale of an individual fuel pellet, the neutron flux distribution can be considered uniform since the mean free path of the neutrons is large compared with the fuel rod dimensions. Consequently the rate of fission and therefore, to a first approximation, the rate of production of heat can be considered uniform within a fuel pellet. Thus the first component of the analysis that follows concentrates on how the heat is transferred from an individual fuel rod to the surrounding coolant.

But, the neutron flux does vary substantially from one fuel rod to another within the reactor core. Consequently, the second component of the analysis that follows focuses on how the heat transfer varies from point to point within the reactor core.

6.1.3 Fuel rod heat transfer

Consider first the heat transfer within an individual fuel rod. The cross-section of a fuel pellet is sketched in figure 6.1. The fuel pellet radius and thermal conductivity are denoted by R_f and k_f and the fuel rod cladding thickness and thermal conductivity by b and k_C. The temperatures in the center of the fuel rod, at the outer surface of the fuel pellet, at the inner surface of the cladding and at the outer surface of the fuel rod will be denoted by T_M, T_{FS}, T_{CS}, and T_S respectively. A small gap and/or a contact resistance is assumed so that $T_{FS} \neq T_{CS}$. It will also be assumed that the gradients of temperature in the axial direction are small compared with those in the radial direction and therefore that the primary heat flux takes place in the radial plane of figure 6.1. Consequently, if the rate of heat production per unit length of a fuel rod is denoted by $\mathcal{Q}$ and if this is uniformly distributed over the cross-section of the rod, then, in steady state operation, the radially outward heat flux (per unit

area) through the radial location, r, must be $\mathcal{Q}r/2\pi R_f^2$. Consequently the heat conduction equation becomes

$$\frac{\mathcal{Q}r}{2\pi R_f^2} = -k\frac{\partial T}{\partial r} \tag{6.1}$$

where $T(r)$ is the temperature distribution and k is the local thermal conductivity (k_f or k_C). Integrating in the fuel pellet, it follows that for $0 < r < R_f$:

$$T(r) = T_M - \frac{\mathcal{Q}}{4\pi R_f^2 k_f} r^2 \tag{6.2}$$

where we have applied the condition that $T = T_M$ at $r = 0$. Consequently the temperature at the surface of the fuel pellet is

$$T_{FS} = T_M - \frac{\mathcal{Q}}{4\pi k_f} \tag{6.3}$$

As a typical numerical example note that with a typical value of $\mathcal{Q}$ of $500 W/cm$ and a thermal conductivity of UO_2 of $k_f = 0.03 W/cm^\circ K$ the temperature difference between the surface and center of the fuel becomes $1400^\circ K$, a very substantial difference.

Assuming that the small gap and/or contact resistance between the fuel and the cladding gives rise to a heat transfer coefficient, h^*, where

$$k_f \left(\frac{\partial T}{\partial r}\right)_{r = R_f \text{ in fuel}} = k_C \left(\frac{\partial T}{\partial r}\right)_{r = R_f \text{ in cladding}} = -h^* \{T_{FS} - T_{CS}\} \tag{6.4}$$

It follows that

$$T_{CS} = T_M - \frac{\mathcal{Q}}{4\pi k_f} - \frac{\mathcal{Q}}{2\pi R_f h^*} \tag{6.5}$$

Integration of equation 6.1 in the cladding ($R_f < r < R_f + b$) leads to

$$T(r) = C - \frac{\mathcal{Q}}{4\pi R_f^2 k_C} r^2 \tag{6.6}$$

where C is an integration constant. Applying the condition that $T = T_{CS}$ at $r = R_f$ yields a value for C and, finally, the fuel rod surface temperature is obtained as

$$T_S = T_M - \frac{\mathcal{Q}}{4\pi}\left[\frac{1}{k_f} + \frac{2}{h^* R_f} + \frac{\left\{(1 + b/R_f)^2 - 1\right\}}{k_C}\right] \tag{6.7}$$

Typical temperature differences in a LWR, across the fuel/cladding gap, across the cladding and between the cladding surface and the bulk of the coolant might be of the order of $200^\circ K$, $80^\circ K$ and $15^\circ K$ respectively so that the temperature difference between the water and the center of the fuel pellet is dominated by

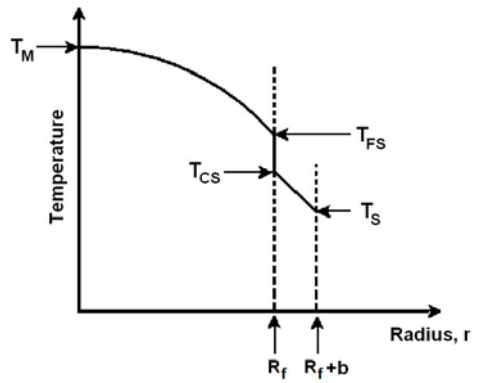

Figure 6.2: The general form of the radial temperature distribution within a fuel rod.

the temperature difference in the fuel and has a magnitude of about $1400°K$. In summary, the radial temperature distribution in a fuel rod is given by equations 6.2, 6.3, 6.5, 6.6 and 6.7 and the general form of this distribution is illustrated in figure 6.2.

Since the objective is to extract heat from the fuel it is desirable to maintain a large heat production rate, $\mathcal{Q}$, using a proportionately large neutron flux. A large $\mathcal{Q}$ and therefore a large power density is desirable for several reasons. First it minimizes the size of the reactor core for a given power production level and thereby reduces the cost of the core and the cost and size of the rest of the structure that contains the core. Second, higher temperature differences across the core lead to higher thermal efficiencies in the turbines driven by the coolant.

But a high $\mathcal{Q}$ implies large temperature differences within the fuel rods and therefore high temperatures. Thus, limiting design factors are the maximum allowable temperature in the fuel, T_M, which must be much less than the melting temperature and, similarly, a maximum temperature in the cladding, T_{CS}. Moreover the temperature of the wall in contact with the coolant, T_S, will also be constrained by boiling limits in the coolant. Any or all of these factors will limit the heat production since the temperature differences are proportional to $\mathcal{Q}$. It is also clear that the temperature differences for a given heat production per unit fuel volume (or a given neutron flux) are reduced by decreasing the size of the fuel pellets, R_f. But to yield the required power from the reactor this means increasing the number of fuel rods and this increases the cost of the core. Consequently a compromise must be reached in which the number of fuel rods is limited but the temperature differences within each rod are maintained so as not to exceed a variety of temperature constraints.

It is valuable to list some secondary effects that must also be factored into this fuel rod analysis:

- The neutron flux in the center of the fuel rod is somewhat less than at larger radii because thermal neutrons that enter the fuel from the mod-

erator or coolant are absorbed in greater number near the surface of the fuel. This helps even out the temperature distribution in the fuel.

- The fuel is often UO_2 whose manufacture causes small voids that decrease the thermal conductivity of the pellet and increase the temperature differences.

- As the fuel is used up the gap between the fuel pellet and the cladding tends to increase causing a decrease in h^* and therefore an increase in the temperature of the fuel.

- The thermal conductivity of the fuel increases with temperature and therefore, as the heat production increases, the temperature differences in the fuel increase with $\mathcal{Q}$ somewhat less than linearly.

- Fission gases are released by nuclear reactions in the fuel and this can lead to significant build up of pressure within the fuel rods that are, of course, sealed to prevent release of these gases. The gas release increases rapidly with temperature and hence there is an important design constraint on the fuel temperature that is required in order to limit the maximum pressure in the fuel rods. This constraint is often more severe than the constraint that T_M be less than the fuel melting temperature.

Despite these complicating factors, it is useful to emphasize that the leading constraint is the maximum allowable temperature in the center of the fuel as we will discuss in sections 6.3 and 6.4.

6.1.4 Heat transfer to the coolant

It is appropriate at this juncture to give a brief summary of the heat transfer to the coolant in order to complete this review of the temperature distribution in the reactor core. In the notation of section 6.1.3, the heat flux, $\dot{q}$, from the fuel rod to the coolant per unit surface area of the fuel rod is given by $\mathcal{Q}/\mathcal{P}$ where $\mathcal{P}$ is the cross-sectional perimeter of the fuel rod. Though it is overly simplistic, the easiest way to relate the temperature differences in the coolant to this heat flux, is by defining a heat transfer coefficient, h, as

$$\dot{q} = \frac{\mathcal{Q}}{\mathcal{P}} = h(T_S - T_C) \tag{6.8}$$

where T_S and T_C are respectively the local temperature of the surface of the fuel cell and the local temperature of the coolant far from that surface. The coefficient, h, is, however, a complicated function of the transport properties of the coolant and of the coolant channel geometry. To express this function we introduce a dimensionless heat transfer coefficient known as the Nusselt number, Nu, defined by hD_h/k_L where D_h is the *hydraulic diameter* of the coolant channel (see section 7.3.4) and k_L is the thermal conductivity of the coolant. The hydraulic diameter is 4 times the cross-sectional area of the channel divided

by the perimeter of that cross-sectional area and applies to a range of cross-sectional geometries of the coolant channel. We also define the *Reynolds number* of the channel flow, $Re = \rho_L U D_h/\mu_L$, where U is the volumetrically averaged coolant velocity and ρ_L and μ_L are the density and viscosity of the coolant and we define a *Prandtl number*, $Pr = \mu_L c_p/k_L$, where c_p is the specific heat of the coolant. It transpires that Nu is a function of Re and Pr; however that functional relation changes depending on a number of factors including whether the Prandtl number is large or small and on whether the channel flow is laminar or turbulent. Commonly used correlations are of the form $Nu = CPr^{C_1}Re^{C_2}$ where C, C_1 and C_2 are *constants*. For details of these correlations the reader is referred to heat transfer texts (for example, Rohsenow and Hartnett 1973). For simplicity and illustrative purposes, we shall assume that h is a known constant that, in the absence of boiling, is uniform throughout the reactor core. The case of boiling, either in a boiling water reactor or during an excursion in a normally non-boiling reactor, will be covered later.

The next step is to subdivide the coolant flow through the reactor core into a volume flow rate, $\dot{V}$, associated with each individual fuel rod. As that flow proceeds through the core it receives heat from the fuel rod at a rate of $\mathcal{Q}dz$ for an elemental length, dz, of the rod. As a result, the temperature rise in the coolant over that length is dT where

$$\rho_L \dot{V} c_p \frac{dT}{dz} = \mathcal{Q} \tag{6.9}$$

We will proceed to integrate this rate in order to obtained the temperature distribution over the length of a coolant channel. In order to do so we need the variation of $\mathcal{Q}$ with z. This is roughly proportional to the variation of the neutron flux with z. As seen in chapter 4 this neutron flux distribution also varies with the radial location, r, within the reactor core; it also depends on control factors such as the extent of the control rod insertion (section 4.7.4).

6.2 Core temperature distributions

As a representative numerical example of the temperature distribution in a reactor core consider a homogeneous cylindrical reactor without reflectors and without control rod insertion. The neutron flux has the form given by equation 4.41 (coordinates defined in figure 4.1) and therefore $\mathcal{Q}$ will be given by

$$\mathcal{Q} = \mathcal{Q}_M \cos\left(\frac{\pi z}{H_E}\right) J_0\left(\frac{2.405r}{R_E}\right) \tag{6.10}$$

where the constant $\mathcal{Q}_M$ is the maximum value at the center of the reactor core. Note for future use that the average heat flux would then be about $0.4\mathcal{Q}_M$. Substituting equation 6.10 into equation 6.9 and integrating, the temperature of the coolant, T_C, within the reactor core becomes

$$T_C = T_{CI} + \frac{\mathcal{Q}_M H_E}{\pi \rho_L \dot{V} c_p} J_0\left(\frac{2.405r}{R_E}\right)\left[\sin\left(\frac{\pi z}{H_E}\right) + 1\right] \tag{6.11}$$

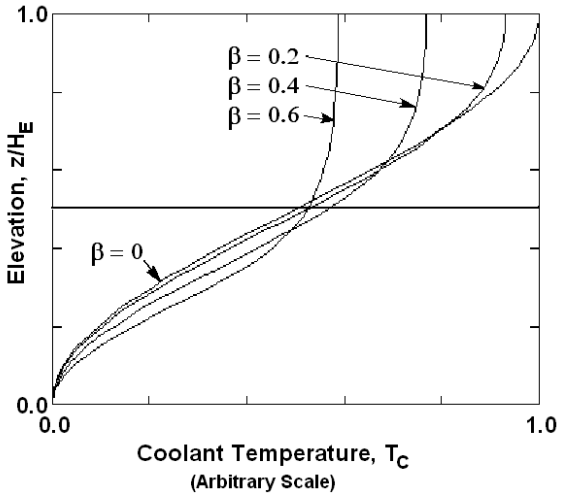

Figure 6.3: Axial coolant temperature distributions within a cylindrical reactor where the horizontal scale may differ for each line plotted. Solid lines: $\beta = 0$ is a homogeneous reactor and the lines for $\beta = 0.2$, 0.4 and 0.6 are for various control rod insertions corresponding to the neutron fluxes in figure 4.7 (for the case of $H_E/R_E = 2.0$ and $L_2/R_E = 0.36$).

where T_{CI} is the coolant inlet temperature. The form of this temperature distribution along the centerline of the reactor core ($r = 0$) is shown labeled $\beta = 0$ in figure 6.3. Similar integrations can readily be performed for the neutron flux distributions at various control rod insertions (see section 4.7.4) and three such examples are also included in figure 6.3. Note that the temperature rise in the upper part of the core is reduced due to the decrease in the heat production in that part of the reactor.

It is important to emphasize that, even in the absence of boiling (which we address in section 6.5), these calculations of the axial temperature distribution are only of very limited validity. In practical reactors variations in the fuel and moderator distributions are used to even out the heat distribution. Moreover, thermal and transport properties like the heat transfer coefficient may vary significantly within the reactor core. Nevertheless the above calculations combined with the knowledge of the radial distribution of temperature implicit in equation 6.11 and coupled with the temperature distribution within each fuel rod as described in section 6.1.3 allow construction of the temperatures throughout the core in a way that is qualitatively correct.

6.3 Core design - an illustrative LWR example

The results of the last few sections allow presentation of a simplistic but illustrative design methodology for the reactor core. In this section we focus on a

LWR example and, in the next section on a LMFBR example.

For the sake of our simplified numerical evaluation of a LWR core, we stipulate that the maximum temperature in the fuel must be well below the melting temperature of uranium dioxide, specifically much less than about $3000°K$. Consequently the usual red-line design maximum is in the range $2000-2300°K$. Since the maximum coolant temperature is about $500°K$ and the maximum temperature difference between the center of the fuel rod and the coolant is therefore about $1500-1800°K$, this effectively limits the heat flux from the fuel rod for a given radius, R_f, of that rod. Clearly from this perspective the smaller the rod the greater the potential power output but there are other considerations (such as the structural strength and the neutronics) that necessarily limit how small the fuel rod radius can be. These compromises led to fuel rod radii, R_f, of $0.53cm$ and $0.71cm$ respectively for the typical PWR and BWR.

Then equation 6.7 (or 6.3) determines the maximum heat flux allowable in the reactor. For a fuel thermal conductivity of $k_f = 0.03W/cm°K$ these equations yield a maximum allowable value of $\mathcal{Q}$ of about $430W/cm$ in the hottest part of the core. This, in turn, implies a red line value for the *average* heat flux of about $180W/cm$.

The next step is to stipulate the desired ratio of moderator volume to fuel volume, α_{mf}. This is primarily determined by nuclear considerations that dictate a moderator to fuel volume ratio of $\alpha_{mf} \approx 1$.

For this example we will seek to find the size of the cylindrical reactor needed for a $1150MW$ electric power plant with efficiency of 34% so that the thermal power generated by the core is $P = 3400MW$. For convenience we choose a cylindrical reactor of diameter, $2R$, and a height equal to that diameter. Then the fuel volume (neglecting the cladding volume) will be $2\pi R^3/(1+\alpha_{mf})$ and the required number of fuel rods, N_f, of the same height as the reactor will be

$$N_f = R^2 / \left[R_f^2(1+\alpha_{mf})\right] \tag{6.12}$$

Moreover the thermal power of the reactor power, P, will clearly be given by the heat added to the coolant during its passage through the core or

$$P = 2R\mathcal{Q}_{av}N_f \tag{6.13}$$

where $\mathcal{Q}_{av}$ is the average heat flux per unit fuel rod length, averaged over the volume of the reactor. If the maximum value of that heat flux is set at $420W/cm$ (see above) then a reasonable, illustrative value of this average would be $\mathcal{Q}_{av} = 180W/cm$. Substituting this value into equation 6.13 as well as the expression 6.12 for N_f and $P = 3400MW$ yields an expression for the dimension of the reactor, R. For the aforementioned values of α_{mf} and R_f this yields:

$$\textit{For PWR:} \quad R = 1.7m \quad ; \quad \textit{For BWR:} \quad R = 2.0m \tag{6.14}$$

values that are close to the actual volumetric-equivalent radii of $1.7m$ and $1.8m$ for the typical PWR and BWR respectively. Despite the crudeness of these calculations they indicate the order of magnitude of the dimensions of light water reactor cores.

In addition substitution back into equation 6.12 yields $N_f \approx 54,000$ and $N_f \approx 46,000$ for the PWR and the BWR respectively, values that are again close to the actual typical numbers of fuel rods, 56,000 and 47,000 respectively.

6.4 Core design - an LMFBR example

An illustrative LMFBR core design follows very similar lines though with numerical differences. The chosen fuel rod diameters are significantly smaller in order to allow higher heat fluxes (typical fuel rod radii are $0.38cm$). Liquid sodium coolant temperatures of the order of $820°K$ mean a maximum temperature difference between the fuel rod center and the sodium coolant of about $1500°K$. According to equation 6.3, this implies a maximum heat flux of $490W/cm$. If we then select an *average* maximum heat flux of $290W/cm$ equations 6.13 and 6.12 imply a reactor radius R of $1.1m$ for a $2600MW$ electric generating plant (we have also assumed that the fuel takes up one-half of the volume of the core). This reactor radius is close to the actual, typical volumetric-equivalent radius of an LMFBR core of $1.1m$, much smaller than a LWR core of the same power.

6.5 Boiling water reactor

6.5.1 Temperature distribution

If the temperature of the coolant reaches the boiling point before the top of the reactor then virtually all the heat generated will go into latent heat to produce vapor and the temperature above that boiling point elevation will remain approximately constant as illustrated in figure 6.4 (an adaption of figure 6.3). This is because the pressure change is small and so the thermodynamic state of the multiphase fluid remains at approximately the same saturated temperature and pressure while the mass quality of the *steam* flow, $\mathcal{X}$, increases with elevation (the mass quality, $\mathcal{X}$, is defined as the ratio of the mass flux of vapor to the total mass flux, see section 7.2.1). This relative constancy of the pressure and temperature will hold until all the liquid has evaporated. Of course, if the critical heat flux is reached (see secions 7.5.2 to 7.5.4 and 6.6 below) and film boiling (see sections 7.5.5 and 7.5.6) sets in the fuel rod temperature would rise rapidly and the potential for meltdown may exist. This critical accident scenario is discussed in chapter 8.

Above the elevation at which boiling starts and assuming that the critical heat flux is not reached, it is roughly true that all the heat flux from the fuel rods, $\mathcal{Q}$, is converted to latent heat. Therefore, it follows that the rate of increase of the mass quality, $d\mathcal{X}/dz$, in the coolant flow will be given by

$$\frac{d\mathcal{X}}{dz} = \frac{\mathcal{Q}}{\dot{m}\mathcal{L}} \tag{6.15}$$

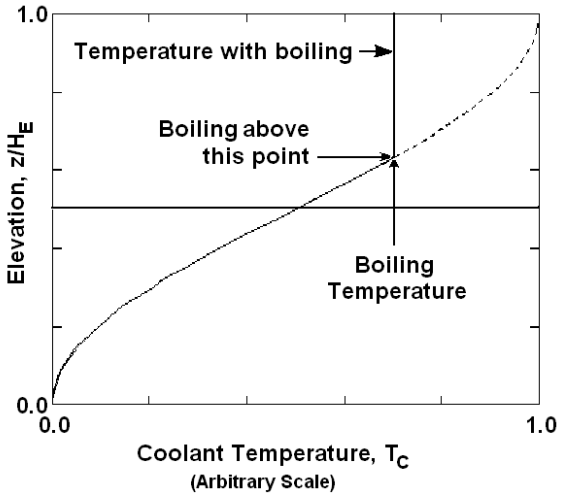

Figure 6.4: Typical modification of the axial coolant temperature distribution due to boiling where the curve below the boiling point is reproduced from figure 6.3.

where $\dot{m}$ is the mass flow rate per fuel rod (equal to $\rho_L \dot{V}$ below the boiling elevation) and $\mathcal{L}$ is the latent heat of the coolant. Since the temperature and pressure do not change greatly above the boiling point elevation, the latent heat, $\mathcal{L}$, is also relatively constant and therefore equation 6.15 can be written in the integrated form

$$\mathcal{X} = \frac{1}{\dot{m}\mathcal{L}} \int_{z_B}^{z} \mathcal{Q} dz \tag{6.16}$$

where z_B is the elevation at which boiling starts and where the mass quality is therefore zero. Note that the rate of increase of the mass quality decreases with the mass flow rate, $\dot{m}$, and increases with the heat flux, $\mathcal{Q}$.

The evaluation of the mass quality (and other multiphase flow properties) is important for a number of reasons, all of which introduce a new level of complexity to the analysis of the core neutronics and thermo-hydraulics. In the next section we consider how the calculations of these quantities might proceed.

6.5.2 Mass quality and void fraction distribution

Boiling in the flow channels changes the moderating properties of the fluid and hence the reactivity and this, in turn, will change the heat flux. Consequently it is necessary to perform simultaneous neutronics and multiphase flow calculations in order to properly establish the heat flux and two-phase flow conditions in the boiling region. Perhaps it is most illustrative to consider approaching the solution iteratively starting with the heat flux distribution that would occur in the absence of boiling (see section 6.2) as sketched with the solid line in the

top graph of figure 6.5. This would imply a coolant temperature given by the solid line to the left of the boiling location in the second graph. We will assume that when this reaches the saturated vapor temperature at the prevailing coolant pressure, boiling begins and the temperature thereafter remains at the saturated vapor temperature (since the pressure decreases with elevation due to a combination of hydrostatic pressure drop and frictional pressure drop the saturated vapor temperature may drop a little as sketched in figure 6.5). For the present we will assume that the critical heat flux (CHF) (see section 7.5.2) is not reached in the reactor core; otherwise the temperature would begin to rise substantially as sketched by the dashed line in the second graph of figure 6.5.

The next step is to integrate the heat flux using equation 6.13 to obtain the mass quality as a function of elevation as sketched in the third graph of figure 6.5; note that the mass quality, $\mathcal{X}$, will begin at zero at the point where boiling begins and that the slope of the line beyond that point will vary like the heat flux, $\mathcal{Q}$. The next step is to deduce the void fraction, α, of the two-phase flow knowing the mass quality, $\mathcal{X}$. This is a more complex step for, as discussed in section 7.2.1, the relation between α and $\mathcal{X}$ involves the velocities of the two phases and these may be quite different. The calculation of the void fraction is necessary since the void fraction changes the moderating properties of the two-phase coolant. The local reactivity will decline as α increases as discussed in section 7.7.2 and will therefore take the qualitative form sketched in the lowest graph of figure 6.5.

But this change in the reactivity means that the heat flux will be different from that which was assumed at the start of the calculation. Therefore the second iteration needs to begin with a revised heat flux determined using the new, corrected reactivity. This will result in a decreased heat flux above the location of boiling initiation and the previous series of steps then need to be repeated multiple times until a converged state is reached.

We should note that the two-phase flow also alters the heat transfer coefficient, h, governing the heat flux from the fuel rods to the coolant. Under these conditions the functional relation between the Nusselt number, Nu, and the Reynolds and Prandtl numbers will change and this, in turn, will change the temperatures in the fuel rod. This complication also needs to be factored into the above calculation.

6.6 Critical heat flux

In the preceding two sections we assumed that the critical heat flux conditions and temperatures were not reached within the reactor. Indeed care is taken to stay well below those temperatures during the designed normal operation of a boiling water reactor. However, since a postulated accident in a PWR, a BWR or any other liquid-cooled reactor core might result in enhanced boiling, analyses similar to those described in the preceding sections need to be carried out in order to predict the evolution of that accident scenario. If burnout and

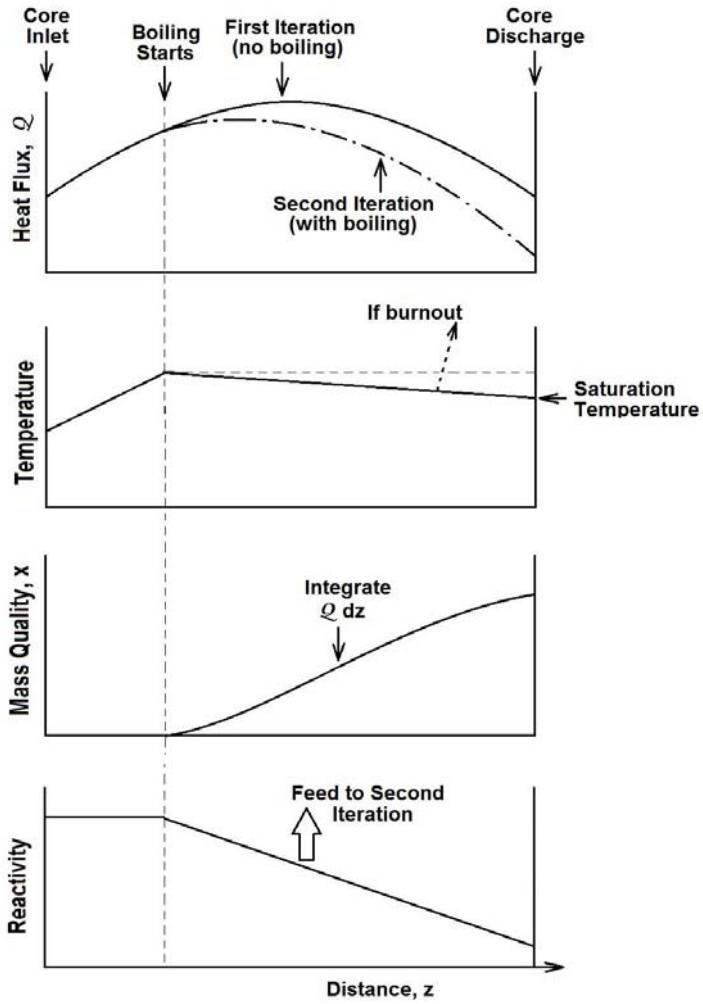

Figure 6.5: Schematic relation between the heat flux, $\mathcal{Q}$, as a function of elevation within the core of a boiling water reactor (top graph) and the coolant temperature, mass quality and reactivity.

critical heat flux conditions were to occur at some elevation within the core this would further modify the conditions described in the last section. The coolant and fuel rod temperatures above that burnout location would rise rapidly as would the mass quality of the coolant which would approach unity. But this would result in yet another decrease in the reactivity and therefore in the local heat generation within the fuel. Moreover, in a LOCA an evolving decrease in the coolant flow rate, $\dot{m}$, will result in an enhanced rate of increase in the mass quality (as illustrated in equation 6.13) and this would promote the chance of

burnout.

Because of the potential for fuel rod damage and meltdown in such a postulated accident scenario it is very important to be able to predict the evolution of such an event. The above description of how such a calculation might proceed only serves to indicate what a complicated multiphase flow calculation that involves. We comment further on these efforts at the end of the next chapter.

References

Gregg King, C.D. (1964). *Nuclear power systems.* The Macmillan Company, New York.

Knief, R.A. (1992). *Nuclear engineering: Theory and practice of commercial nuclear power.* Hemisphere Pub. Corp.

Rohsenow, W.M. and Hartnett, J.P. (1973.) *Handbook of heat transfer.* McGraw-Hill Book Company.

Todres, N.E. and Kazimi, M.S. (1990). *Nuclear systems I. Thermal hydraulic fundamentals.* Hemisphere Publ. Co.

Tong, L.S. and Weisman, J. (1970). *Thermal analysis of pressurized water reactors.* American Nuclear Society monograph.

Chapter 7

MULTIPHASE FLOW

7.1 Introduction

A multiphase flow is the flow of a mixture of phases or components. Such flows occur in the context of nuclear power generation either because the reactor (such as a BWR) is designed to function with a cooling system in which the primary coolant consists of several phases or components during normal operation or because such flows might occur during a reactor accident. In the latter context, predictions of how the accident might progress or how it might be ameliorated may involve analyses of complicated and rapidly changing multiphase flows. Consequently some familiarity with the dynamics of multiphase flows is essential to the nuclear reactor designer and operator. In this chapter we provide a summary of the fundamentals of the dynamics of multiphase flows. In general this is a subject of vast scope that ranges far beyond the limits of this book. Consequently the reader will often be referred to other texts for more detailed analyses and methodologies.

7.2 Multiphase flow regimes

From a practical engineering point of view one of the major design difficulties in dealing with multiphase flow is that the mass, momentum, and energy transfer rates and processes can be quite sensitive to the geometric distribution or topology of the components within the flow. For example, the topology may strongly effect the interfacial area available for mass, momentum or energy exchange between the phases. Moreover, the flow within each phase or component will clearly depend on that geometric distribution. Thus we recognize that there is a complicated two-way coupling between the flow in each of the phases or components and the geometry of the flow (as well as the rates of change of that geometry). The complexity of this two-way coupling presents a major challenge in the analysis and prediction of multiphase flows.

7.2.1 Multiphase flow notation

The notation that will be used for multiphase flow is as follows. Uppercase subscripts will refer to the property of a specific phase or component, for example, C for a continous phase, D for a disperse phase, L for liquid, G for gas, V for vapor. In some contexts generic subscripts N, A, or B will be used for generality. Specific properties frequently used are as follows. The densities of individual components or phases are denoted by ρ_N. *Volumetric fluxes* (volume flow per unit area) of individual components will be denoted by j_N and the *total volumetric flux* is denoted by $j = j_A + j_B$. *Mass fluxes* will then be given by $\rho_N j_N$ and velocities of the individual components or phases will be denoted by u_N.

The volume fraction of a component or phase is denoted by α_N and in the case of two components or phases, A and B, it follows that $\alpha_B = 1 - \alpha_A$. Then the mixture density, denoted by ρ, is given by

$$\rho = \alpha_A \rho_A + \alpha_B \rho_B \tag{7.1}$$

It also follows that the volume flux of a component, N, and its velocity are related by $j_N = \alpha_N u_N$.

Two other fractional properties are the *volume quality*, β_N, defined as the ratio of the volumetric flux of the component, N, to the total volumetric flux so that, for example, $\beta_A = j_A/j$. Note that, in general, β is not necessarily equal to α. The *mass fraction*, x_A, of a phase or component, A, is simply given by $\rho_A\alpha_A/(\rho_A\alpha_A + \rho_B\alpha_B)$. On the other hand the *mass quality*, $\mathcal{X}_A$, often referred to simply as *the quality*, is the ratio of the mass flux of component, A, to the total mass flux, or

$$\mathcal{X}_A = \frac{\rho_A j_A}{\rho_B j_B + \rho_A j_A} \tag{7.2}$$

Furthermore, when only two components or phases are present it is often redundant to use subscripts on the volume fraction and the qualities since $\alpha_A = 1 - \alpha_B, \beta_A = 1 - \beta_B$ and $\mathcal{X}_A = 1 - \mathcal{X}_B$. Thus unsubscripted quantities α, β and $\mathcal{X}$ will often be used in these circumstances.

Finally, we note for future use, that the relation between the volume fraction, α_A, and the mass quality, $\mathcal{X}_A$, for a given phase or component, A, in a two-phase or two-component mixture of A and B follows from equation 7.2, namely

$$\mathcal{X}_A = \frac{\rho_A \alpha_A u_A}{\rho_B (1 - \alpha_A) u_B + \rho_A \alpha_A u_A} \tag{7.3}$$

where u_A and u_B are the velocities of the two phases or components. Therefore $\mathcal{X}_A$ and α_A may be quite different.

7.2.2 Multiphase flow patterns

An appropriate starting point in any analysis of multiphase flow is a phenomenological description of the geometric distributions that are observed in these flows.

A particular type of geometric distribution of the components is called a *flow pattern* or *flow regime* and many of the names given to these flow patterns (such as annular flow or bubbly flow) are now quite standard. Usually the flow patterns are recognized by visual inspection, though other means such as analysis of the spectral content of the unsteady pressures or the fluctuations in the volume fraction have been devised for those circumstances in which visual information is difficult to obtain (Jones and Zuber, 1974).

For some of the simpler flows, such as those in vertical or horizontal conduits, a substantial number of investigations have been conducted to determine the dependence of the flow pattern on component volume fluxes, (j_A, j_B), on volume fraction and on the fluid properties such as density, viscosity, and surface tension. The results are often displayed in the form of a *flow regime map* that identifies the flow patterns occurring in various parts of a parameter space defined by the component flow rates. The flow rates used may be the volume fluxes, mass fluxes, momentum fluxes, or other similar quantities depending on the author. Summaries of these flow pattern studies and the various empirical laws extracted from them are a common feature in reviews of multiphase flow (see, for example, Brennen 2005, Wallis 1969 or Weisman 1983).

The boundaries between the various flow patterns in a flow pattern map occur because a regime becomes unstable as the boundary is approached and growth of this instability causes transition to another flow pattern. Like the laminar-to-turbulent transition in single phase flow, these multiphase transitions can be rather unpredictable since they may depend on otherwise minor features of the flow, such as the roughness of the walls or the entrance conditions. Hence, the flow pattern boundaries are not distinctive lines but more poorly defined transition zones.

But there are other serious difficulties with most of the existing literature on flow pattern maps. One of the basic fluid mechanical problems is that these maps are often dimensional and therefore apply only to the specific pipe sizes and fluids employed by the investigator. A number of investigators (for example Baker 1954, Schicht 1969 or Weisman and Kang 1981) have attempted to find generalized coordinates that would allow the map to cover different fluids and conduits of different sizes. However, such generalizations can only have limited value because several transitions are represented in most flow pattern maps and the corresponding instabilities are governed by different sets of fluid properties. Hence, even for the simplest duct geometries, there exist no universal, dimensionless flow pattern maps that incorporate the full, parametric dependence of the boundaries on the fluid characteristics.

Beyond these difficulties there are a number of other troublesome questions. In single phase flow it is well established that an entrance length of 30 to 50 diameters is necessary to establish fully developed turbulent pipe flow. The corresponding entrance lengths for multiphase flow patterns are less well established and it is quite possible that some of the reported experimental observations are for temporary or developing flow patterns. Moreover, the implicit assumption is often made that there exists a unique flow pattern for given fluids with given flow rates. It is by no means certain that this is the case. Consequently, there

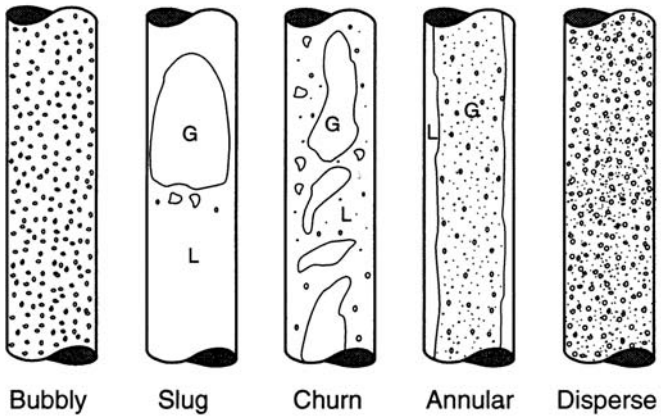

Figure 7.1: Sketches of flow regimes for two-phase flow in a vertical pipe. Adapted from Weisman (1983).

may be several possible flow patterns whose occurence may depend on the initial conditions, specifically on the manner in which the multiphase flow is generated.

7.2.3 Flow regime maps

Despite the issues and reservations discussed in the preceding section it is useful to provide some examples of flow regime maps along with the definitions that help distinguish the various regimes. Perhaps the most widely studied multiphase flow is that of a gas/liquid mixture in a horizontal conduit and here some progress has been made in understanding the scaling of the boundaries in a flow regime map (see, for example, Hubbard and Dukler 1966, Weisman 1983, Mandhane *et al.* 1974, Brennen 2005). However, the focus in nuclear power generation is more frequently on vertical gas/liquid flow and the typical definitions of these flow regimes are as displayed graphically in figures 7.1 (see, for example, Hewitt and Hall Taylor 1970, Butterworth and Hewitt 1977, Hewitt 1982, Whalley 1987). An example of a vertical flow regime map is shown in figure 7.2, this one using momentum flux axes rather than volumetric or mass fluxes. Note the wide range of flow rates in this flow regime map by Hewitt and Roberts (1969) and the fact that they correlated both air/water data at atmospheric pressure and steam/water flow at high pressure.

It should be added that flow regime information such as that presented in figure 7.2 appears to be valid both for flows that are not evolving with axial distance along the pipe and for flows, such as those in a reactor, in which the volume fraction is increasing with axial position. Figure 7.3 provides a sketch of the kind of evolution one might expect in a vertical fluid passage within a reactor core based on the flow regime maps given above.

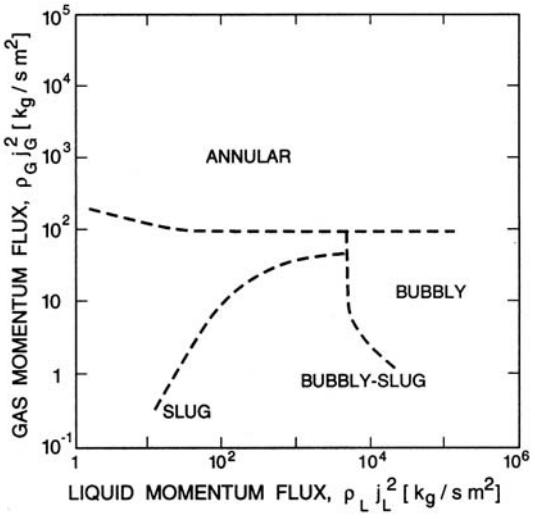

Figure 7.2: The vertical flow regime map of Hewitt and Roberts (1969) for flow in a 3.2cm diameter tube, validated for both air/water flow at atmospheric pressure and steam/water flow at high pressure.

7.2.4 Flow pattern classifications

One of the most fundamental characteristics of a multiphase flow pattern is the extent to which it involves global separation of the phases or components. At the two ends of the spectrum of separation characteristics are those flow patterns that are termed *disperse* and those that are termed *separated.* A *disperse* flow pattern is one in which one phase or component is widely distributed as drops, bubbles, or particles in the other *continuous* phase. On the other hand, a *separated* flow consists of separate, parallel streams of the two (or more) phases. Even within each of these limiting states there are various degrees of component separation. The asymptotic limit of a disperse flow in which the disperse phase is distributed as an infinite number of infinitesimally small bubbles or drops is termed a *homogeneous* multiphase flow. Since the relative velocity of a tiny bubble or drop approaches zero as its size decreases, this limit implies zero relative motion between the phases. However, there are many practical disperse flows, such as bubbly or mist flow in a pipe, in which the flow is quite disperse in that the particle size is much smaller than the pipe dimensions but in which the relative motion between the phases is significant.

Within separated flows there are similar gradations or degrees of phase separation. The low velocity flow of gas and liquid in a pipe that consists of two single phase streams can be designated a *fully separated* flow. On the other hand, most annular flows in a vertical pipe consist of a film of liquid on the walls and a central core of gas that contains a significant number of liquid droplets. These droplets are an important feature of annular flow and therefore the flow can

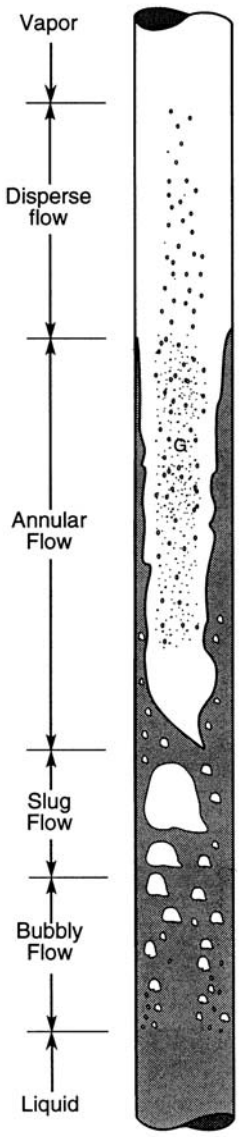

Figure 7.3: The evolution of the steam/water flow in a reactor.

only be regarded as partially separated.

To summarize: one of the basic characteristics of a flow pattern is the degree of separation of the phases into streamtubes of different concentrations. The degree of separation will, in turn, be determined by (a) some balance between the fluid mechanical processes enhancing dispersion and those causing segregation, or (b) the initial conditions or mechanism of generation of the multiphase flow, or (c) some mix of both effects.

A second basic characteristic that is useful in classifying flow patterns is the level of intermittency in the volume fraction. An example of intermittent flow patterns is slug flow in a vertical pipe. The first separation characteristic was the degree of separation of the phases between streamtubes; this second, intermittency characteristic, can be viewed as the degree of periodic separation in the streamwise direction. The slugs or waves are kinematic or concentration waves (sometimes called continuity waves) and the reader is referred to Brennen (2005) for a general discussion of the structure and characteristics of such waves. Intermittency is the result of an instability in which kinematic waves grow in an otherwise nominally steady flow to create significant streamwise separation of the phases.

In the sections which follow we briefly describe how these ideas of cross-streamline separation and intermittency can lead to an understanding of the limits of specific multiphase flow regimes. Both the limits on disperse flow regimes and the limits on separated flow regimes are briefly addressed.

7.2.5 Limits of disperse flow regimes

In order to determine the limits of a disperse phase flow regime, it is necessary to identify the dominant processes enhancing separation and those causing dispersion. By far the most common process causing phase separation is due to the difference in the densities of the phases and the mechanisms are therefore functions of the ratio of the density of the disperse phase to that of the continuous phase. Then the buoyancy forces caused either by gravity or, in a non-uniform or turbulent flow by the Lagrangian fluid accelerations will create a relative velocity between the phases that may lead to phase separation.

While the primary mechanism of phase separation in a quiescent multiphase mixture is sedimentation, in flowing mixtures the mechanisms are more complex and, in most applications, are controlled by a balance between the buoyancy/gravity forces and the hydrodynamic forces. In high Reynolds number, turbulent flows, the turbulence can cause either dispersion or segregation. Segregation may occur when, for example, solid particles suspended in a gas flow are centrifuged out of the more intense turbulent eddies and collect in the shear zones in between (see for example, Squires and Eaton 1990, Elghobashi and Truesdell 1993) or when bubbles in a liquid collect in regions of low pressure such as in the wake of a body or in the centers of vortices (see for example Pan and Banerjee 1997). Counteracting these separation processes are dispersion processes and in many engineering contexts the principal dispersion is caused by the turbulent or other unsteady motions in the continuous phase.

The shear created by unsteady velocities can also cause either fission or fusion of the disperse phase bubbles or drops. Quantitative evaluation of these competing forces of segregation and dispersion can lead to criteria determining the boundary between seperated and disperse flow in a flow regime map (see, for example, Brennen 2005).

As a postscript, we note from the above that an evaluation of the disperse flow separation process will normally require knowledge of the bubble or droplet size and this is not usually known, *a priori*. This is a serious complication because the size of the bubbles or drops is often determined by the flow itself since the flow shear tends to cause fission and therefore limit the maximum size of the surviving bubbles or drops. Then the flow regime may depend upon the particle size that in turn depends on the flow and this two-way interaction can be difficult to unravel. When the bubbles or drops are very small, a variety of forces may play a role in determining the effective size. But often the bubbles or drops are sufficiently large that the dominant force resisting fission is due to surface tension while the dominant force promoting fission is the shear in the flow. Typical regions of high shear occur in boundary layers, in vortices or in turbulence. Frequently, the larger drops or bubbles are fissioned when they encounter regions of high shear and do not subsequently coalesce to any significant degree. For further analyses and criteria the reader is referred to Mandhane *et al.* (1974), Taitel and Dukler (1976), and Brennen (2005).

7.2.6 Limits on separated flow

We now turn to the limits on separated flow regimes and the primary mechanism that determines that limit is the Kelvin-Helmholtz instability. Separated flow regimes such as stratified horizontal flow or vertical annular flow can become unstable when waves form on the interface between the two fluid streams (subscripts 1 and 2). As indicated in figure 7.4, the densities of the fluids will be denoted by ρ_1 and ρ_2 and the velocities by u_1 and u_2. If these waves continue to grow in amplitude they cause a transition to another flow regime, typically one with greater intermittency and involving plugs or slugs. Therefore, in order to determine this particular boundary of the separated flow regime, it is necessary to investigate the potential growth of the interfacial waves, whose wavelength will be denoted by λ (wavenumber, $\kappa = 2\pi/\lambda$). Studies of such waves have a long history originating with the work of Kelvin and Helmholtz and the phenomena they revealed have come to be called Kelvin-Helmholtz instabilities (see, for example, Yih 1965). In general this class of instabilities involves the interplay between at least two of the following three types of forces:

- a buoyancy force due to gravity and proportional to the difference in the densities of the two fluids. In a horizontal flow in which the upper fluid is lighter than the lower fluid this force is stabilizing. When the reverse is true the buoyancy force is destabilizing and this causes Rayleigh-Taylor instabilities. When the streams are vertical as in vertical annular flow the role played by the buoyancy force is less clear.

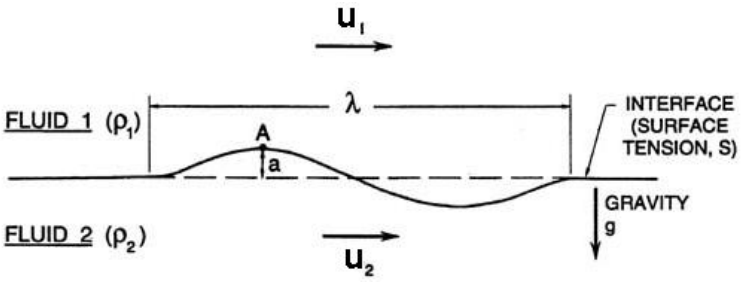

Figure 7.4: Sketch showing the notation for Kelvin-Helmholtz instability.

- a surface tension force that is always stabilizing.
- a Bernoulli effect that implies a change in the pressure acting on the interface caused by a change in velocity resulting from the displacement, a, of that surface. For example, if the upward displacement of the point A in figure 7.5 were to cause an increase in the local velocity of fluid 1 and a decrease in the local velocity of fluid 2, this would imply an induced pressure difference at the point A that would increase the amplitude of the distortion, a.

The interplay between these forces is most readily illustrated by a simple example. Neglecting viscous effects, one can readily construct the planar, incompressible potential flow solution for two semi-infinite horizontal streams separated by a plane horizontal interface (as in figure 7.4) on which small amplitude waves have formed. Then it is readily shown (Lamb 1879, Yih 1965) that Kelvin-Helmholtz instability will occur when

$$\frac{g\Delta\rho}{\kappa} + \mathcal{S}\kappa - \frac{\rho_1\rho_2(\Delta u)^2}{\rho_1+\rho_2} < 0 \tag{7.4}$$

where $\mathcal{S}$ is the surface tension of the interface. The contributions from the three previously mentioned forces are self-evident. Note that the surface tension effect is stabilizing since that term is always positive, the buoyancy effect may be stabilizing or destabilizing depending on the sign of $\Delta\rho$ and the Bernoulli effect is always destabilizing. Clearly, one subset of this class of Kelvin-Helmholtz instabilities are the Rayleigh-Taylor instabilities that occur in the absence of flow ($\Delta u = 0$) when $\Delta\rho$ is negative. In that static case, the above relation shows that the interface is unstable to all wave numbers less than the critical value, $\kappa = \kappa_c$, where

$$\kappa_c = \left(\frac{g(-\Delta\rho)}{\mathcal{S}}\right)^{\frac{1}{2}} \tag{7.5}$$

The Bernoulli effect is frequently the primary cause of instability in a separated flow and can lead to transition to a plug or slug flow regime. As a first

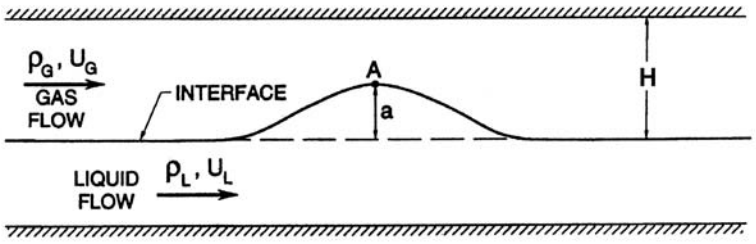

Figure 7.5: Sketch showing the notation for stratified flow instability.

example of the instability induced by the Bernoulli effect, consider the stability of the horizontal stratified flow depicted in figure 7.5 where the destabilizing Bernoulli effect is primarily opposed by a stabilizing buoyancy force. An approximate instability condition is readily derived by observing that the formation of a wave (such as that depicted in figure 7.5) will lead to a reduced pressure, p_A, in the gas in the orifice formed by that wave. The reduction below the mean gas pressure, $\bar{p}_G$, will be given by Bernoulli's equation as

$$p_A - \bar{p}_G = -\rho_G u_G^2 a/H \tag{7.6}$$

provided $a \ll H$. The restraining pressure is given by the buoyancy effect of the elevated interface, namely $(\rho_L - \rho_G)ga$. It follows that the flow will become unstable when

$$u_G^2 > gH\Delta\rho/\rho_G \tag{7.7}$$

In this case the liquid velocity has been neglected since it is normally small compared with the gas velocity. Consequently, the instability criterion provides an upper limit on the gas velocity that is, in effect, the velocity difference. Taitel and Dukler (1976) compared this prediction for the boundary of the stratified flow regime in a horizontal pipe with the experimental observations of Mandhane *et al.* (1974) and found substantial agreement.

As a second example consider vertical annular flow that becomes unstable when the Bernoulli force overcomes the stabilizing surface tension force. From equation 7.4, this implies that disturbances with wavelengths greater than a critical value, λ_c, will be unstable and that

$$\lambda_c = 2\pi\mathcal{S}(\rho_1 + \rho_2)/\rho_1\rho_2(\Delta u)^2 \tag{7.8}$$

For a liquid stream and a gas stream (as is normally the case in annular flow) and with $\rho_L \ll \rho_G$ this becomes

$$\lambda_c = 2\pi\mathcal{S}/\rho_G(\Delta u)^2 \tag{7.9}$$

Now consider the application of this criterion to a well-developed annular flow at high gas volume fraction in which $\Delta u \approx j_G$. Then for a water/air mixture equation 7.9 predicts critical wavelengths of $0.4cm$ and $40cm$ for $j_G = 10m/s$

and $j_G = 1m/s$ respectively. In other words, at low values of j_G only larger wavelengths are unstable and this seems to be in accord with the break-up of the flow into large slugs. On the other hand at higher j_G flow rates, even quite small wavelengths are unstable and the liquid gets torn apart into the small droplets carried in the core gas flow.

7.3 Pressure drop

7.3.1 Introduction

An obvious objective of the analysis of the flow in the primary coolant loop is the prediction and understanding of the pressure drop in the flow through the core and the corresponding pressure increase in the flow through the primary coolant pumps. As long as these remain single phase flow, the analyses do not differ greatly from the parallel features in any power plant and it will be assumed herein that the reader has some familiarity with such single phase flow analyses. However, when boiling occurs either by design or because of some abnormal excursion, the resulting multiphase flow requires more complicated analyses and we touch upon those methods in the next few sections. It should be noted that the literature contains a plethora of engineering correlations for multiphase flow pipe friction and some data for other components such as pumps. This section will provide an overview and some references to illustrative material, but does not pretend to survey these empirical methodologies.

7.3.2 Horizontal disperse flow

As might be expected, frictional losses in straight uniform pipe flows have been the most widely studied and so we begin with a discussion of that subject, focusing first on disperse or nearly disperse flows and then on separated flows.

Beginning with disperse horizontal flow, it is noted that there exists a substantial body of data relating to the frictional losses or pressure gradient, $(-dp/ds)$, in a straight pipe of circular cross-section (the coordinate s is measured along the axis of the pipe). Clearly $(-dp/ds)$ is a critical factor in the design of many systems (for example slurry pipelines). This pressure gradient is usually non-dimensionalized using the pipe diameter, d, the density of the continuous phase (ρ_C), and either the total volumetric flux, j, or the volumetric flux of the continuous fluid (j_C). Thus, commonly used friction coefficients are

$$C_f = \frac{d}{2\rho_C j_C^2}\left(-\frac{dp}{ds}\right) \quad \textbf{or} \quad C_f = \frac{d}{2\rho_C j^2}\left(-\frac{dp}{ds}\right) \tag{7.10}$$

and, in parallel with the traditional Moody diagram for single phase flow, these friction coefficients are usually presented as functions of a Reynolds number for various mixture ratios as characterized by the volume fraction, α, or the volume quality, β, of the disperse phase. Commonly used Reynolds numbers are based on the pipe diameter, the viscosity of the continuous phase (ν_C) and

either the total volumetric flux, j, or the volumetric flux of the continuous phase, j_C. For boiling flows or for gas/liquid flows, the reader is referred to the reviews of Hsu and Graham (1976) and Collier and Thome (1994). For a review of slurry pipeline data the reader is referred to Shook and Roco (1991) and Lazarus and Neilsen (1978). For the solids/gas flows associated with the pneumatic conveying of solids, Soo (1983) provides a good summary.

7.3.3 Homogeneous flow friction

When the multiphase flow or slurry is thoroughly mixed the pressure drop can be approximated by the friction coefficient for a single-phase flow with the mixture density, ρ (equation 7.1) and the same total volumetric flux, j, as the multiphase flow. Then the ratio of the multiphase flow friction coefficient (based on j), $C_f(\alpha)$, at a particular void fraction, α, to the friction coefficient for the continuous phase flowing alone, $C_f(0)$, will given by

$$\frac{C_f(\alpha)}{C_f(0)} = \frac{(1 + \alpha\rho_D/\rho_C)}{(1-\alpha)^2} \tag{7.11}$$

where it is assumed that $\beta \approx \alpha$. An example of the comparison of this expression with measured friction coefficient ratios in horizontal disperse flows shows good agreement up to large volume fractions (Brennen 2005).

Thus a flow regime that is homogeneous or thoroughly mixed can usually be modeled as a single phase flow with an effective density, volume flow rate and viscosity. In these circumstances the orientation of the pipe appears to make little difference. Often these correlations also require an effective mixture viscosity. In the above example, an effective kinematic viscosity of the multiphase flow could have been incorporated in the expression 7.11; however, this often has little effect especially under the turbulent conditions.

Wallis (1969) includes a discussion of homogeneous flow friction correlations for both laminar and turbulent flow. Turbulence in multiphase flows introduces another set of complicated issues. Nevertheless the above-mentioned single phase approach to the pipe friction seems to produce moderately accurate results in homogeneous flows as is illustrated by the data of figure 7.6. The presence of drops, bubbles or particles can act like surface roughness, enhancing turbulence in many applications. Consequently, turbulent friction factors for homogeneous flow tend to be similar to the values obtained for single phase flow in rough pipes, values around 0.005 being commonly experienced (Wallis 1969).

Vertically-oriented pipe flow can experience partially separated flows in which large relative velocities develop due to buoyancy and the difference in the densities of the two-phases or components. These large relative velocities complicate the problem of evaluating the pressure gradient and can lead to friction coefficients much larger than suggested by a homogeneous flow friction factor.

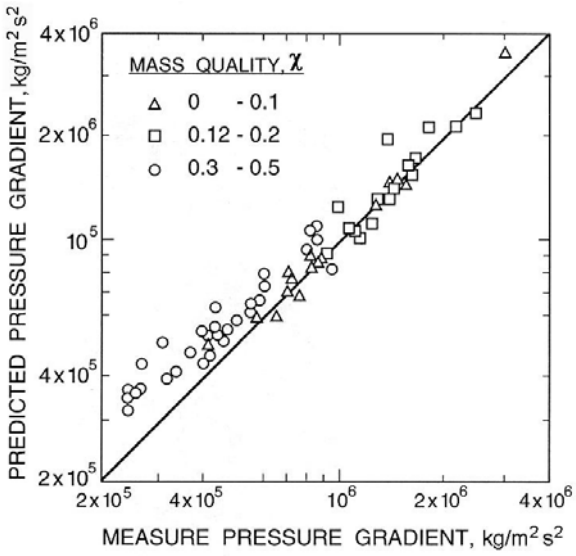

Figure 7.6: Comparison of the measured friction coefficient with that using the homogeneous prediction for steam/water flows of various mass qualities in a $0.3cm$ diameter tube. Adapted from Owens (1961).

7.3.4 Frictional loss in separated flow

Having discussed homogeneous and disperse flows we now turn our attention to the friction in separated flows and, in particular, describe the commonly used Martinelli correlations. The Lockhart-Martinelli (Lockhart and Martinelli, 1949) and Martinelli-Nelson (Martinelli and Nelson, 1948) correlations are widely documented in multiphase flow texts (see, for example, Wallis 1969 or Brennen 2005). These attempt to predict the frictional pressure gradient in two-component or two-phase pipe flows. It is assumed that these flows consist of two separate co-current streams that, for convenience, we will refer to as the liquid and the gas though they could be any two immiscible fluids. The correlations use the results for the frictional pressure gradient in single phase pipe flows of each of the two fluid streams. In two-phase flow, the volume fraction is often changing as the mixture progresses along the pipe and such phase change necessarily implies acceleration or deceleration of the fluids. Associated with this acceleration is an additional acceleration component of the pressure gradient that is addressed with the Martinelli-Nelson correlation. Obviously, it is convenient to begin with the simpler, two-component case (the Lockhart-Martinelli correlation); this also neglects the effects of changes in the fluid densities with distance, s, along the pipe axis so that the fluid velocities also remain invariant with s. Moreover, in all cases, it is assumed that the hydrostatic pressure gradient has been accounted for so that the only remaining contribution to the pressure gradient, $-dp/ds$, is that due to the wall shear stress, τ_w. A simple

balance of forces requires that

$$-\frac{dp}{ds} = \frac{P}{A}\tau_w \tag{7.12}$$

where P and A are the perimeter and cross-sectional area of the stream or pipe. For a circular stream or pipe, $P/A = 4/d$, where d is the stream/pipe diameter. For non-circular cross-sections, it is convenient to define a *hydraulic diameter*, $4A/P$. Then, defining the dimensionless friction coefficient, C_f, as

$$C_f = \tau_w / \frac{1}{2}\rho j^2 \tag{7.13}$$

the more general form of equation 7.10 becomes

$$-\frac{dp}{ds} = C_f \rho j^2 \frac{P}{2A} \tag{7.14}$$

In single phase flow the coefficient, C_f, is a function of the Reynolds number, $\rho dj/\mu$, of the form

$$C_f = \mathcal{K}\left\{\frac{\rho dj}{\mu}\right\}^{-m} \tag{7.15}$$

where $\mathcal{K}$ is a constant that depends on the roughness of the pipe surface and will be different for laminar and turbulent flow. The index, m, is also different, being 1 in the case of laminar flow and 1/4 in the case of turbulent flow.

These relations from single phase flow are applied to the two cocurrent streams in the following way. First, we define hydraulic diameters, d_L and d_G, for each of the two streams and define corresponding area ratios, κ_L and κ_G, as

$$\kappa_L = 4A_L/\pi d_L^2 \quad ; \quad \kappa_G = 4A_G/\pi d_G^2 \tag{7.16}$$

where $A_L = A(1-\alpha)$ and $A_G = A\alpha$ are the actual cross-sectional areas of the two streams. The quantities κ_L and κ_G are shape parameters that depend on the geometry of the flow pattern. In the absence of any specific information on this geometry, one might choose the values pertinent to streams of circular cross-section, namely $\kappa_L = \kappa_G = 1$, and the commonly used form of the Lockhart-Martinelli correlation employs these values. (Note that Brennen (2005) also presents results for an alternative choice.)

The basic geometric relations yield

$$\alpha = 1 - \kappa_L d_L^2/d^2 = \kappa_G d_G^2/d^2 \tag{7.17}$$

Then, the pressure gradient in each stream is assumed given by the following coefficients taken from single phase pipe flow:

$$C_{fL} = \mathcal{K}_L\left\{\frac{\rho_L d_L u_L}{\mu_L}\right\}^{-m_L} \quad ; \quad C_{fG} = \mathcal{K}_G\left\{\frac{\rho_G d_G u_G}{\mu_G}\right\}^{-m_G} \tag{7.18}$$

and, since the pressure gradients must be the same in the two streams, this imposes the following relation between the flows:

$$-\frac{dp}{ds} = \frac{2\rho_L u_L^2 \mathcal{K}_L}{d_L}\left\{\frac{\rho_L d_L u_L}{\mu_L}\right\}^{-m_L} = \frac{2\rho_G u_G^2 \mathcal{K}_G}{d_G}\left\{\frac{\rho_G d_G u_G}{\mu_G}\right\}^{-m_G} \tag{7.19}$$

In the above, m_L and m_G are 1 or 1/4 depending on whether the stream is laminar or turbulent.

Equations 7.17 and 7.19 are the basic relations used to construct the Lockhart-Martinelli correlation. The solutions to these equations are normally and most conveniently presented in non-dimensional form by defining the following dimensionless pressure gradient parameters:

$$\phi_L^2 = \frac{\left(\frac{dp}{ds}\right)_{actual}}{\left(\frac{dp}{ds}\right)_L} \quad ; \quad \phi_G^2 = \frac{\left(\frac{dp}{ds}\right)_{actual}}{\left(\frac{dp}{ds}\right)_G} \tag{7.20}$$

where $(dp/ds)_L$ and $(dp/ds)_G$ are respectively the hypothetical pressure gradients that would occur in the same pipe if only the liquid flow were present and if only the gas flow were present. The ratio of these two hypothetical gradients, Ma, given by

$$Ma^2 = \frac{\phi_G^2}{\phi_L^2} = \frac{\left(\frac{dp}{ds}\right)_L}{\left(\frac{dp}{ds}\right)_G} = \frac{\rho_G j_G^2}{\rho_L j_L^2}\frac{\mathcal{K}_G}{\mathcal{K}_L}\frac{\left\{\frac{\rho_G j_G d}{A\mu_G}\right\}^{-m_G}}{\left\{\frac{\rho_L j_L d}{A\mu_L}\right\}^{-m_L}} \tag{7.21}$$

has come to be called the Martinelli parameter and allows presentation of the solutions to equations 7.17 and 7.19 in a convenient parametric form. Using the definitions of equations 7.20, the non-dimensional forms of equations 7.17 become

$$\alpha = 1 - \kappa_L^{(3-m_L)/(m_L-5)}\phi_L^{4/(m_L-5)} = \kappa_G^{(3-m_G)/(m_G-5)}\phi_G^{4/(m_G-5)} \tag{7.22}$$

and the solution of these equations produces the Lockhart-Martinelli prediction of the non-dimensional pressure gradient.

To summarize: for given values of (a) the fluid properties, ρ_L, ρ_G, μ_L and μ_G (b) the nature of the flow, laminar or turbulent, in the two streams and the phase correlation constants, m_L, m_G, $\mathcal{K}_L$ and $\mathcal{K}_G$ (c) the parameters defined by the flow pattern geometry, κ_L and κ_G and (d) a given value of α equations 7.22 can be solved to find the non-dimensional solution to the flow, namely the values of ϕ_L^2 and ϕ_G^2. The value of Ma^2 also follows and the rightmost expression in equation 7.21 then yields a relation between the liquid mass flux, $\rho_L j_L$, and the gas mass flux, $\rho_G j_G$. Thus, if one is also given just **one** mass flux (often this will be the total mass flux, $\dot{m} = \rho_L j_L + \rho_G j_G$), the solution will yield the individual mass fluxes, the mass quality and other flow properties. Alternatively one could begin the calculation with the mass quality rather than the void fraction and

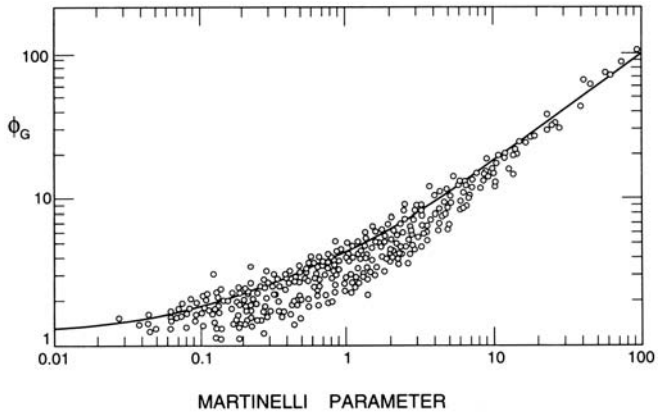

Figure 7.7: Comparison of the Lockhart-Martinelli correlation (the TT case) for ϕ_G (solid line) with experimental data. Adapted from Turner and Wallis (1965).

find the void fraction as one of the results. Finally the pressure gradient, dp/ds, follows from the values of ϕ_L^2 and ϕ_G^2.

Charts for the results are presented by Wallis (1969), Brennen (2005) and others. Charts like these are commonly used in the manner described above to obtain solutions for two-component gas/liquid flows in pipes. A typical comparison of the Lockhart-Martinelli prediction with the experimental data is presented in figure 7.7. Note that the scatter in the data is significant (about a factor of 3 in ϕ_G) and that the Lockhart-Martinelli prediction often yields an overestimate of the friction or pressure gradient. This is the result of the assumption that the entire perimeter of both phases experiences static wall friction. This is not the case and part of the perimeter of each phase is in contact with the other phase. If the interface is smooth this could result in a decrease in the friction; on the other hand a roughened interface could also result in increased interfacial friction.

It is important to recognize that there are many deficiencies in the Lockhart-Martinelli approach. First, it is assumed that the flow pattern consists of two parallel streams and any departure from this topology could result in substantial errors. Second, there is the previously discussed deficiency regarding the suitability of assuming that the perimeters of both phases experience friction that is effectively equivalent to that of a static solid wall. A third source of error arises because the multiphase flows are often unsteady and this yields a multitude of quadratic interaction terms that contribute to the mean flow in the same way that Reynolds stress terms contribute to turbulent single phase flow.

The Lockhart-Martinelli correlation was extended by Martinelli and Nelson (1948) to include the effects of phase change. This extension includes evaluation of the additional pressure gradient due to the acceleration of the flow caused by the phase change. To evaluate this one must know the variation of the mass

quality, $\mathcal{X}$, with distance, s, along the pipe. In many boilers, evaporators or condensers, the rate of heat supply or removal per unit length of the pipe, $\mathcal{Q}_\ell$, is roughly uniform and the latent heat, $\mathcal{L}$, can be also be considered constant. It follows that for a flow rate of $\dot{m}$ in a pipe of cross-sectional area, A, the mass quality varies linearly with distance, s, since

$$\frac{d\mathcal{X}}{ds} = \frac{\mathcal{Q}_\ell}{A\dot{m}\mathcal{L}} \tag{7.23}$$

Given the quantities on the right-hand side this allows evaluation of the mass quality as a function of distance along the conduit and also allows evaluation of the additional acceleration contributions to the pressure gradient. For further details the reader is referred to Brennen (2005).

7.4 Vaporization

7.4.1 Classes of vaporization

There are two classes of rapid vaporization of importance in the context of nuclear reactors and we identify them here as homogeneous and heterogeneous vaporization. Homogeneous vaporization occurs when the principal source of the latent heat supply to the interface is the liquid itself. Examples are the formation and growth of a cavitation bubble in a liquid body far from a solid boundary or the vapor explosions described in section 7.4.3. On the other hand, heterogeneous vaporization occurs when the principal source of the latent heat supply to the interface is a different nearby substance or object such as a heated wall. Examples are pool boiling near a heated surface or many of the fuel-coolant interactions described in section 8.5.5. Though there is overlap between the two classes, the definitions are convenient in distinguishing the contributing features.

Moreover, each of these two classes can be subdivided into one of two circumstances. The first circumstance is that in which the growth of the vapor volume is only limited by the inertia of the surroundings, liquid or solid. In the second the vapor volume growth is more severely limited by the rate of supply of latent heat to the interface to produce the vaporization. Both of these rate-limiting growth mechanisms will be examined in the sections that follow since the rate of volume growth essentially controls the rate of damage (if any) to the structure in contact with the liquid.

7.4.2 Homogeneous vaporization

Homogeneous vaporization is identified as vaporization in which the principal source of the latent heat supply to the interface is the liquid itself rather than some nearby heat source. As a model, we present here a simplified version of the equations governing the dynamics of a simple spherical bubble of radius, $R(t)$. The reader who seeks greater detail is referred to the presentation in Brennen (1995) that includes many of the lesser features omitted here. Lord Rayleigh

(1917) first derived the equation governing the radius, $R(t)$, of a spherical vapor/gas bubble in a liquid of density, ρ_L, when the pressure inside the bubble is $p_B(t)$ and the pressure far away in the liquid is $p_\infty(t)$, namely:

$$\frac{p_B(t) - p_\infty(t)}{\rho_L} = R\frac{d^2R}{dt^2} + \frac{3}{2}\left(\frac{dR}{dt}\right)^2 \tag{7.24}$$

The pressure in the bubble, $p_B(t)$, may be comprised of a component due to any non-condensable gas present as well as the vapor pressure of the surrounding liquid *at the prevailing temperature in the bubble*, $T_B(t)$. The first component, that due to any non-condensable gas, is important but will not be central to the current presentation. On the other hand the vapor pressure, and, in particular, the prevailing temperature in the bubble play a key role in the phenomena that are manifest.

In any liquid volume that is mostly at a temperature close to its triple point, the vapor density is so small that only a very small mass of liquid on the surface of the bubble needs to evaporate in order to supply the increase in bubble volume associated with the bubble growth. Moreover, that small mass of liquid means that only a small supply of heat to the interface is needed to effect the evaporation. And, in turn, that small heat flux only creates a small thermal boundary layer on the bubble surface so that the temperature in the bubble, $T_B(t)$, is only very slightly depressed below the prevailing temperature in the bulk of the liquid, T_∞.

The converse of this is a liquid that is mostly at a higher temperature, so that the density of the vapor is such that a significant mass of liquid must be vaporized at the bubble surface in order to provide the volume needed for the bubble growth. This implies a substantial heat flux to the interface in order to provide the latent heat for that evaporation; and that heat flux, in turn, usually causes a significant reduction in the temperature of the bubble contents, $T_B(t)$ (see below for an exception to this consequence). It follows that the vapor pressure in the bubble decreases so that the pressure difference driving the bubble growth, namely $p_B(t) - p_\infty$, decreases and, therefore, according to equation 7.24, the rate of bubble growth decreases. This effect of the liquid temperature in depressing the rate of bubble growth is called the *thermal effect on bubble growth* and it can cause quite a dramatic difference in the resulting bubble dynamics. Perhaps this is most dramatically recognized in the bubble growth in water at normal temperatures. Bubble growth at room temperatures (which are close to the triple point of water) are most frequently observed as cavitation (see Brennen 1995), a phenomenon in which the growth (and the subsequent collapse) of bubbles is extremely explosive and violent. On the other hand, bubble growth in a pot of boiling water on the stove at $100°C$ is substantially inhibited by thermal effects and is therefore much less explosive, much less violent.

We can quantify these effects with the following analyses. First, in the case of no thermal effect, the temperature of the bubble contents will be close to the liquid temperature and therefore the bubble pressure will be roughly constant

(neglecting the effect of any non-condensable gas). Then, if the pressures are assumed constant, equation 7.24 can be integrated to yield

$$\frac{dR}{dt} = \left[\frac{2(p_B - p_\infty)}{3\rho_L}\right]^{\frac{1}{2}} \quad \text{and} \quad R = \left[\frac{2(p_B - p_\infty)}{3\rho_L}\right]^{\frac{1}{2}} t \tag{7.25}$$

where the integration constant is absorbed into the origin of t. This result implies explosive bubble growth, with a volume increasing like t^3; it is the kind of bubble growth characteristic of cavitation (Brennen 1995).

For contrast, consider the thermally-inhibited growth characteristic of boiling in which the growth is controlled by the rate at which heat can diffuse through an interfacial thermal boundary layer to provide the latent heat of vaporization. The rate of volume growth of the bubble, $4\pi R^2 dR/dt$, requires a mass rate of evaporation equal to $4\pi R^2 (dR/dt)/\rho_V$ where ρ_V is the vapor density in the bubble. To evaporate this mass requires a rate of heat supply to the interface equal to

$$4\pi R^2 (dR/dt)/(\mathcal{L}\rho_V) \tag{7.26}$$

where $\mathcal{L}$ is the latent heat of evaporation. This heat must diffuse through the thermal boundary layer that builds up in the liquid on the bubble surface and causes the bubble temperature, T_B, to fall below the liquid temperature outside of the boundary layer, T_∞. It is this temperature difference, $(T_\infty - T_B)$, that drives heat to the bubble surface at a rate given approximately by

$$4\pi R^2 k_L (T_\infty - T_B)/\delta \tag{7.27}$$

where k_L is the thermal conductivity of the liquid and δ is the thickness of the thermal boundary layer. For growth that begins at time $t = 0$ this thickness will be given approximately by

$$\delta \approx (\alpha_L t)^{\frac{1}{2}} \tag{7.28}$$

where α_L is the thermal diffusivity of the liquid. Furthermore, since T_B is the temperature of the interface it should be roughly equal to the vapor temperature at the bubble pressure, p_B, and using the Clausius-Clapeyron relation (Brennen 2005):

$$T_\infty - T_B = \frac{(p_B - p_V)T_B}{\rho_V \mathcal{L}} \tag{7.29}$$

Therefore, equating the expressions 7.26 and 7.27 and using the expressions 7.28 and 7.29 we find that

$$\frac{dR}{dt} = \frac{k_L T_B (p_B - p_V)}{(\alpha t)^{\frac{1}{2}}} \quad \text{and so} \quad R \propto t^{\frac{1}{2}} \tag{7.30}$$

This rate of growth is much slower than given by the expression 7.25 and is characteristic of boiling in water at normal pressures.

To summarize, the above analyses (given in much more detail in Brennen 1995) lead, naturally, to two technologically important multiphase phenomena,

Figure 7.8: Typical photographs of a rapidly growing bubble in a droplet of superheated ether suspended in glycerine. The bubble is the dark, rough mass; the droplet is clear and transparent. The photographs, which are of different events, were taken 31, 44, and 58 μs after nucleation and the droplets are approximately $2mm$ in diameter. Reproduced from Frost and Sturtevant (1986).

namely cavitation and boiling. The essential difference is that bubble growth (and collapse) in boiling is inhibited by limitations on the heat transfer at the interface whereas bubble growth (and collapse) in cavitation is not limited by heat transfer but only by the inertia of the surrounding liquid. Cavitation is therefore an explosive (and implosive) process that is far more violent and damaging than the corresponding bubble dynamics of boiling.

7.4.3 Effect of interfacial roughness

One of the features that can alter the thermal inhibition of bubble growth occurs when the bubble surface becomes sufficiently roughened to effectively eliminate the thermal boundary layer. This may occur because of an interfacial instability or because of some external interference with the interface. Shepherd and Sturtevant (1982) and Frost and Sturtevant (1986) examined rapidly growing bubbles near the limit of superheat and found growth rates substantially larger than expected when the bubble was in the thermally inhibited range of parameters. Photographs of those bubbles (see figure 7.8) show that the interface is rough and irregular in places. The enhancement of the heat transfer caused by this roughening is probably responsible for the larger than expected growth rates. Shepherd and Sturtevant (1982) attribute the roughness to the development of a baroclinic interfacial instability. In other circumstances, Rayleigh-Taylor instability of the interface could give rise to a similar effect (Reynolds and Berthoud 1981). A flow with a high turbulence level could have the same consequence and it seems clear that this suppression of the thermal inhibition plays a key role in the phenomenon of vapor explosions (section 8.5.4).

7.5 Heterogeneous vaporization

7.5.1 Pool boiling

We now shift attention to the heat transfer phenomena associated with heterogeneous vaporization and begin with the most common version of this namely, pool boiling, in which the vapor bubbles form and grow as a result of the conduction of heat through a bounding solid surface (in a nuclear reactor the surface of the fuel rods). The most obvious application of this information is the boiling that occurs in a BWR. The heat flux per unit area through the solid surface is denoted by $\dot{q}$; the wall temperature is denoted by T_w and the bulk liquid temperature by T_b (or T_L). The temperature difference $\Delta T = T_w - T_b$ is a ubiquitous feature of all these problems. Moreover, in almost all cases the pressure differences within the flow are sufficiently small that the saturated liquid/vapor temperature, T_e, can be assumed uniform. Then, to a first approximation, boiling at the wall occurs when $T_w > T_e$ and $T_b \leq T_e$. The label *sub-cooled boiling* refers to the circumstances when $T_b < T_e$ and the liquid must be heated to T_e before bubbles occur. On the other hand vapor condensation at the wall occurs when $T_w < T_e$ and $T_b \geq T_e$. The label *super-heated condensation* refers to the circumstances in which $T_b > T_e$ and the vapor must be cooled to T_e before liquid appears at the wall.

The solid surface may be a plane vertical or horizontal containing surface or it may be the interior or exterior of a conduit. Another factor influencing the phenomena is whether there is a substantial fluid flow (convection) parallel to the solid surface. For some of the differences between these various geometries and imposed flow conditions the reader is referred to texts such as Collier and Thome (1994), Hsu and Graham (1976) or Whalley (1987). In the next section we review the phenomena associated with a plane horizontal boundary with no convection. Later sections deal with vertical surfaces.

7.5.2 Pool boiling on a horizontal surface

Perhaps the most common configuration, known as *pool boiling* is when a pool of liquid is heated from below through a horizontal surface. For present purposes we assume that the heat flux, $\dot{q}$, is uniform. A uniform bulk temperature far from the wall is maintained because the mixing motions generated by natural convection (and, in boiling, by the motions of the bubbles) mean that most of the liquid is at a fairly uniform temperature. In other words, the temperature difference ΔT occurs within a thin layer next to the wall.

In pool boiling the relation between the heat flux, $\dot{q}$, and ΔT is as sketched in figure 7.9 and events develop with increasing ΔT as follows. When the pool as a whole has been heated to a temperature close to T_e, the onset of nucleate boiling occurs. Bubbles form at nucleation sites on the wall and grow to a size at which the buoyancy force overcomes the surface tension forces acting at the line of attachment of the bubble to the wall. The bubbles then break away and rise through the liquid.

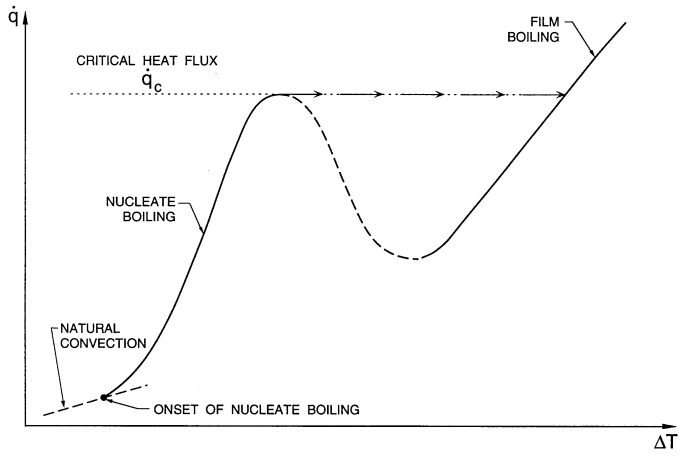

Figure 7.9: Pool boiling characteristics.

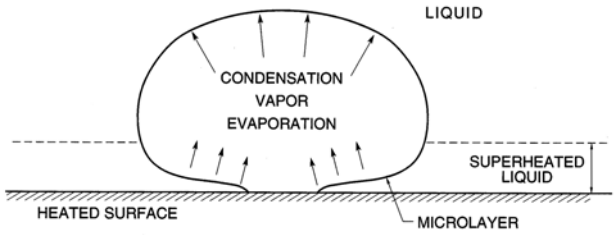

Figure 7.10: Sketch of nucleate boiling bubble with microlayer.

In a steady state process, the vertically-upward heat flux, $\dot{q}$, should be the same at all elevations above the wall. Close to the wall the situation is complex for several mechanisms increase the heat flux above that for pure conduction through the liquid. First the upward flux of vapor away from the wall must be balanced by an equal downward mass flux of liquid and this brings cooler liquid into closer proximity to the wall. Second, the formation and movement of the bubbles enhances mixing in the liquid near the wall and thus increases heat transfer from the wall to the liquid. Third, the flux of heat to provide the latent heat of vaporization that supplies vapor to the bubbles increases the total heat flux. While a bubble is still attached to the wall, vapor may be formed at the surface of the bubble closest to the wall and then condense on the surface furthest from the wall thus creating a heat pipe effect. This last mode of heat transfer is sketched in figure 7.10 and requires the presence of a thin layer of liquid under the bubble known as the *microlayer*.

At distances further from the wall (figure 7.11) the dominant component of $\dot{q}$ is simply the enthalpy flux difference between the upward flux of vapor and the downward flux of liquid. Assuming this enthalpy difference is given

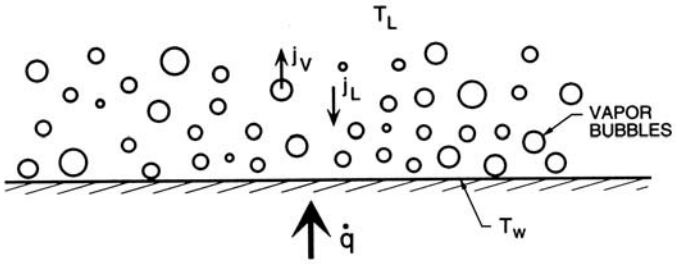

Figure 7.11: Nucleate boiling.

approximately by the latent heat, $\mathcal{L}$, it follows that the upward volume flux of vapor, j_V, is given by $\dot{q}/\rho_V\mathcal{L}$, where ρ_V is the saturated vapor density at the prevailing pressure. Since mass must be conserved the downward mass flux of liquid must be equal to the upward mass flux of vapor and it follows that the downward liquid volume flux should be $\dot{q}/\rho_L\mathcal{L}$, where ρ_L is the saturated liquid density at the prevailing pressure.

To complete the analysis, estimates are needed for the number of nucleation sites per unit area of the wall ($N^*\ m^{-2}$), the frequency (f) with which bubbles leave each site and the equivalent volumetric radius (R) upon departure. Given the upward velocity of the bubbles (u_V) this allows evaluation of the volume fraction and volume flux of vapor bubbles from:

$$\alpha = \frac{4\pi R^3 N^* f}{3u_V} \quad ; \quad j_V = \frac{4}{3}\pi R^3 N^* f \tag{7.31}$$

and it then follows that

$$\dot{q} = \frac{4}{3}\pi R^3 N^* f \rho_V \mathcal{L} \tag{7.32}$$

As ΔT is increased both the site density N^* and the bubble frequency f increase until, at a certain critical heat flux, $\dot{q}_c$, a complete film of vapor blankets the wall. This is termed *boiling crisis* and the heat flux at which it occurs is termed the *critical heat flux (CHF)* . Normally one is concerned with systems in which the heat flux rather than the wall temperature is controlled, and, because the vapor film provides a substantial barrier to heat transfer, such systems experience a large increase in the wall temperature when the boiling crisis occurs. This development is sketched in figure 7.9. The large increase in wall temperature can be very hazardous and it is therefore important to be able to predict the boiling crisis and the heat flux at which this occurs. There are a number of detailed analyses of the boiling crisis and for such detail the reader is referred to Zuber *et al.* (1959, 1961), Rohsenow and Hartnett (1973), Hsu and Graham (1976), Whalley (1987) or Collier and Thome (1994). This important fundamental process is discussed below in section 7.5.4.

7.5.3 Nucleate boiling

As equation 7.32 illustrates, quantitative understanding and prediction of nucleate boiling requires detailed information on the quantities N^*, f, R and u_V and thus knowledge not only of the number of nucleation sites per unit area, but also of the cyclic sequence of events as each bubble grows and detaches from a particular site. Though detailed discussion of the nucleation sites is beyond the scope of this book, it is well-established that increasing ΔT activates increasingly smaller (and therefore more numerous) sites (Griffith and Wallis 1960) so that N^* increases rapidly with ΔT. The cycle of events at each nucleation site as bubbles are created, grow and detach is termed the *ebullition cycle* and consists of

1. a period of bubble growth during which the bubble growth rate is directly related to the rate of heat supply to each site, $\dot{q}/N^*$. In the absence of inertial effects and assuming that all this heat is used for evaporation (in a more precise analysis some fraction is used to heat the liquid), the bubble growth rate is then given by

$$\frac{dR}{dt} = CR^{-2}\frac{\dot{q}}{4\pi\rho_V \mathcal{L} N^*} \tag{7.33}$$

   where C is some constant that will be influenced by complicating factors such as the geometry of the bubble attachment to the wall and the magnitude of the temperature gradient in the liquid normal to the wall (see, for example, Hsu and Graham 1976).

2. the moment of detachment when the upward buoyancy forces exceed the surface tension forces at the bubble-wall contact line. This leads to a bubble size, R_d, upon detachment given qualitatively by

$$R_d = C^* \left[\frac{\mathcal{S}}{g(\rho_L - \rho_V)}\right]^{\frac{1}{2}} \tag{7.34}$$

   where the constant C will depend on surface properties such as the contact angle but is of the order of 0.005 (Fritz 1935). With the growth rate from the growth phase analysis this fixes the time for growth.

3. the waiting period during which the local cooling of the wall in the vicinity of the nucleation site is diminished by conduction within the wall surface and after which the growth of another bubble is initiated.

Obviously the sum of the growth time and the waiting period leads to the bubble frequency, f. In addition, the rate of rise of the bubbles, u_V, must be estimated using the methods such as those described in Brennen (2005); note that the downward flow of liquid must also be taken into account in evaluating u_V.

These are the basic elements involved in characterizing nucleate boiling though there are many details for which the reader is referred to the texts by Rohsenow and Hartnett (1973), Hsu and Graham (1976), Whalley (1987)

or Collier and Thome (1994). Note that the concepts involved in the analysis of nucleate boiling on an inclined or vertical surface do not differ greatly. The addition of an imposed flow velocity parallel to the wall will alter some details since, for example, the analysis of the conditions governing bubble detachment must include consideration of the resulting drag on the bubble.

7.5.4 Pool boiling crisis

In this section we will follow the approach taken by Zuber, Tribius and Westwater (1961) who demonstrated that the phenomenon of boiling crisis can be visualized as a flooding phenomenon (see, for example, Brennen 2005). Consider first the nucleate boiling process depicted in figure 7.11. As liquid is turned to vapor at or near the solid surface, this results in an upward flux of vapor in the form or bubbles and, neccessarily, an equal downward mass flux of liquid. As the heat transfer rate increases these two mass fluxes increase proportionately and the interaction force between the two streams increases. This force inhibits the mass flow rate and there exists a maximum for which this flow pattern cannot sustain any further increase in heat or mass flux. This is known as the flooding point for this flow pattern and the maximum or critical heat flux, $\dot{q}_{c1}$, can be estimated (see, for example, Brennen 2005) to be

$$\dot{q}_{c1} = C_1 \rho_V \mathcal{L} \left\{ \frac{\mathcal{S} g (\rho_L - \rho_V)}{\rho_L^2} \right\}^{\frac{1}{4}} \tag{7.35}$$

where $\mathcal{L}$ is the latent heat, $\mathcal{S}$ is the surface tension, ρ_L and ρ_V are the liquid and vapor densities, and the typical bubble radius, R, is estimated to be given by

$$R = \left\{ \frac{3\mathcal{S}}{2g(\rho_L - \rho_V)} \right\}^{\frac{1}{2}} \tag{7.36}$$

Now consider the alternative flow pattern sketched in figure 7.12 in which there is a layer of vapor next to the wall. The flow within that vapor film consists of water droplets falling downward through an upward vapor flow. Analysis

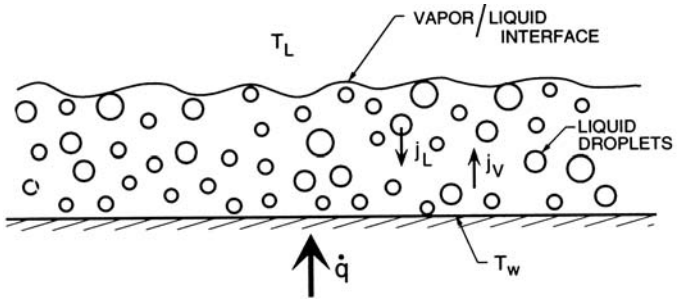

Figure 7.12: Sketch of the conditions close to film boiling.

of the Rayleigh-Taylor instability of the upper surface of that film leads to the conclusion that the size of the droplets is given by a similar expression as equation 7.36 except that the factor of proportionality is different. Further analyis of the interaction of downward mass flux of droplets flowing through the upward flux of vapor leads to the conclusion that in this flow pattern there exists a flooding condition with a maximum possible heat flux and mass flow rate. This maximum heat flux, $\dot{q}_{c2}$, can be estimated (Brennen 2005) to be

$$\dot{q}_{c2} = C_2 \rho_V \mathcal{L} \left\{ \frac{\mathcal{S} g (\rho_L - \rho_V)}{\rho_V^2} \right\}^{\frac{1}{4}} \tag{7.37}$$

where C_2 is some other constant of order unity.

The two model calculations presented above (and leading, respectively, to critical heat fluxes given by equations 7.35 and 7.37) allow the following interpretation of the pool boiling crisis. The first model shows that the bubbly flow associated with nucleate boiling will reach a critical state at a heat flux given by $\dot{q}_{c1}$ at which the flow will tend to form a vapor film. However, this film is unstable and vapor droplets will continue to be detached and fall through the film to wet and cool the surface. As the heat flux is further increased a second critical heat flux given by $\dot{q}_{c2} = (\rho_L/\rho_V)^{\frac{1}{2}} \dot{q}_{c1}$ occurs beyond which it is no longer possible for the water droplets to reach the surface. Thus, this second value, $\dot{q}_{c2}$, will more closely predict the true boiling crisis limit. Then, the analysis leads to a dimensionless critical heat flux, $(\dot{q}_c)_{nd}$, from equation 7.37 given by

$$(\dot{q}_c)_{nd} = \frac{\dot{q}_c}{\rho_V \mathcal{L}} \left\{ \frac{\mathcal{S} g (\rho_L - \rho_V)}{\rho_V^2} \right\}^{-\frac{1}{4}} = C_2 \tag{7.38}$$

Kutateladze (1948) had earlier developed a similar expression using dimensional analysis and experimental data; Zuber *et al.* (1961) placed it on a firm analytical foundation.

Borishanski (1956), Kutateladze (1952), Zuber *et al.* (1961) and others have examined the experimental data on critical heat flux in order to determine the value of $(\dot{q}_c)_{nd}$ (or C_2) that best fits the data. Zuber *et al.* (1961) estimate that value to be in the range $0.12 \rightarrow 0.15$ though Rohsenow and Hartnett (1973) judge that 0.18 agrees well with most data. Figure 7.13 shows that the values from a wide range of experiments with fluids including water, benzene, ethanol, pentane, heptane and propane all lie within the $0.10 \rightarrow 0.20$. In that figure $(\dot{q}_C)_{nd}$ (or C_2) is presented as a function of the Haberman-Morton number, $Hm = g\mu_L^4 (1 - \rho_V/\rho_L)/\rho_L \mathcal{S}^3$, since the appropriate type and size of bubble that is likely to form in a given liquid will be governed by Hm (see, for example, Brennen 2005).

Lienhard and Sun (1970) showed that the correlation could be extended from a simple horizontal plate to more complex geometries such as heated horizontal tubes in which the typical dimension (for example, the tube diameter) is denoted by d. Explicitly Lienhard and Sun recommend

$$(\dot{q}_c)_{nd} = 0.061/C^{**} \quad \text{where} \quad C^{**} = d/\left\{ \frac{\mathcal{S}}{g(\rho_L - \rho_V)} \right\}^{\frac{1}{2}} \tag{7.39}$$

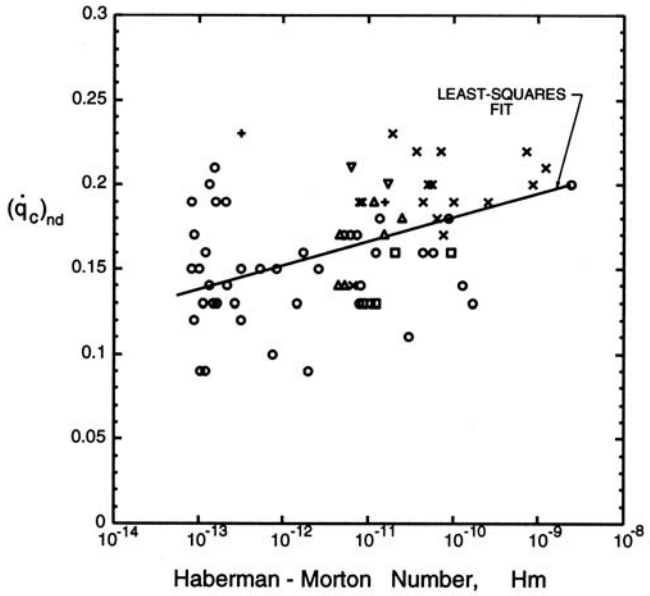

Figure 7.13: Data on the dimensionless critical heat flux, $(\dot{q}_c)_{nd}$ (or C_2), plotted against the Haberman-Morton number, $Hm = g\mu_L^4(1-\rho_V/\rho_L)/\rho_L\mathcal{S}^3$, for water (+), pentane (×), ethanol (⊡), benzene (△), heptane(▽) and propane (∗) at various pressures and temperatures. Adapted from Borishanski (1956) and Zuber *et al.* (1961).

where the constant, 0.061, was determined from experimental data; the result 7.39 should be employed when $C^{**} < 2.3$. For very small values of C^{**} (less than 0.24) there is no nucleate boiling regime and film boiling occurs as soon as boiling starts.

For useful reviews of the extensive literature on the critical heat flux in boiling, the reader is referred to Rohsenow and Hartnet (1973), Collier and Thome (1994), Hsu and Graham (1976) and Whalley (1987).

7.5.5 Film boiling

At or near boiling crisis a film of vapor is formed that coats the surface and substantially impedes heat transfer. This vapor layer presents the primary resistance to heat transfer since the heat must be conducted through the layer. It follows that the thickness of the layer, δ, is given approximately by

$$\delta = \frac{\Delta T k_V}{\dot{q}} \tag{7.40}$$

However, these flows are usually quite unsteady since the vapor/liquid interface is unstable to Rayleigh-Taylor instability (see section 7.2.5). The result of this

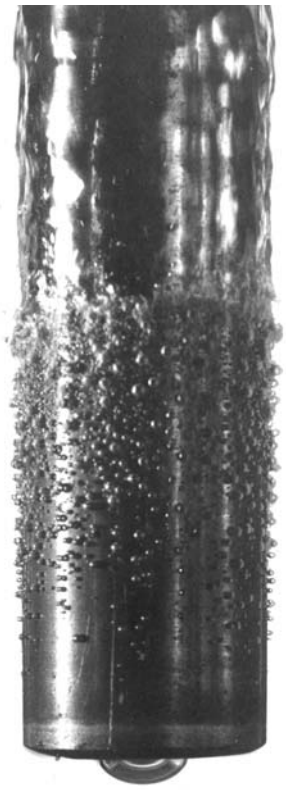

Figure 7.14: The evolution of convective boiling around a heated rod, reproduced from Sherman and Sabersky (1981).

unsteadiness of the interface is that vapor bubbles are introduced into the liquid and travel upwards while liquid droplets are also formed and fall down through the vapor toward the hot surface. These droplets are evaporated near the surface producing an upward flow of vapor. The relation 7.40 then needs modification in order to account for the heat transfer across the thin layer under the droplet.

The droplets do not normally touch the hot surface because the vapor created on the droplet surface nearest the wall creates a lubrication layer that suspends the droplet. This is known as the Leidenfrost effect. It is readily observed in the kitchen when a drop of water is placed on a hot plate. Note, however, that the thermal resistance takes a similar form to that in equation 7.40 though the temperature difference in the vicinity of the droplet now occurs across the much thinner layer under the droplet rather than across the film thickness, δ.

7.5.6 Boiling on vertical surfaces

Boiling on a heated vertical surface is qualitatively similar to that on a horizontal surface except for the upward liquid and vapor velocities caused by natural convection. Often this results in a cooler liquid and a lower surface temperature at lower elevations and a progression through various types of boiling as the flow proceeds upwards. Figure 7.14 provides an illustrative example. Boiling begins near the bottom of the heated rod and the bubbles increase in size as they are convected upward. At a well-defined elevation, boiling crisis (section 7.5.4 and figure 7.9) occurs and marks the transition to film boiling at a point about 5/8 of the way up the rod in the photograph. At this point, the material of the rod or pipe experiences an abrupt and substantial rise in surface temperature as described in section 7.5.2.

The first analysis of film boiling on a vertical surface was due to Bromley (1950) and proceeds as follows. Consider a small element of the vapor layer of length dz and thickness, $\delta(z)$, as shown in figure 7.15. The temperature difference between the wall and the vapor/liquid interface is ΔT. Therefore the mass rate of conduction of heat from the wall and through the vapor to the vapor/liquid interface per unit surface area of the wall will be given approximately by $k_V \Delta T/\delta$ where k_V is the thermal conductivity of the vapor. In general some of this heat flux will be used to evaporate liquid at the interface and some will be used to heat the liquid outside the layer from its bulk temperature, T_b to the saturated vapor/liquid temperature of the interface, T_e. If the subcooling is small, the latter heat sink is small compared with the former and, for simplicity in this analysis, it will be assumed that this is the case. Then the mass rate of evaporation at the interface (per unit area of that interface) is $k_V \Delta T/\delta\mathcal{L}$. Denoting the mean velocity of the vapor in the layer by $u(z)$, continuity of vapor mass within the layer requires that

$$\frac{d(\rho_V u\delta)}{dz} = \frac{k_V \Delta T}{\delta \mathcal{L}} \tag{7.41}$$

Assuming that we use mean values for ρ_V, k_V and $\mathcal{L}$ this is a differential relation between $u(z)$ and $\delta(z)$.

A second relation between these two quantities can be obtained by considering the equation of motion for the vapor in the element dz. That vapor mass will experience a pressure denoted by $p(z)$ that must be equal to the pressure in the liquid if surface tension is neglected. Moreover, if the liquid motions are neglected so that the pressure variation in the liquid is hydrostatic, it follows that the net force acting on the vapor element as a result of these pressure variations will be $\rho_L g\delta dz$ per unit depth normal to the sketch. Other forces per unit depth acting on the vapor element will be its weight $\rho_V g\delta dz$ and the shear stress at the wall that we will estimate to be given roughly by $\mu_V u/\delta$. Then if the vapor momentum fluxes are neglected the balance of forces on the vapor element yields

$$u = \frac{(\rho_L - \rho_V) g\delta^2}{\mu_V} \tag{7.42}$$

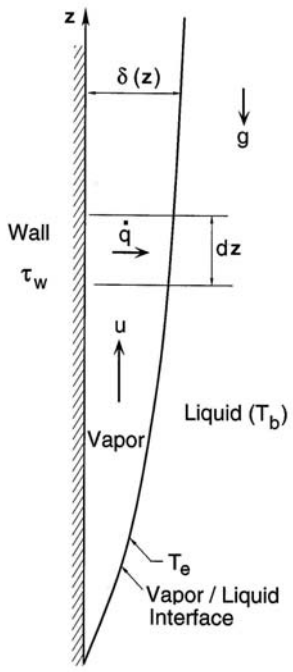

Figure 7.15: Sketch for the film boiling analysis.

Substituting this expression for u into equation 7.41 and solving for $\delta(z)$ assuming that the origin of z is chosen to be the origin or virtual origin of the vapor layer where $\delta = 0$ we obtain the following expression for $\delta(z)$

$$\delta(z) = \left[\frac{4k_V \Delta T \mu_V}{3\rho_V(\rho_L - \rho_V)g\mathcal{L}}\right]^{\frac{1}{4}} z^{\frac{1}{4}} \tag{7.43}$$

This defines the geometry of the film.

The heat flux per unit surface area of the plate, $\dot{q}(z)$, can then be evaluated and the local heat transfer coefficient, $\dot{q}/\Delta T$, becomes

$$\frac{\dot{q}(z)}{\Delta T} = \left[\frac{3\rho_V(\rho_L - \rho_V)g\mathcal{L}k_V^3}{4\Delta T \mu_V}\right]^{\frac{1}{4}} z^{-\frac{1}{4}} \tag{7.44}$$

Note that this is singular at $z = 0$. It also follows by integration that the overall heat transfer coefficient for a plate extending from $z = 0$ to $z = H$ is

$$\left(\frac{4}{3}\right)^{\frac{3}{4}} \left[\frac{\rho_V(\rho_L - \rho_V)g\mathcal{L}k_V^3}{\Delta T \mu_V H}\right]^{\frac{1}{4}} \tag{7.45}$$

This characterizes the film boiling heat transfer coefficients in the upper right of figure 7.9. Though many features of the flow have been neglected this relation

gives good agreement with the experimental observations (Westwater 1958). Other geometrical arrangements such as heated circular pipes on which film boiling is occurring will have a similar functional dependence on the properties of the vapor and liquid (Collier and Thome 1994, Whalley 1987).

7.6 Multiphase flow instabilities

7.6.1 Introduction

Multiphase flows in general are susceptible to a wide range of instabilities over and above those that occur in single phase flows. A broad review of the state of knowledge of these is beyond the scope of this; for that, the reader is referred to texts such as Brennen (2005). Nevertheless a brief review of the various types of instability that can occur in multiphase flows is appropriate and we will follow this with some examples that are pertinent to nuclear reactor applications.

We should begin a list of the types of instability with mention of the basic local instabilities that can occur in these flows. Well known and previously described are some of the local instabilities that can lead to changes in the flow regime, for example, the Kelvin-Helmholtz instability (section 7.2.5) or boiling crisis (section 7.5.4).

A second type can be identified as system instabilities within a internal flow system that lead to pressure, flow rate and volume fraction oscillations. These system instabilities can be further subdivided into those that can be analyzed using quasistatic methods (see Brennen 2005) assuming the oscillations progress through a series of quasisteady states and, on the other hand, those that are dynamic. An example of a quasistatic instabilibity is the Ledinegg instability described below in section 7.6.3. An even simpler quasistatic example are the concentration waves that can develop in some circulating systems (section 7.6.2). However there are also instabilities that do not have a simple quasistatic explanation and occur in flows that are quasistatically stable. An example of a fundamentally dynamic instability is the chugging instability described in section 7.6.4.

7.6.2 Concentration wave oscillations

Often in multiphase flow processes, one encounters a circumstance in which one part of the flow loop contains a mixture with a concentration that is somewhat different from that in the rest of the system. Such an inhomogeneity may be created during start-up or during an excursion from the normal operating point. It is depicted in figure 7.19, in which the closed loop has been somewhat arbitrarily divided into a *pipeline* component and a *pump* component. As indicated, a portion of the flow has a mass quality that is larger by $\Delta\mathcal{X}$ than the mass quality in the rest of the system. Such a perturbation could be termed a concentration wave though it is also called a density wave or a continuity wave; more generally, it is known as a kinematic wave. Clearly, the perturbation will move

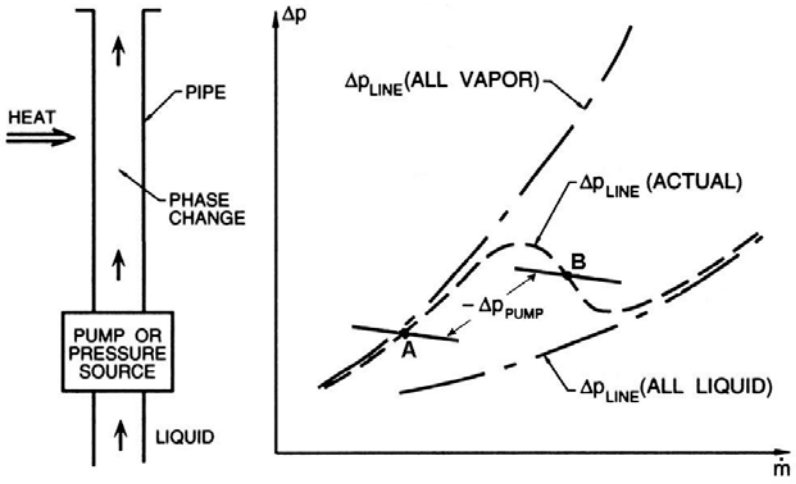

Figure 7.16: Sketch illustrating the Ledinegg instability.

round the circuit at a speed that is close to the mean mixture velocity though small departures can occur in vertical sections in which there is significant relative motion between the phases. The mixing processes that would tend to homogenize the fluid in the circuit are often quite slow so that the perturbation may persist for an extended period.

It is also clear that the pressures and flow rates may vary depending on the location of the perturbation within the system. These fluctuations in the flow variables are termed concentration wave oscillations and they arise from the inhomogeniety of the fluid rather than from any instability in the flow. The characteristic frequency of the oscillations is simply related to the time taken for the flow to complete one circuit of the loop (or some multiple if the number of perturbed fluid pockets is greater than unity). This frequency is usually small and its calculation often allows identification of the phenomenon.

7.6.3 Ledinegg instability

Sometimes a multiphase flow instability is the result of a non-monotonic pipeline characteristic. Perhaps the best known example is the Ledinegg instability (Ledinegg 1983) which is depicted in figure 7.16. This occurs in boiler tubes through which the flow is forced either by an imposed pressure difference or by a pump as sketched in figure 7.16. If the heat supplied to the boiler tube is roughly independent of the flow rate, then, at high flow rates, the flow will remain mostly liquid since, as discussed in section 7.2.5, $d\mathcal{X}/ds$ is inversely proportional to the flow rate (see equation 7.23). Therefore $\mathcal{X}$ remains small. On the other hand, at low flow rates, the flow may become mostly vapor since $d\mathcal{X}/ds$ is large. The pipeline characteristic for such a flow (graph of pressure drop

versus mass flow rate) is constructed by first considering the two hypothetical characteristics for all-vapor flow and for all-liquid flow. The rough form of these are shown in figure 7.16; since the frictional losses at high Reynolds numbers are proportional to $\dot{m}^2/\rho$, the all-vapor characteristic lies above the all-liquid line because of the lower density. However, as the flow rate, $\dot{m}$, increases, the actual characteristic must make a transition from the all-vapor line to the all-liquid line, and may therefore have the non-monotonic form sketched in figure 7.16. Now the system will operate at the point where this characteristic intersects the pump characteristic (or pressure characteristic) driving the flow. This is shown by the solid line(s) in figure 7.16. Several examples are shown in figure 7.16. An operating point such as A where the slope of the pipeline characteristic is greater than the slope of the pump characteristic will be a stable operating point. This is almost always the case with single phase flow (see Brennen (2005) for further detail). On the other hand an operating point such as B is unstable and leads in this example to the Ledinegg instability in which the operation oscillates back and forth across the unstable region producing periods of mostly liquid flow interspersed with periods of mostly vapor flow. The instability is most familiar as the phenomenon that occurs in a coffee percolator.

7.6.4 Chugging and condensation oscillations

As an example of a dynamic instability involving a two-phase flow we describe the oscillations that occur when steam is forced down a vent into a pool of water. The situation is sketched in figure 7.17 and is clearly relevant to the pressure suppression systems used in BWRs (see section 8.3), a context in which the phenomena have been extensively studied (see, for example, Wade 1974, Koch and Karwat 1976, Class and Kadlec 1976, Andeen and Marks 1978). The phenomena do however also occur in other systems in which steam (or other vapor) is injected into a condensing liquid (Kiceniuk 1952). The instabilities that result from the dynamics of a condensation interface can take a number of forms including those known as *chugging* and *condensation oscillations*.

The basic components of the system are as shown in figure 7.17 and consist of a vent or pipeline of length, ℓ, the end of which is submerged to a depth, H, in a pool of water. The basic instability is illustrated in figure 7.18. At relatively low steam flow rates the rate of condensation at the steam/water interface is sufficiently high that the interface remains within the vent. However, at higher flow rates the pressure in the steam increases and the interface is forced down and out of the end of the vent. When this happens both the interface area and the turbulent mixing in the vicinity of the interface increase dramatically. This greatly increases the condensation rate which, in turn, causes a marked reduction in the steam pressure. Thus the interface collapses back into the vent, often quite violently. Then the cycle of growth and collapse, of oscillation of the interface from a location inside the vent to one outside the end of the vent, is repeated. The phenomenon is termed condensation instability and, depending on the dominant frequency, the violent oscillations are known as *chugging* or *condensation oscillations* (Andeen and Marks 1978)

The frequency of the phenomenon tends to lock in on one of the natural modes of oscillation of the system in the absence of condensation. There are two obvious natural modes and frequencies. The first, is the manometer mode of the liquid inside the end of the vent. In the absence of any steam flow, this manometer mode will have a typical small amplitude frequency, $\omega_m = (g/H)^{\frac{1}{2}}$, where g is the acceleration due to gravity. This is usually a low frequency of the order of $1Hz$ or less and, when the condensation instability locks into this low frequency, the phenomenon is known as *chugging*. The pressure oscillations resulting from chugging can be quite violent and can cause structural loads that are of concern to the safety engineer. Another natural mode is the first acoustic mode in the vent whose frequency, ω_a, is approximately given by $\pi c/\ell$ where c is the sound speed in the steam. There are also observations of lock-in to this higher frequency and these oscillations are known as *condensation oscillations*. They tend to be of smaller amplitude than the chugging oscillations.

Figure 7.19 illustrates the results of a linear stability analysis of the suppression pool system (Brennen 1979). Constructing dynamic transfer functions for each basic component of this system (see Brennen 2005), one can calculate the linearized input impedance of the system viewed from the steam supply end of the vent. In such a linear stability analysis, a positive input resistance implies that the system is absorbing fluctuation energy and is therefore stable; a negative input resistance implies an unstable system. In figure 7.19, the input resistance is plotted against the perturbation frequency for several steam flow rates. Note that, at low steam flow rates, the system is stable for all frequen-

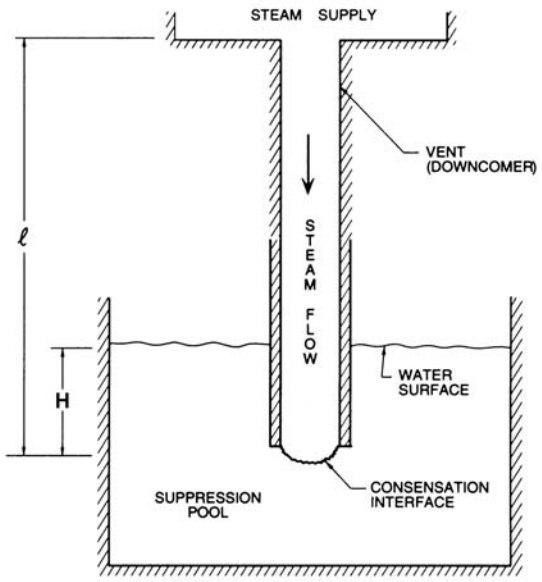

Figure 7.17: Components of a pressure suppression system.

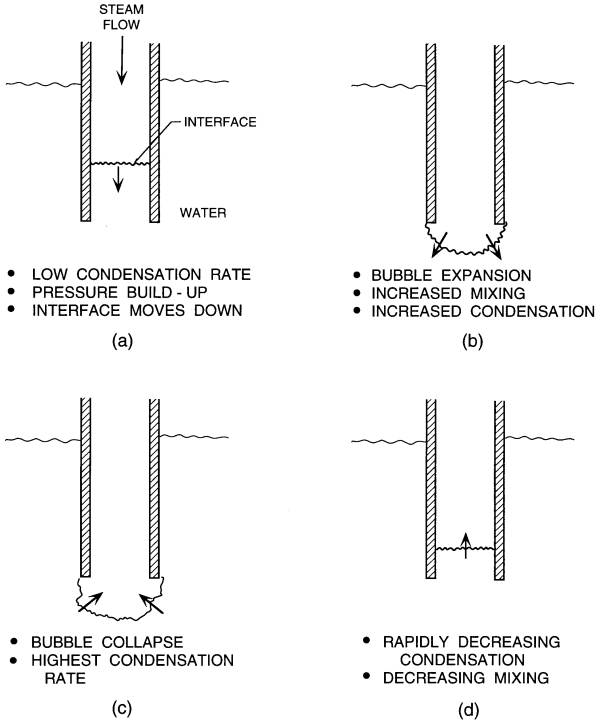

Figure 7.18: Sketches illustrating the stages of a condensation oscillation.

cies. However, as the steam flow rate is increased, the system first becomes unstable over a narrow range of frequencies close to the manometer frequency, ω_m. Thus chugging is predicted to occur at some critical steam flow rate. At still higher flow rates, the system also becomes unstable over a narrow range of frequencies close to the first vent acoustic frequency, ω_a; thus the possibility of condensation oscillations is also predicted. Note that the quasistatic input resistance at small frequencies remains positive throughout and therefore the system is quasistatically stable for all steam flow rates. Thus, chugging and condensation oscillations are true, dynamic instabilities.

It is, however, important to observe that a linear stability analysis cannot model the highly non-linear processes that occur during a *chug* and, therefore, cannot provide information on the subject of most concern to the practical engineer, namely the magnitudes of the pressure excursions and the structural loads that result from these condensation instabilities. While models have been developed in an attempt to make these predictions (see, for example, Sargis *et al.* 1979) they are usually very specific to the particular problem under investigation. Often, they must also resort to empirical information on unknown factors such as the transient mixing and condensation rates.

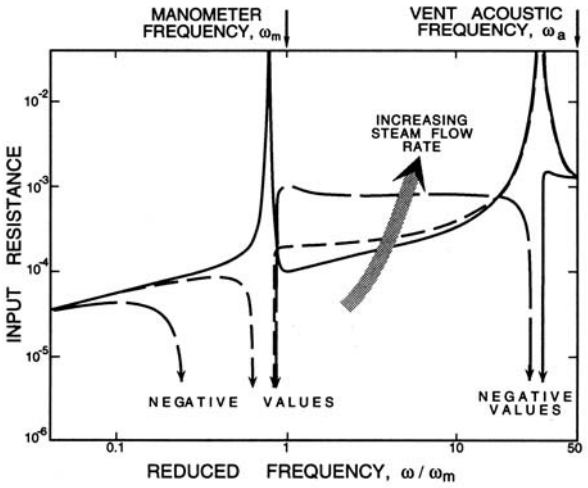

Figure 7.19: The real part of the input impedance (the input resistance) of the suppression pool as a function of the perturbation frequency for several steam flow rates. Adapted from Brennen (1979).

Finally, we note that these instabilities have been observed in other contexts. For example, when steam was injected into the wake of a streamlined underwater body in order to explore underwater jet propulsion, the flow became very unstable (Kiceniuk 1952).

7.7 Nuclear reactor context

In this and the following sections we describe how multiphase flow is pertinent to the understanding and analysis of nuclear power generation. Here we refer to those multiphase issues in the reactor itself and leave aside the many multiphase flow issues associated with the conventional components of the power generation process such as the steam generators and the steam turbine operation.

Multiphase flows that might or do occur in a nuclear reactor are most conveniently subdivided into those that occur during nominal reactor operation and those that might occur during a reactor accident. Both sets of issues are complex and multifaceted and many of the complexities are beyond the scope of this monograph. The reader is referred to texts such as Hsu and Graham (1976), Jones and Bankhoff (1977a & b), Jones (1981), Hewitt and Collier (1987), Todres and Kazimi (1990) for a broader perspective on these issues.

7.7.1 Multiphase flow in normal operation

The most obvious multiphase flow occuring during normal operation is the process of boiling in a BWR core. Sections 7.5.4, 7.5.5 and 7.5.6 described how

boiling is initiated within a BWR reactor core (section 7.5.3), how the flow pattern within the coolant passages would change from bubbly flow to annular flow as the fluid rose (sections 7.2.3) and the circumstances under which the wall film might undergo burnout (section 7.5.4) leading to the critical heat flux condition (CHF) and a rapid rise in the temperature (figure 7.9) of the interface between the fuel rod cladding and the coolant. Boiling water reactors are designed to operate at a comfortable margin short of CHF at any location within the reactor. This requires a coupled calculation of the multiphase flow and the neutronics (section 6.5) as well as an criterion that determines the CHF. For a review of the thermohydraulic data on CHF in nuclear reactors the reader is referred to Groeneveld and Gardiner (1977).

7.7.2 Void fraction effect on reactivity

In most reactors it is important to recognize that any change in the geometry of the core or change of phase of its components may alter the reactivity of the reactor. Any positive change in the reactivity, ρ, (or multiplication factor, k) that resulted from an unexpected change in the geometry would clearly be a serious safety issue. Therefore an important objective in the design of a reactor core is to achieve as negative an effect on the reactivity as possible in the event of a change of the geometry of the structure or coolant in the core.

In so far as the design of the structure of the core (particularly the topological distribution of the fuel, coolant, moderator, etc.) is concerned the objective is to create an arrangement whose reactivity would decrease in the event of any structural deformation. Examples: (1) the CANDU reactor design incorporates such an effect (see section 5.3) (2) analyses of a hypothetical core disruptive accident in an LMFBR suggest that expansion of the core in a serious accident would also result in a decrease in the reactivity (see section 8.5.3).

However, perhaps the most important effect in this category occurs in liquid-cooled reactors where any change of phase, any boiling in a PWR or LMFBR or increased boiling in a BWR can substantially effect the neutronics of the core and the reactivity of the reactor. Thus, one important objective of the multiphase flow analyses of postulated accidents is to assess the *void coefficient*, the change of the reactivity, ρ, as a result of a change in the void fraction, α, or

$$\text{Void Coefficent} \;=\; \frac{d\rho}{d\alpha} \tag{7.46}$$

This may, of course, be a function not only of time and location in the core but of other topological effects. As we discuss elsewhere, one of the substantial safety features of water-cooled thermal reactors is that boiling and loss of coolant that result from overheating causes a strong negative void coefficient since the thermal neutron supply is decreased by the reduction in the moderator (section 8.3). In contrast, most LMFBR designs have a positive void coefficient (see section 8.5.3) because the loss of the neutron slowing effect of the sodium coolant results in an increase in the population of fast neutrons. However, modified design of the geometry of the LMFBR core could reverse this dangerous attribute.

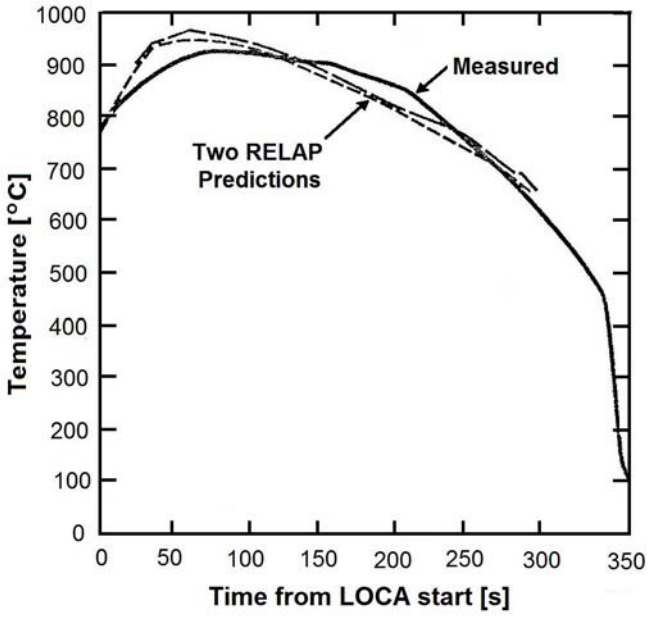

Figure 7.20: An example of a comparison between the measured cladding temperature following a simulated LOCA in a PWR model test facility (FLECHT) and the predictions of the RELAP code with two different choices of coefficients. Adapted from Hsu and Sullivan (1977).

7.7.3 Multiphase flow during overheating

In any light water reactor, it is clear that in the event of any departure from normal operation whether through unexpected depressurization or through decrease in the coolant flow (for example a LOCA), conditions in the reactor core may lead to the critical heat flux (CHF) condition being exceeded with the concominant large increase in the fuel rod temperatures. Such a circumstance could be the precursor for a core meltdown and hence the importance of being able to predict the CHF.

As we commented at the end of the preceding chapter (section 6.6) the prediction of the flows and temperatures following postulated reactor excursions and accidents is an important input to the evaluation of reactor safety. Much effort has gone into the development and validation of multiphase flow computer codes for this purpose. The objective is to make reliable predictions for the purposes of designing effective safety systems for reactors. An example of the multiphase flow and heat transfer codes developed is the extensively used RELAP code (Aerojet Nuclear Co. 1976, and, for example, Jackson *et al.* 1981, Wagner and Ransom, 1982). The details of these codes are beyond the scope of this text and the reader is referred to the references listed below for further

information. As with most multiphase numerical methods, validation presents a real challenge for the scaling of many of the phenomena involved contains uncertainties and the coefficients that govern the flow and heat transfer are hard to predict accurately. Consequently there is a need for large scale test facilities and experimental measurements that can be used for validation of these codes. Examples of these facilities and test programs, summarized by Hsu and Sullivan (1977), are the FLECHT program at Westinghouse (see, for example, Hassan 1986) and the LOFTand other facilities at the Idaho National Engineering Laboratory. As one example of a comparison between a large scale facility measurement and a computer code we include in figure 7.20 a comparison between a measured cladding temperature in a FLECHT experiment simulating a LOCA and two corresponding predictions using the RELAP code. The discrepancies are typical of the uncertainities in these complex multiphase flow predictions.

References

Aerojet Nuclear Company (1976). RELAP4/MOD5: A computer program for transient thermal-hydraulic analysis of nuclear reactors and related systems (3 volumes). *ANCR-NUREG 1335.*

Andeen, G.B. and Marks, J.S. (1978). Analysis and testing of steam chugging in pressure systems. *Electric Power Res. Inst. Report NP-908.*

Baker, O. (1954). Simultaneous flow of oil and gas. *Oil Gas J.*, **53**, 185.

Borishanski, V.M. (1956). An equation generalizing experimental data on the cessation of bubble boiling in a large volume of liquid. *Zh. Tekh. Fiz.*, **26**, No.7, 452-456.

Brennen, C.E. (1979). A linear, dynamic analysis of vent condensation stability. In *Basic Mechanisms in Two-Phase Flow and Heat Transfer* (eds. P.H. Rothe and R.T. Lahey, Jr.), ASME (No. G00179).

Brennen, C.E. (1995). *Cavitation and bubble dynamics.* Oxford Univ. Press.

Brennen, C.E. (2005). *Fundamentals of Multiphase Flow.* Cambridge Univ. Press.

Bromley, L.A. (1950). Heat transfer in stable film boiling. *Chem. Eng. Prog. Ser.*, **46**, 221-227.

Butterworth, D., and Hewitt, G.F. (1977). *Two-phase flow and heat transfer*, Oxford Univ. Press.

Class, G. and Kadlec, J. (1976). Survey of the behavior of BWR pressure suppression systems during the condensation phase of LOCA. *Paper presented at Amer. Nucl. Soc. Int. Conf., Washington, D.C., Nov. 1976.*

Collier, J.G., and Thome, J.R. (1994). *Convective boiling and condensation.* Clarendon Press, Oxford.

Elghobashi, S.E. and Truesdell, G.C. (1993). On the two-way interaction between homogeneous turbulence and dispersed solid particles. I: Turbulence modification. *Phys. Fluids*, **A5**, 1790-1801.

Fritz, W. (1935). Berechnung des Maximal Volume von Dampfblasen. *Phys. Z.*, **36**, 379.

Frost, D. and Sturtevant, B. (1986). Effects of ambient pressure on the instability of a liquid boiling explosively at the superheat limit. *ASME J. Heat Transfer*, **108**, 418–424.

Griffith, P. and Wallis, J.D. (1960). The role of surface conditions in nucleate boiling. *Chem. Eng. Prog. Symp.*, Ser. 56, **30**, 49-63.

Groeneveld, D.C. and Gardiner, S.R.M. (1977). *Post-CHF heat transfer under forced convective conditions.* In Jones, O.C. and Bankhoff, S.G.(1977).

Hassan, Y.A. (1986). Analysis of FLECHT and FLECHT-SEASET reflood tests with RELAP5 MOD2. *Nucl. Tech.*, **74**, No.2, 176-188.

Hewitt, G.F., and Roberts, D.N. (1969). Studies of two-phase flow patterns by simultaneous X-ray and flash photography. *U.K.A.E.A. Rep. No. AERE-M2159.*

Hewitt, G.F., and Hall-Taylor, N.S. (1970). *Annular two-phase flow.* Pergamon Press.

Hewitt, G.F. (1982). Flow regimes. In *Handbook of multiphase systems* (ed: G. Hetsroni). McGraw-Hill Book Co.

Hewitt, G.F. and Collier, J.G. (1987). *Introduction to nuclear power.* Taylor & Francis Group.

Hsu, Y.-Y. and Graham, R.W. (1976). *Transport processes in boiling and two-phase systems.* Hemisphere Publ. Co. and McGraw-Hill Book Co.

Hsu, Y.-Y. and Sullivan, H. (1977). *Thermal hydraulic aspects of PWR safety research.* In Jones, O.C. and Bankhoff, S.G.(1977).

Hubbard, N.G. and Dukler, A.E. (1966). *The characterization of flow regimes in horizontal two-phase flow.* Heat Transfer and Fluid Mechanics Inst., Stanford Univ.

Jackson, J.F., Liles, D.R., Ransom, D.H., and Ybarrondo, L.J. (1981). *LWR system safety analysis.* In Jones, O.C. (ed.) (1981).

Jones, O.C. and Zuber, N. (1974). Statistical methods for measurement and analysis of two-phase flow. *Proc. Int. Heat Transfer Conf., Tokyo.*

Jones, O.C. and Bankhoff, S.G. (editors) (1977a). *Symposium on the Thermal and Hydraulic Aspects of Nuclear Reactor Safety. Volume 1: Light Water Reactors.* ASME, New York.

Jones, O.C. and Bankhoff, S.G. (editors) (1977b). *Symposium on the Thermal and Hydraulic Aspects of Nuclear Reactor Safety. Volume 2: Liquid Metal Fast Breeder Reactors.* ASME, New York.

Jones, O.C. (ed.) (1981). *Nuclear reactor safety heat transfer.*Hemisphere Publ. Co.

Kiceniuk, T. (1952). A preliminary investigation of the behavior of condensible jets discharging in water. *Calif. Inst. of Tech. Hydro. Lab. Rept.*, E-24.6.

Koch, E. and Karwat, H. (1976). Research efforts in the area of BWR pressure suppression containment systems. *Proc. 4th Water Reactor Safety Research Meeting, Gaithersburg, MD, Sept. 1976.*

Kutateladze, S.S. (1948). On the transition to film boiling under natural convection. *Kotloturbostroenie*, **3**, 10.

Kutateladze, S.S. (1952). Heat transfer in condensation and boiling. *U.S. AEC Rep. AEC-tr-3770.*

Lamb, H. (1932). *Hydrodynamics.* Cambridge Univ. Press.

Lazarus, J.H. and Neilson, I.D. (1978). A generalized correlation for friction head losses of settling mixtures in horizontal smooth pipelines. *Hydrotransport 5. Proc. 5th Int. Conf. on Hydraulic Transport of Solids in Pipes.*, **1**, B1-1-B1-32.

Ledinegg, M. (1983). Instabilität der Strömung bei Natürlichen und Zwangumlaut. *Warme*, **61**, No.8, 891-898.

Lienhard, J.H. and Sun, K. (1970). Peak boiling heat flux on horizontal cylinders. *Int. J. Heat and Mass Transfer*, **13**, 1425-1440.

Lockhart, R.W. and Martinelli, R.C. (1949). Proposed correlation of data for isothermal two-phase two-component flow in pipes. *Chem. Eng. Progress*, **45**, 39-48.

Mandhane, J.M., Gregory, G.A. and Aziz, K.A. (1974). A flow pattern map for gas-liquid flow in horizontal pipes. *Int. J. Multiphase Flow*, **1**, 537-553.

Martinelli, R.C. and Nelson, D.B. (1948). Prediction of pressure drop during forced circulation boiling of water. *Trans. ASME*, **70**, 695-702.

Owens, W.L. (1961). Two-phase pressure gradient. International developments in heat transfer. *ASME Paper no. 41*, **2**, 363-368.

Pan, Y. and Banerjee, S. (1997). Numerical investigation of the effects of large particles on wall-turbulence. *Phys. Fluids*, **9**, 3786-3807.

Rayleigh, Lord. (1917). On the pressure developed in a liquid during the collapse of a spherical cavity. *Phil. Mag.*, **34**, 94–98.

Reynolds, A.B. and Berthoud, G. (1981). Analysis of EXCOBULLE two-phase expansion tests. *Nucl. Eng. and Design*, **67**, 83–100.

Rohsenow, W.M. and Hartnett, J.P. (1973). *Handbook of heat transfer*, Section 13. McGraw-Hill Book Co.

Sargis, D.A., Stuhmiller, J.H. and Wang, S.S. (1979). Analysis of steam chugging phenomena, Volumes 1, 2 and 3. *Electric Power Res. Inst. Report NP-962.*

Schicht, H.H. (1969). Flow patterns for an adiabatic two-phase flow of water and air within a horizontal tube. *Verfahrenstechnik*, **3**, No.4, 153-161.

Shepherd, J.E. and Sturtevant, B. (1982). Rapid evaporation near the superheat limit. *J. Fluid Mech.*, **121**, 379–402.

Sherman, D.C. and Sabersky, R.H. (1981). Natural convection film boiling on a vertical surface. *Lett. in Heat and Mass Transfer*, **8**, 145-153.

Shook, C.A. and Roco, M.C. (1991). *Slurry flow. Principles and practice.* Butterworth-Heinemann.

Soo, S.L. (1983). Pneumatic transport. Chap. 29 in *Handbook of fluids in motion* (eds: N.P.Cheremisinoff and R.Gupta), Ann Arbor Science.

Squires, K.D. and Eaton, J.K. (1990). Particle response and turbulence modification in isotropic turbulence. *Phys. Fluids*, **A2**, 1191-1203.

Taitel, Y. and Dukler, A.E. (1976). A model for predicting flow regime transitions in horizontal and near horizontal gas-liquid flow. *AIChE J.*, **22**, 47-55.

Todres, N.E. and Kazimi, M.S. (1990). *Nuclear systems I. Thermal hydraulic fundamentals.* Hemisphere Publ. Co.

Turner, J.M. and Wallis, G.B. (1965). The separate-cylinders model of two-phase flow. *AEC Report NYO-3114-6.*

Wade, G.E. (1974). Evolution and current status of the BWR containment system. *Nuclear Safety*, **15**, No.2.

Wagner, R.J. and Ransom, V.H. (1982). RELAP5 nuclear-plant analyzer capabilities. *Trans. Amer. Nucl, Soc.*, **43**, 381-382.

Wallis, G.B. (1969). *One-dimensional two-phase flow.* McGraw-Hill Book Co.

Weisman, J. (1983). Two-phase flow patterns. Chapter 15 in *Handbook of Fluids in Motion* (eds: N.P. Cheremisinoff and R. Gupta), Ann Arbor Science Publ., 409-425.

Weisman, J., and Kang, S.Y. (1981). Flow pattern transitions in vertical and upwardly inclined lines. *Int. J. Multiphase Flow*, **7**, 27.

Westwater, J.W. (1958). Boiling of liquids. *Adv. in Chem. Eng.*, **2**, 1-56.

Whalley, P.B. (1987). *Boiling, condensation and gas-liquid flow.* Oxford Science Publ.

Yih, C.-S. (1969). *Fluid mechanics.* McGraw-Hill Book Co.

Zuber, N. (1959). Hydrodynamic aspects of boiling heat transfer. *Ph.D. Thesis, UCLA.*

Zuber, N., Tribus, M. and Westwater, J.W. (1961). The hydrodynamic crisis in pool boiling of saturated and subcooled liquids. *Proc. 2nd Int. Heat Tranf. Conf.*, Section A, Part II, 230-237.

Chapter 8

NUCLEAR POWER ACCIDENTS

8.1 Introduction

This chapter will review the safety concerns that are critical to the public acceptance of nuclear power plants as well as the systems that have been developed and improved to address those concerns. The three major accidents to date, Three Mile Island, Chernobyl and Fukushima are briefly described and the lessons learned from those and other lesser accidents are emphasized since they have led to substantial improvement of the world's nuclear power stations.

By way of light relief and as a way of demonstrating how much public perceptions have changed we include figure 8.1. In this postcard which is undated but was probably printed in the 1950s, Aerojet-General advertises a personal nuclear reactor, the $AGN201$. The blurb on the back of the postcard is particularly disingenuous.

8.2 Safety concerns

There are two coupled, major concerns for the designer, manufacturer and operator of a nuclear power station. The first of these is to avoid any hazard associated with uncontrolled criticality of the reactor and the second is to eliminate any possible release of radioactive material to the environment surrounding the plant. The designer, manufacturer and operator seek to minimize the likelihood of any accident and this requires not only constant vigilance but also continuing improvement in the monitoring instrumentation and in the training of the plant operators.

Over the years, partly because of both the major and lesser accidents that have occurred at nuclear power stations, a great deal of time and effort has gone into examining every conceivable failure (both mechanical and human)

Figure 8.1: Postard advertising a personal reactor, circa 1950. Top: front; Bottom: obverse.

that might lead to a departure from controlled operation of a nuclear reactor power station (USAEC 1957, 1973). Fault trees (Bodansky 1996) have been exhaustively explored in order to try to eliminate any combination of malfunction and/or operator mis-management that might have serious consequences. Experience, for example during the Three Mile Island accident, has shown that a relatively minor equipment failure combined with human operator error can lead to a serious accident, even to a release of radioactivity.

Moreover, technical and operational analyses must be carried well beyond the initial failure and until a safe and controlled state has again been established. Thus the failure trees must postulate quite unlikely initial failures and then follow the progression of events that necessarily unfold in the seconds, minutes, hours and weeks that follow. Thus, for example, much attention has been given

to the hypothetical *loss of coolant accident* (LOCA) (see sections 8.5.2 and 8.5.3) that would occur if part of the primary coolant circuit were to fail so that coolant were to escape into the secondary containment and the heat produced in the reactor were no longer being removed by the coolant. The subsequent build-up of heat within the reactor could lead to a meltdown of the core and its containment, a scenario that became popularized by the movie *The China Syndrome* (see, for example, Lewis 1977, Okrent 1981, Collier and Hewitt 1987). The likelihood that such a meltdown would also lead to a release of radioactive material led to exhaustive study of this particular developing fault path.

These explorations of conceivable fault trees and accidents led to the installation of equipment designed to mitigate the effects of these unlikely events. Indeed, to minimize the potential of human error it is also desirable that these safety systems be *passive* (not requiring human or mechanical intervention and not requiring power) though this is not always possible. In the next section we describe some of the installed safety systems, with particular focus on those systems designed to mitigate the consequences of a loss of coolant accident.

Another class of concerns is the vulnerability of nuclear reactors to large external events and forces, such as earthquakes, tsunamis, volcanoes, hurricanes, power outages, and terrorist attacks. Many of these involve the choice of the site of a nuclear power plant. Particularly in California, a great deal of attention has been given to the proximity of earthquake faults and the need to ensure that the reactor, its containment structures and emergency power systems are as impervious as possible to a major earthquake (Bodansky 1996, Okrent 1981). Moreover, these power plants require copious external cooling water and are therefore often sited close to the ocean. The Fukushima accident (see section 8.4.3 below) demonstrated that more thought should have been given to protecting the plant and its surrounding auxiliary facilities from the tsunami danger. Another scenario which needed to be examined in the aftermath of the 9/11 disaster in 2001 was the possibility of a direct hit by a fully loaded airliner. Analyses and tests have shown that under no circumstances would there be any penetration of the containment building; the airliner would simply disintegrate.

Of course, public imagination conjures up the possibility of an even more drastic accident, namely a nuclear explosion. It is, however, contrary to the fundamental laws of physics for any commercial nuclear reactor containing fuel enriched to less than 5% to explode like a nuclear bomb. It is also important to emphasize that, apart from the Chernobyl accident, *no one* (neither a member of the public nor a plant worker) has ever died as a result of exposure to a commercial nuclear reactor incident. Moreover, as we discuss below, the world has put any future Chernobyl incident beyond the realm of possibility.

8.3 Safety systems

The safety systems installed in modern nuclear reactors for electricity generation have three basic purposes: (1) to control the reactivity of the reactor, to maintain it in a marginally critical state during power production and to shut

the reactor down when that is required (2) to cool the fuel and prevent overheating and (3) to contain all radioactive substances and radiation even in the event of radical, hypothetical accidents. While detailed description of each of these strategic objectives is beyond the scope of this text we will comment on each individually.

Though the control of a nuclear power plant is a complex and multi-faceted issue (see, for example, Schultz 1955), the reactivity of a normally operating reactor is primarily controlled by the insertion or withdrawal of the control rods whose effect was demonstrated in section 4.7.4. One of the most reassuring features of water cooled and moderated nuclear reactors (in effect most of the present commercial reactors) is that any overheating of the core that is sufficient to vaporize the cooling water within it will automatically result in a decrease in the reactivity (since thermal neutrons are not being fed back to the fuel) and consequently a shutdown of the nuclear reactor core. Of course, the fuel will still produce decay heat and therefore special cooling systems are needed to prevent the decay heat from causing an excessive overheating of the core.

Consequently, all modern nuclear reactors are equipped with redundant *Emergency Core Cooling Systems (ECCS)* that force cooling water into the primary containment vessel and the core in the event of an uncontrolled build up of heat. Some of these systems are passive (needing no power so they function in the absence of emergency generating power) and some are active. In addition, containment structure (see figure 5.5) is designed to prevent any escape of radioactive substances even if the primary containment were to fail or leak. As described in section 7.7.3, extensive multiphase flow analyses and simulated experiments (see, for example, Hochreiter 1985) have been carried out in order to evaluate the effectiveness of these cooling systems following a postulated LOCA.

8.3.1 PWR safety systems

In a PWR the ECCS (see figure 8.2) consist of a number of water injection and spray systems each with multiple injection points. There is a passive accumulator injection system consisting of two or more large tanks of water connected via a check valve to the primary coolant cold leg and maintained under a nitrogen pressure of $15 - 50atm$ so that they inject water when the pressure in the primary coolant loop drops below a critical level. There are also several active water injection systems, typically a high pressure coolant injection system (HPCI) designed to operate when the primary coolant loop pressure is high and therefore to operate for small breaks. There is also a low pressure coolant injection system (LPCI) designed to operate for large breaks or when the primary coolant loop pressure is low. These injection systems are intended to flood the reactor core from below.

In a PWR the secondary containment structure (see figure 8.3)is designed to withstand the pressure that would be generated if all of the primary cooling water were released into that containment, a circumstance that is estimated to result in a maximum possible pressure of $5atm$. As shown it is also equipped

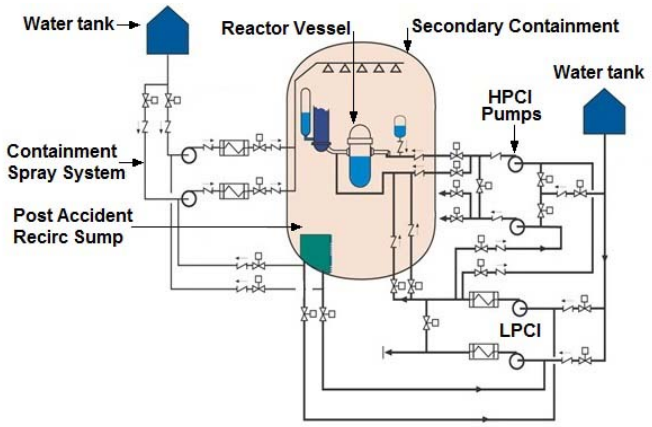

Figure 8.2: Schematic of the ECCS system in a PWR.

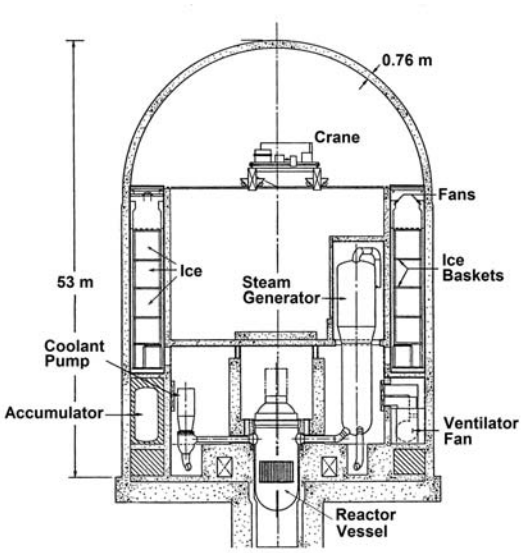

Figure 8.3: Typical PWR primary coolant loop and containment system. Adapted from USAEC (1973).

with cold water spray systems (see figure 8.2) and sometimes ice to prevent the build up of excessive heat and pressure within that containment in the event of cooling water and other substances escaping from the primary containment.

8.3.2 BWR safety systems

A typical BWR ECCS (figure 8.4) has similar HPCI and LPCI systems as well as spray systems above the core and within the reactor vessel itself (see figure 8.5). Usually one spray system is designed to operate while the pressure within the reactor vessel is high (the High Pressure Core Spray, HPCS) and another for lower reactor vessel pressures (the Low Pressure Core Spray, LPCS). There is also a spray system outside the reactor vessel and inside the secondary containment structure whose purpose is to cool the primary containment vessel and its contents from the outside.

In a BWR the potential consequences of the release of all of the primary cooling water are handled differently than in a PWR. As described in section 7.6.4, the steam would be forced down into a *pressure suppression pool* or *wetwell* where it would condense and thus prevent a build-up of pressure in the primary containment. The first Mark I configuation of this suppression pool was a toroidal shape as shown in figure 8.6; General Electric introduced later Mark II and Mark III versions that are sketched in figure 8.7. Concerns about the oscillatory condensation phenomema that might occur if these suppression pools were to be brought into action raised issues of the structural loads that might result and the ability of the suppression pool structure to withstand those loads. Several very large scale experiments were carried out in order to answer those questions.

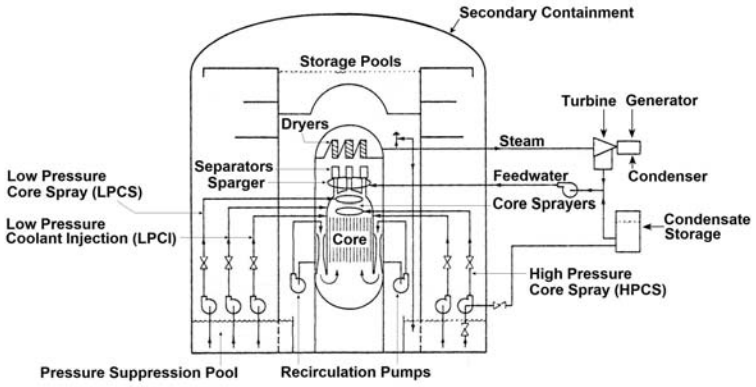

Figure 8.4: Schematic of the ECCS system in a GE Mark III BWR. Adapted from Dix and Anderson (1977), Lahey (1977).

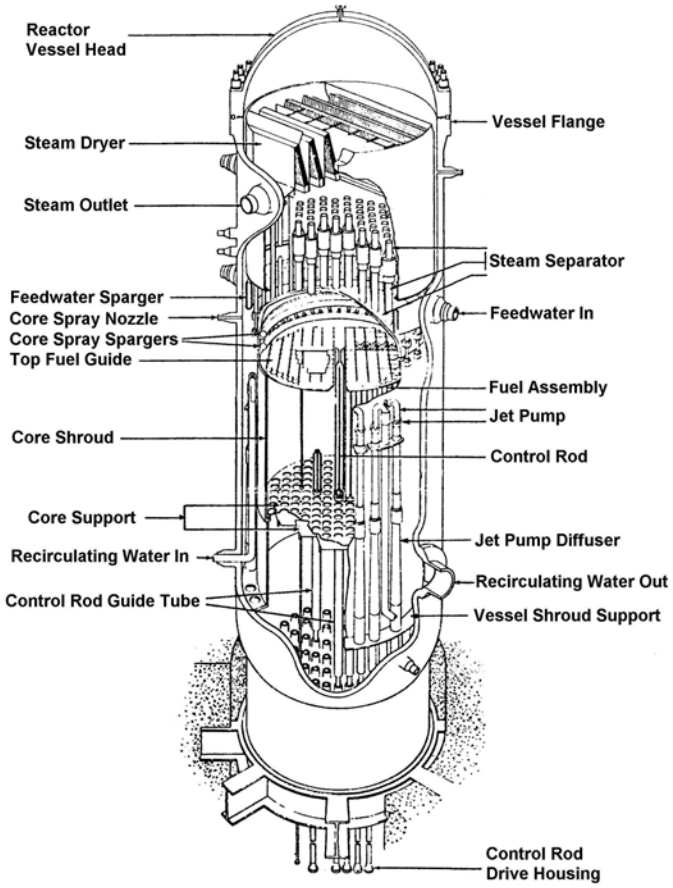

Figure 8.5: Typical BWR reactor vessel. Adapted from USAEC (1973).

8.4 Major accidents

There have been three major accidents at nuclear power stations. Each of these has not only had a major political effect on the future of nuclear power but has also driven home some important lessons that have greatly improved the safety of nuclear power plants. The political implications are beyond the scope of this text though it is clear that they will cause any future developments in the industry to be very conservative. For example, it is hard to visualize that any reactor with positive or near positive void coefficient of reactivity (see section 7.7.2) would be politically acceptable in the foreseeable future and this may eliminate many FBR designs.

The engineering lessons learned are, however, within the scope of this text and demand a description of all three of the major accidents. Of course there have also been a number of lesser accidents and mention of these will be made

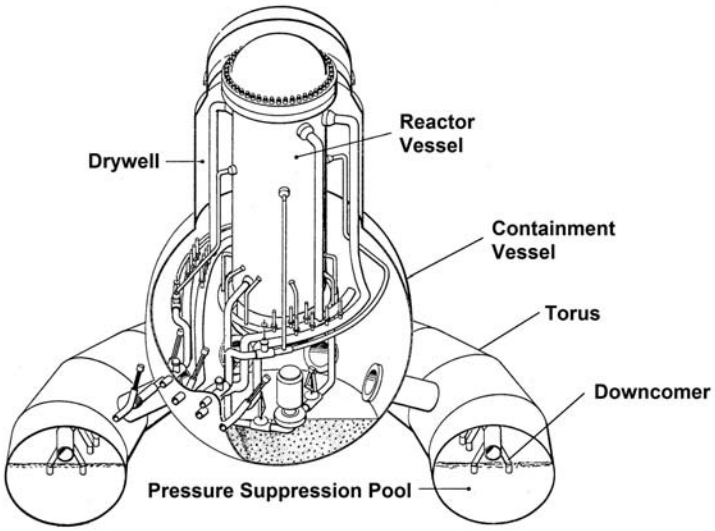

Figure 8.6: Schematic of the BWR (Mark I) primary containment and pressure suppression systems. Adapted from USAEC (1973).

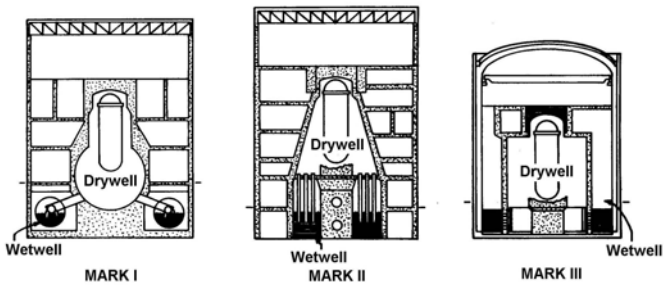

Figure 8.7: Mark I, Mark II and Mark III BWR pressure suppression systems. Adapted from Lahey (1977).

where appropriate.

8.4.1 Three Mile Island

In March 1979 the operational PWR at Three Mile Island experienced a loss of coolant accident (LOCA) (see sections 8.5.2 and 8.5.3) when a pressure relief valve in the pressurizer (figure 5.4) stuck open without the operators realizing what had happened (Cameron 1982). The primary coolant drained out of the core which then overheated. The operators injected emergency cooling water with little effect partly because, unknown to the them, water continued to drain out of the jammed pressure relief valve. Meanwhile, unexpectedly, a large bubble

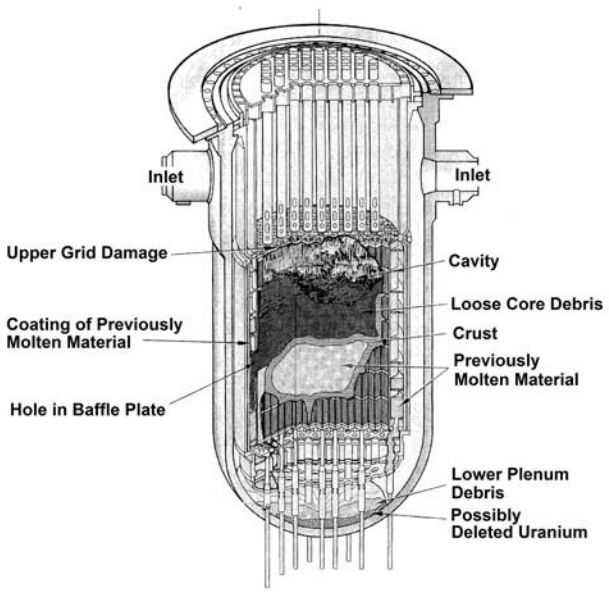

Figure 8.8: State of the Three Mile Island reactor after the accident. Adapted from Osif *et al.* (2004).

of steam and gas formed at the top of the core and prevented water from rising into it and cooling it. Half of the reactor melted and, in the process, the operators were forced to release a little radioactive steam to the atmosphere in order to prevent excessive pressure build up in the containment building. Parenthetically there was some build up of hydrogen due to the high temperature interaction of steam with the zircaloy cladding and this may have exploded in the upper core. Eventually, sufficient water was forced into the core to cool it and bring the situation under control. The reactors other protection systems functioned as they should and the concrete containment building prevented any further release of radioactive material.

For some months after the accident it was assumed that there had been no core meltdown because there was no indication of serious radioactive release within the secondary containment structure. However, as depicted in figure 8.8 (Osif *et al.* 2004), it transpired that almost half the core had melted. Despite this the reactor vessel remained almost completely in tact and there was no major escape of radioactive material into the secondary containment structure. This helped allay the worst fears of the consequences of core meltdown in other LWR plants.

The principal conclusion in the aftermath was that improved instrumentation was needed to ensure the operators had reliable information on the state of the reactor systems. If they had known the relief valve was open the damage to the reactor would have been much less. In addition, it was concluded that

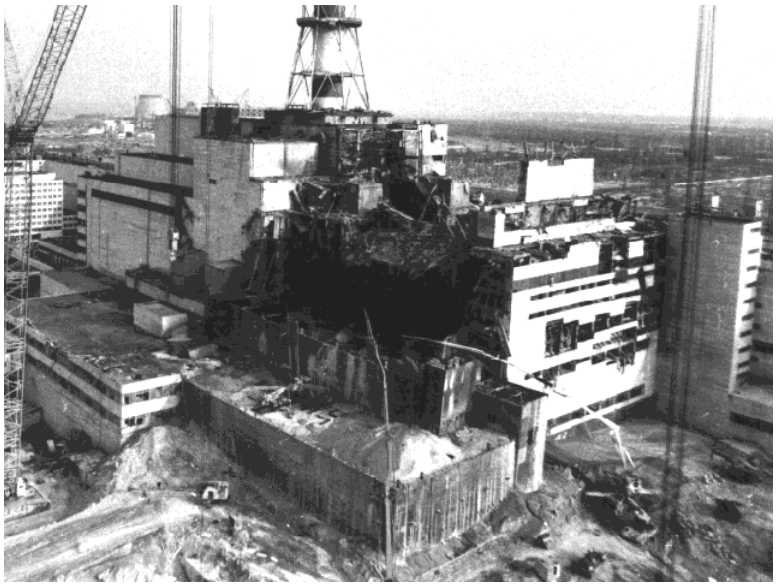

Figure 8.9: Photograph of the Chernobyl accident site taken shortly after the accident (http://gallery.spaceman.ca/d/4383-3/fruin4m.gif).

operator error also contributed to the accident and therefore improved training was also needed.

8.4.2 Chernobyl

The worst nuclear reactor accident occurred in the Ukraine in April 1986 when an old Russian RBMK boiling water reactor (see figure 5.12) suffered an intense fire in the nuclear core that resulted in destruction of the reactor and the death of 56 people. It also caused radiation sickness in another 200-300 workers and firemen and contaminated a large area in Ukraine and the neighboring country of Belarus (see figure 8.10). It is estimated that 130,000 people in the vicinity of the reactor received radiation above international limits. The photograph in figure 8.9 demonstrates how extensive the damage was to the reactor building. The accident and its aftermath have been extensively documented (see, for example, Marples 1986, Mould 2000) and exhaustively analyzed.

This reactor not only did not have a secondary containment structure that might have prevented much death, injury and contamination but it was also of the type that could have a positive void coefficient (see section 7.7.2) though this is not believed to have contributed to the accident. Eventually the remains of that reactor were covered in concrete; plans to enclose the whole mess with an additional $107m$ tall, semi-cylindrical sarcophagus are currently underway (see figure 8.11).

The Chernobyl disaster clearly demonstrated the serious safety deficiencies

Figure 8.10: Map of the location and restricted area of the Chernobyl reactor. (https://encrypted-tbn0.gstatic.com/images?q=tbn:ANd9GcQCtPzUmokYg-Bs6lSMWhbZgN GDs7wKZ47thXTwlFIBXI9B4evqw).

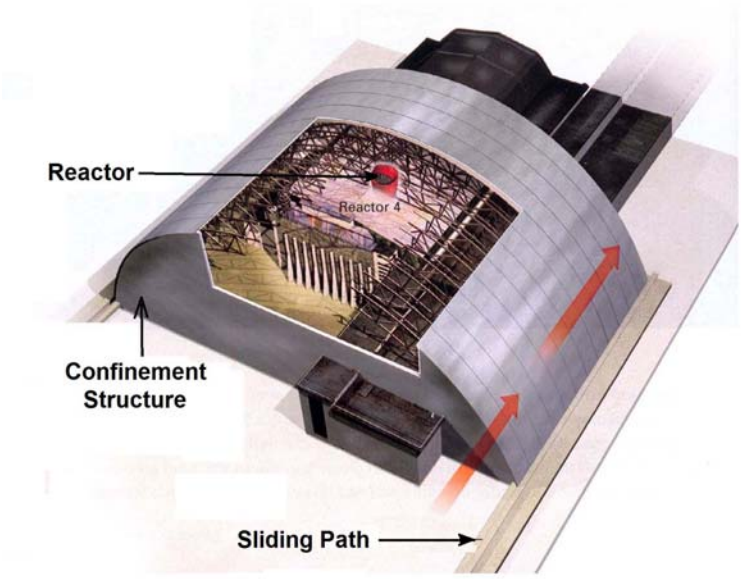

Figure 8.11: Schematic of the removable containment building planned for the Chernobyl reactor. Drawing reproduced from National Geographic Magazine, April 2006.

Figure 8.12: Tsunami wave striking the Fukushima Daiichi nuclear power plant. From ANS Nuclear Cafe website.

in these old Russian nuclear power plants and the wisdom in other designs of several layers of reactor confinement, particularly a carefully designed secondary confinement structure. These old reactors have now been removed from service or radically altered and similar hypothetical mishaps have been carefully analyzed to ensure that there could be no repeat of the Chernobyl disaster.

8.4.3 Fukushima

On March 11, 2011, three operating Mark 1 BWRs at a power station in Fukushima, Japan (out of the six at the site - the other 3 were not operating), shutdown automatically and successfully when they experienced a huge magnitude 9.0 earthquake. One hour later cooling, driven by the backup generators, was proceeding normally when the generators were swamped by a large tsunami (see figure 8.12), causing the generators to stop and the ECCS systems to fail. The cores heated up uncontrollably and partially melted before the situation was brought under control though not before several hydrogen explosions occurred. Despite this series of failures, the secondary containment was largely successful. There were no deaths though some workers received non-lethal radiation doses. Figure 8.13 shows the location and various exclusion zones around the damaged Fukushima Daiichi nuclear power plant.

This accident did confirm the viability of the secondary containment system but showed that more attention needed to paid to the siting of nuclear power plants (see Okrent 1981) and to the emergency provision of power for the safety systems at nuclear power plants. Many plants are situated near large bodies of water so as to provide cooling water; therefore, they may be susceptible to

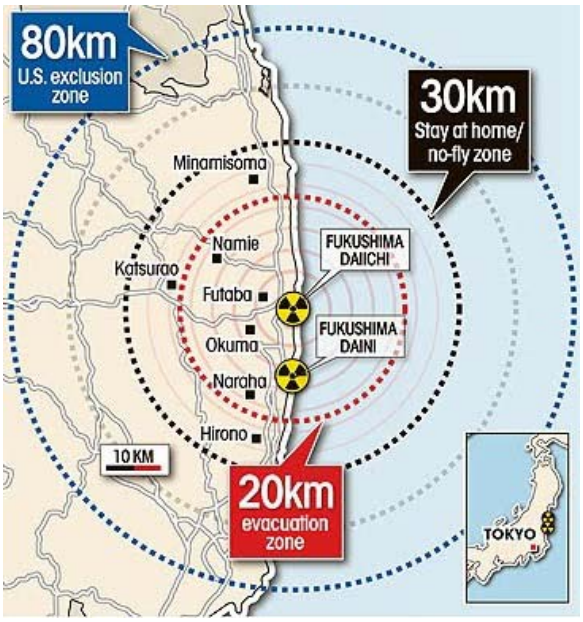

Figure 8.13: Location and exclusion zones around the Fukushima Daiichi plant.

floods, tides and tsunamis. Upgrading of the protection from such hazards has been occurring around the world, most notably in France.

8.4.4 Other accidents

There have, of course, been other lesser accidents during about 15,000 cumulative reactor-years of commercial nuclear power plant operation throughout the world. There has also been extensive experience in other reactors, mostly military and experimental; in particular the US Navy who have operated nuclear power plants since 1955 have an excellent safety record. Among the non-military plants, aside from the three major accidents there have been about ten core meltdowns mostly in non-commercial reactors and none of these generated any hazard outside the plant. One of the reasons for the fine record of the US Navy is that there was broad standardization in the design, construction and management of their power plants. This allowed for safety experience to be broadly applied with subsequent widespread benefit. It is now recognized that a corresponding lack of standardization in commercial power plants significantly impaired their safety margins. In the aftermath, both national and international agencies charged with nuclear plant oversight are actively involved in pressing for standardization not only in the construction of new plants but also in the upgrading of older plants. In a broader context, global cooperation on safety issues has increased greatly in the aftermath of Chernobyl and Fukushima (see, for example, OCED 1996).

8.5 Hypothetical accident analyses

Safety concerns with nuclear plants, particularly the fear of the release of radioactive materials, have led to very careful analyses of all the conceived deviations from normal operation of the reactor and of all the conceived accidents that might have serious consequences. Of course, about $15,000 hrs$ of accumulated experience with nuclear power generation around the world have contributed substantial validity to these conceivable accidents and their likelihood of occurrence. One of the lessons from this experience, is that the combination of minor events can sometimes lead to major problems. This makes accident prediction even more complex since it requires investigation of many more accidental permutations.

Conceivable events in a nuclear generating plant are classified as (A) normal operating transients that require no special action (B) faults that may require reactor shutdown but which allow fairly rapid return to normal operation (C) faults that result in unplanned shutdown that will result in extended shutdown and (D) limiting faults that may result in the release of radioactive material.

8.5.1 Hypothetical accident analyses for LWRs

First, we focus on the last category of faults, limiting faults, in light water reactors (see USAEC 1973, URNRC 1975); this category includes but is not confined to the following postulated accidents:

1. Major rupture of primary coolant loop pipes (PWR and BWR) leading to a *loss of coolant accident* (LOCA).
2. Major rupture of secondary coolant loop pipes (PWR)
3. Steam generator rupture (PWR)
4. Locked rotor on a coolant pump
5. Fuel handling accident
6. Failure of control rod mechanism housing
7. Tornadoes, flooding, earthquakes, etc.

We will not attempt to detail each of these postulated accidents but rather focus on the first item, the loss of coolant accident (LOCA) since it has been judged the postulated accident most likely to lead to the release of radioactive material.

8.5.2 Loss of coolant accident: LWRs

The worst scenario leading to a LOCA envisages an instantaneous double-ended or guillotine break in the primary coolant piping in the cold leg between the primary containment vessel and the primary coolant pump. This would result

in the rapid expulsion of reactor coolant into the primary containment, loss of coolant in the reactor core and rapid increase of the temperature of the core. This, in turn, might lead to a rapid increase in the pressure and temperature in the secondary containment; consequently the secondary containment must be designed to withstand these temperatures and pressures as well as potential complications that might follow (see below). Moreover, even though the loss of coolant in the core would result in shutdown of the chain reaction (see section 7.7.2), the decay heat could result in core meltdown unless the emergency core cooling systems were effective. Core meltdown might result in radioactive materials being released into the secondary containment and hence that secondary barrier needed to be designed to contain those radioactive materials.

The progress of a hypothetical LOCA and the steps taken to bring the accident under control can be divided into three phases, namely the blowdown phase, the refill phase and the reflood phase. During the first or blowdown phase the coolant is visualized as flashing to steam with two-phase flow proceeding through the primary cooling system and out through the guillotine break. Such multiphase flows are not easy to simulate with confidence and much effort has gone into developing computer codes for this purpose (see section 7.7.3) and into experimental validation of the results of those codes. These validation experiments needed to be conducted at large scale due to the uncertainty on how these multiphase flows scaled (see, for example, Holowach *et al.* 2003, Grandjean 2007). In order to evaluate the behavior of in a PWR LOCA, a large scale facility called the *Loss of Fluid Test Facility* (LOFT) was constructed at the Idaho National Laboratory for this purpose. Advantage was also taken of a decommissioned reactor structure at Marviken, Sweden, to conduct additional blowdown tests mimicking a LOCA. For BWRs, General Electric conducted special full-scale blowdown tests at Norco in California. Key outcomes from these experiments were estimates of (a) the rate of steam and enthalpy ejection from the primary containment, a process that probably involved critical or choked flow through the effective orifice created by the break (b) the forces placed on the system by this flow in order to evaluate the possibility of further structural damage (c) the amount of heat removed from the core by this flow which, in turn, defines the role of the subsequent refill and reflood phases (some analyses assume, conservatively that no heat is removed).

About $10-20sec$ after the start of the blowdown, the emergency core cooling system (ECCS) (described in section 8.3) begins operation and this marks the beginning of the second or refill phase. Accurate prediction of the complex two-phase flows generated by the injection and spray systems is essential to ensure that the accident can be brought under control. This relies on a combination of well-tested computational tools backed up by both small and large scale experiments. Using these tools predictions can be made of the development of the LOCA and its amelioration. An example of the information obtained is presented in figure 8.14 which shows how the maximum temperature in the cladding might change during the three phases of the accident using either conservative assumptions or best estimates.

By definition the refill stage ends when the liquid coolant level in the lower

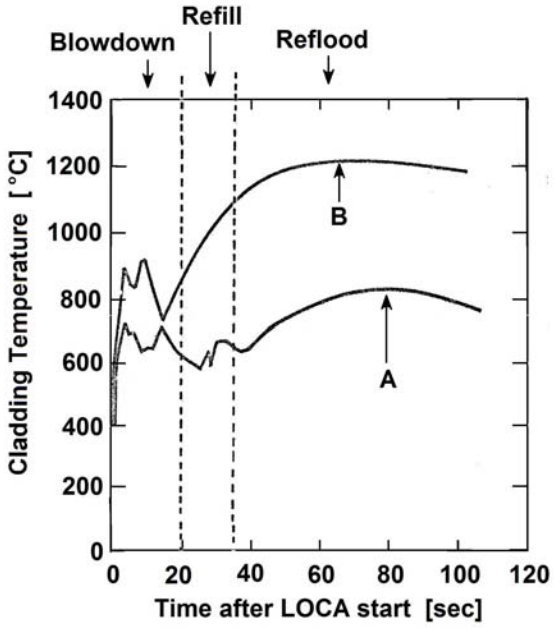

Figure 8.14: Estimated maximum temperature in the cladding during a postulated LOCA in a PWR as a function of time: (A) using realistic assumptions and (B) using conservative assumptions. Adapted from Hsu (1978).

plenum rises to the bottom of the core; the last or reflood stage begins at this time. Reflood involves the quenching of the hot core as the liquid coolant rises within it (see, for example, Hochreiter and Riedle 1977). The liquid coolant may be coming from the spray and injection system above the core or from the injection below the core. In the former case quenching may be delayed as the water is entrained by the updraft of steam originating either in the core or in the lower plenum as a result of continuing flashing of the coolant. Such a *counter-current flooding condition* (CCFL) (see Brennen 2005) may delay quenching either throughout the core or only in the hotter central region of the core. Indeed a strong steam circulating flow is likely in which a steam/water droplet flow rises in a central column of the core and descends outside this central region. Other important differences can be manifest during reflood. For example, the *fast reflood* is defined as occuring when the liquid velocity exceeds the quench front velocity at the surface of the fuel rods (typically about $0.04m/s$ while a *slow reflood* involves coolant velocities less than the quench front velocity. Consequently, the two-phase flow conditions during reflood are unsteady, complex and three-dimensional and require substantial computational and experimental efforts in order to anticipate their progress.

8.5.3 Loss of coolant accident: LMFBRs

Studies of postulated loss of coolant accidents in LMFBRs necessarily begin with two basic differences between LMFBRs and LWRs. The first and most obvious is that the coolant in the LMFBR (and we confine our attention here to sodium) is contained at low pressure and at a temperature well below its boiling temperature. Consequently a primary coolant loop depressurization does not lead to the kind of rapid vaporization that occurs during the initial phase of a LOCA in a LWR. However, the second major difference is that in most LMFBR designs overheating of the coolant in the core that leads to boiling and increased void fraction then produces an increase in the reactivity and therefore increase in the heat generated. Accident analyses and safety systems necessarily take into account these major differences in the reactor designs.

Specifically, boiling and loss of sodium in the core of an LMFBR would cause changes in the reactivity as follows. The sodium would no longer slow down the neutrons and hence there would be proportionately more fast neutrons. The neutron absorption by the sodium would be absent but this is a lesser effect than the increase in the number of fast neutrons. The net effect is an increase in the reactivity of the reactor giving it a *positive void coefficient* (see section 7.7.2) though, to some extent, this potential increase is reduced by the increase in the flux of neutrons out of the reactor at its *edges*. In most designs this is not sufficient to overcome the positive void coefficient of the bulk of the reactor and the resulting reactivity increase would therefore result in an increase in the core heat production. This is in contrast to the LWR response and means that a LOCA in an LMFBR could have more serious consequences and could more readily result in a core meltdown. This is the reason for a focus on the *hypothetical core disassembly accident* discussed below. It is, however, valuable to point out that there have been efforts to redesign an LMFBR core in order to achieve a negative as opposed to positive void coefficient. One way this could be done would be to change the geometry of the core and the blanket so that the negative effect of an increased leakage of neutrons as a result of the voidage more than negates the positive void effect in the bulk of the core (Wilson 1977).

The most likely scenario for a LOCA in an LMFBR is considered to be a blockage in one of the core coolant channels that leads to overheating in that channel, boiling and increased void fraction of the core coolant. With a positive void coefficient this might lead to escalating temperatures and to possible melting of the cladding of the fuel rods. While this series of events could be avoided by prompt reactor shutdown, nevertheless the consequences of such a cladding melt have been exhaustively analyzed in order to understand the events that might follow. The conceivable scenarios are termed *hypothetical core disassembly accidents (HCDA)* and, within that context, it is possible that a *vapor explosion* or a *fuel coolant interaction (FCI)* event might occur. We discuss these phenomena below.

8.5.4 Vapor explosions

One of the accident scenarios that is of concern and that has been studied in the context of both LMFBRs and LWRs is possibility of a *vapor explosion*. In order to assess the potential for and consequences of a vapor explosion (or of a fuel coolant interaction as described in the section that follows) note must first be made of the basic classes of vaporization identified in section 7.4.1. A vapor explosion is defined as the explosive growth of a vapor bubble(s) within a liquid due to the presence of a large, nearby heat source. As described in section 7.4.1, explosive growth of this kind only occurs under a set of particular conditions when the growth is not limited by thermal or heat transfer effects but only by the inertia of the surrounding liquid that is accelerated outward during the bubble(s) growth. Vapor explosions can occur in a number of other technological circumstances. Cavitation at normal pressures is an example of a vapor explosion caused by depressurization of a liquid (Brennen 1995). Vapor explosions also occur when one, highly volatile liquid mixes with another at a higher initial temperature. One example of this occurs when liquid natural gas (or methane) is spilled into water at normal temperatures (Burgess *et al.* 1972) (this is a particular issue in LNG transportation accidents).

In other circumstances the thermal boundary layer at the interface of the bubble(s) inhibits the supply to the interface of the necessary latent heat of vaporization. This is what happens when water is boiled on the stove at normal pressures and this effect radically slows the rate of vaporization and the rate of bubble growth as described in section 7.4.2, in effect eliminating the *explosion*. Such thermally-inhibited growth is manifest in many technological contexts, for example in the growth of bubbles in the liquid hydrogen pumps of liquid-propelled rocket engines (Brennen 1994). Thermally-inhibited growth tends to occur when the saturation condition of the liquid/vapor at higher saturation pressures and temperatures, whereas non-thermally-inhibited growth tends to occur closer to the triple point of the liquid/vapor.

As described in section 7.4.3, other factors that can effect whether explosive growth or thermally-inhibited growth occurs are the conditions at the interface. If the thermal boundary layer is disrupted by instability or by substantial turbulence in the flow then the rate of vaporization will substantially increase and explosive growth will occur or be re-established. Indeed in a cloud of bubbles the growth itself can cause sufficient disruption to eliminate the thermal inhibition. The vapor explosion would then be self-perpetuating.

However, at the kinds of normal operating temperatures for the water coolant in a LWR or the sodium coolant in an LMFBR, all bubble growth in the absence of other effects as described in the following section would be strongly thermally inhibited (Brennen 1995) and highly unlikely to cause a self-perpetuating vapor explosion. To the author's knowledge no such event has been identified in any nuclear reactor.

8.5.5 Fuel coolant interaction

A fuel coolant interaction (FCI) event is a modified vapor explosion in which a second material (a liquid or solid) is brought into close proximity to the vaporizing liquid interface and provides the supply of latent heat of vaporization that generates vapor bubble growth. It belongs to a class of vaporization phenomena caused by the mixing of a very hot liquid or solid with a volatile liquid which then experiences vaporization as a result of the heat transfer from the injected material. Of course, the result may be either relatively benign thermally-inhibited vapor bubble growth or it may be explosive, non-thermally-inhibited growth. Both have been observed in a wide range of different technological and natural contexts, the latter often being described as an *energetic* fuel/coolant explosion. Examples of such energetic explosions have been observed as a result of the injection of molten lava into water (Colgate and Sigurgeirsson 1973) or of molten metal into water (Long 1957). The key to energetic fuel/coolant explosions is the very rapid transfer of heat that requires substantial surface area of the injected liquid (or solid): fragmentation of the liquid (or solid) can provide this necessary surface area. The studies by Witte *et al.* (1973) and their review of prior research showed that such energetic explosions always appear to be associated with fragmentation of the injected material. Research suggests that an energetic fuel/coolant interaction consists of three phases: (1) an initial mixing phase in which the fuel and coolant are separated by a vapor film (2) breakdown in the vapor film that leads to greater heat transfer and vaporization rates and (3) an explosive or energetic phase in which the fluid motions promote even greater heat transfer and vaporization. In this last phase the explosive behavior appears to propagate through the fuel/coolant mixture like a shock wave.

Examples of reviews of the wide range of experiments on fuel/coolant interactions can be found in Witte *et al.* (1970) and Board and Caldarola (1977) among others. However, none of the experiments and analyses on sodium and uranium dioxide showed any significant energetic interaction and most of the experts agree that energetic fuel/coolant interactions will not occur in liquid-sodium LMFBRs (Fauske 1977b, Board and Caldarola 1977b, Dickerman *et al.* 1976).

8.6 Hypothetical accident analyses for FBRs

Even though the possibility of an energetic fuel/coolant interaction can be essentially (though not completely) eliminated in the analyses of hypothetical accident analyses in a liquid sodium cooled LMFBR, there still remain the questions of how the reactor core meltdown would proceed, of whether the containment would be breached, of whether radioactive materials could be released into the surroundings and how the heat generated in the disassembled core would be dissipated (Wilson 1977). Studies and experiments on the core meltdown show that the resulting sodium/uranium mix in the reactor contains sufficient sodium to take away the decay heat by boiling for many hours while the decay heat de-

clines. In this regard the pool-type reactors are superior to the loop-type (see section 5.7) since they contain more sodium. Moreover, large scale experiments have shown that mixtures of boiling sodium and molten fuel and cladding can coexist for many hours without energetic interactions. Despite these reassuring studies, even the most remote possibilities must be explored to allay public fears regarding fast breeder reactors.

8.6.1 Hypothetical core disassembly accident

Detailed analyses of hypothetical core disassembly accidents in LMFBRs have been conducted by Fauske (1976, 1977, 1981) and others. Much of this analysis begins with the hypothetical melting of the cladding that allows molten fuel to mix with the sodium coolant. As Wilson (1977) observes, the questions that necessarily follow are complex and difficult to answer. What is the potential for a fuel coolant interaction involving the molten fuel, the coolant and pieces solid or liquid cladding? Does the cladding melting then progress to other parts of the core? Where does the fuel end up? Is there a physical argument that could be used to place a limit on the damage to the core? And most importantly, does the reactivity increase or decrease during the various scenarios that follow? While many of these complex questions will need to be addressed, primary focus needs to be placed on the maximum possible accident for public acceptance of LMFBRs will depend on the design of safety systems to contain such an accident. As with LWRs, computational analyses will need to be coupled with experimental programs to validate those predictions. For a comprehensive summary of these issues the reader is referred to the review by Wilson (1977).

References

Board, S.J. and Caldarola, L. (1977). *Fuel coolant interactions in fast reactors.* In Jones, O.C. and Bankhoff, S.G. (1977b).

Bodansky, D. (1996). *Nuclear energy. Principles, practices and prospects.* Springer-Verlag New York, Inc.

Brennen, C.E. (1994). *Hydrodynamics of pumps.* Concepts ETI and Oxford Univ. Press.

Brennen, C.E. (1995). *Cavitation and bubble dynamics.* Oxford Univ. Press.

Brennen, C.E. (2005). *Fundamentals of Multiphase Flow.* Cambridge Univ. Press.

Burgess, D.S., Biordi, J. and Murphy, J. (1972). *Hazards of spillage of LNG into water.* U.S.Bureau of Mines, PMSRC Rept. No. 4177.

Cameron, I.R. (1982). *Nuclear fission reactors.* Plenum Press, New York & London.

Colgate, S.A. and Sigurgeirsson, T. (1973). Dynamic mixing of water and lava. *Nature*, **244**, 552-555.

Collier, J.G. and Hewitt, G.F. (1987). *Introduction to nuclear power.* Hemisphere Publ. Co.

Dickerman, C.E., Barts, E.W., De Volpi, A., Holtz, R.E., Murphy, W.F. and Rothman, A.B. (1976). Recent results from TREAT tests on fuel, cladding and coolant motion. *Ann. Nucl. Energy*, **3**, 315-322.

Dix, G.E. and Andersen, J.G.M. (1977). *Spray cooling heat transfer for a BWR fuel bundle.* In Jones, O.C. and Bankhoff, S.G. (1977a).

Fauske, H.K. (1976). The role of core disruptive accidents in design and licensing of LMFBR's. *Nucl. Safety*, **17**, No.5, 550.

Fauske, H.K. (1977). *Liquid metal fast breeder reactor safety: an overview including implications of alternate fuel cycles.* In Jones, O.C. and Bankhoff, S.G.(1977b).

Fauske, H.K. (1981). *Core disruptive accidents.* In Jones, O.C. (ed.) (1981).

Frost, D. and Sturtevant, B. (1986). Effects of ambient pressure on the instability of a liquid boiling explosively at the superheat limit. *ASME J. Heat Transfer*, **108**, 418–424.

Grandjean, C. (2007). Coolability of blocked regions in a rod bundle after ballooning under LOCA conditions - Main findings from a review of past experimental programmes. *Nucl. Eng. & Design*, **237**, No.15-17, 1872-1886.

Hochreiter, L.E. and Riedle, K. (1977). *Reflood heat transfer and hydraulics in pressurized water reactors.* In Jones, O.C. and Bankhoff, S.G.(1977a).

Hochreiter, L.E. (1985). *FLECHT SEASET program final report.* NUREG/CR-4167.

Holowach, M.J., Hochreiter, L.E., Cheung, F.B., Aumiller, D.L. and Houser, R.J. (2003). Scaling of quench front and entrainment-related phenomena. *Nucl. Eng. & Design*, **223**, No.2, 197-209.

Hsu, Y.Y. (1978). *Two-phase problems in PWRs.* In *Two phase flows in nuclear reactors*, Von Karman Institute for Fluid Dynamics, Lecture Series 1978-5, **1**.

Jones, O.C. and Bankhoff, S.G. (editors) (1977a). *Symposium on the thermal and hydraulic aspects of nuclear reactor safety. Volume 1: Light water reactors.* ASME, New York.

Jones, O.C. and Bankhoff, S.G. (editors) (1977b). *Symposium on the thermal and hydraulic aspects of nuclear reactor safety. Volume 2: Liquid metal fast breeder reactors.* ASME, New York.

Jones, O.C. (ed.) (1981). *Nuclear reactor safety heat transfer.*Hemisphere Publ. Co.

Lahey, R.T. Jr. (1977). *The status of boiling water nuclear reactor safety analysis.* In Jones, O.C. and Bankhoff, S.G. (1977a).

Lewis, E.E. (1977). *Nuclear power reactor safety.* John Wiley & Sons.

Long, G. (1957). Explosions of molten aluminum in water: cause and prevention. *Metal Progr.*, **75**, No.1, 107.

Marples, D.R. (1986). *Chernobyl and nuclear power in the USSR.* St. Martin's Press, New York.

Mould, R.F. (2000). *Chernobyl record : the definitive history of the Chernobyl catastrophe.* Publ. Institute of Physics.

National Geographic Magazine, April 2006.

OCED (Organization for Economic Co-operation and Development). (1996). *Implementing severe accident management in nuclear power plants.* Nuclear Energy Agency, OCED.

Okrent, D. (1981). *Nuclear reactor safety.* Univ. Wisconsin Press.

Osif, B.A., Baratta, A.J. and Conkling, T.W. (2004). *TMI 25 years later : the Three Mile Island nuclear power plant accident and its impact.* Pennsylvania State Univ. Press.

USAEC (1957). Theoretical possibilities and consequences of major accidents in large nuclear power plants. *U.S. Atomic Energy Commission*, Rep. WASH-740.

USAEC (1973). The safety of nuclear power reactors (light water cooled) and related facilities. *U.S. Atomic Energy Commission*, Rep. WASH-1250.

Wilson, R. (1977). Physics of liquid metal fast breeder reactor safety. *Rev. Mod. Phys.*, **49**, No.4, 893-924.

Witte, L.C., Cox, J.E. and Bouvier, J.E. (1970). The vapour explosion. *J. Metals*, Feb.1970, 39-44.

Witte, L.C., Vyas, T.J. and Gelabert, A.A. (1973). Heat transfer and fragmentation during molten-metal/water interactions. *ASME J. Heat Transfer*, **95**, No.4, 521-527.

Index